UNIVERSITY OF THE WITWATERSRAND

Department of Mining Engineering

JOHANNESBURG

DETERMINATION OF MODE I (K_{IC}) FRACTURE TOUGHNESS OF THE BRITTLE ROCK TYPES ENCOUNTERED IN THE SOUTH AFRICAN MINING ENVIRONMENT

K. N. Karparov PrEng

August 1998

A Dissertation submitted to the Faculty of Engineering, University of the Witwatersrand, Johannesburg, in fulfilment of the requirements for the Degree of the Master of Science

ABSTRACT

Dri...ed specimens from four types of rocks, namely Quartzite, Norite, Sandstone and Coal encountered in the South Africa mining environment were tested to determine their fracture toughness coefficients, using International Society for Rock Mechanics (ISRM) standards.

The tests were conducted using a MTS servo-controlled testing machine in displacement control mode.

Level I tests were run under load control until the specimen failed. The loading rate during the tests was increased gradually until failure occurred within 10 seconds of the initial load application or reached crack velocity of 0.001 mm/sec. The average stress intensity rate during the tests was not less than 0.25 MPa m/sec. The average fracture toughness coefficient of Quartzite, calculated on this basis was 1.89 MPa m, of Norite - 1.97 MPa m, of Sandstone - 1.40 MPa m and of Coal - 0.45MPa m.

Level II fracture toughness tests were ran under axial displacement (LVDT) control. Template containing procedures were set up for different stages of testing. The stress intensity rate during the test. The loading rate of investigated rock specimens was 0.001 mm/sec. Fracture toughness coefficient of Quartzite was - 2.20 MPa m, of Norite - 2.29 MPa m, of Sandstone - 0.34 MPa/m and of Coal - 0.14 MPa m. Influence of a loading rate on the tensile strength of specimens was confirmed. Estimated yield and ultimate tensile strength can be used for energy related investigations.

The fracto graphic studies show different behaviour between fatigue crack growth of investigated brittle rock types. For example, the main crack in Quartzite specimens occur through the boundary of the quartz grains and keep approximately straight direction in the core of specimen. Fracturing in Norite specimens begins with clear fracture process zone and the crack does not keep a straight direction in the core of specimen. The fatigue region shows more evidence of intergranular cracking and grain pull-out, and the quartz grains appear dulled, possibly by crack locking.

Yield and ultimate tensile strength were estimated on a basis of developed equation for three point bending tests. Influence of a loading rate on the tensile strength of specimens was confirmed. For example, by increasing the loading rate of hard rocks, their tensile strength also increased. With soft rock increasing the loading rate decreases the tensile strength.

Used J-integral technique shows its application in determining of fracture toughness coefficient in mode I. The critical values of J-integral (J_{IC}), which were estimated show their relation to K_{IC}. Backward calculation of K_{IC} from J_{IC} was with acceptable small deviation, compared to K_{IC} estimated tests. Calculated square deviation of K_{IC} from J_{IC} for Quartzite specimens is between 0.9364 and 0.924, for Norite specimens between 0.9107 and 0.9007 and for Sandstone specimens between 0.900 and 0.8135.

DECLARATION

I declare that this dissertation contains only my own original work, except where reference is made with acknowledgement to contributions from others. I also declare that this material has not been submitted for any purpose or examination to any other department or University.

Signed this...19th...............day of...August...1998

....
Krassimir N Karparov PrEng

ACKNOWLEDGEMENTS

I would like to thank the following:

- Prof. M U Ozbay who supervised the project and gave help and support at all times.
- The CSIR - Mining Technology for funding the project and in particular the help of Dr. R G Gurtunca.
- Mr A Tarnar from CSIR - Mining Technology for help with fracto graphic studies.
- Mr D Henderson, Mr H Brenner and all staff in the Mining Department laboratory.
- Mrs D E McKee from the Mining Department for editing of the work.
- My colleagues and fellow post graduate students in the Mining Department.
- All the administrative staff in the Mining Department.
- All staff at WITS - Engineering Library, SIMERA Library and ESKOM Library for their assistance.

CONTENTS

LIST OF NOTATIONS

a	Crack length (Major semi-axis of an elliptical crack)
a_c	Critical crack length
A	Crack surface area
b	Uncracked ligament
B	Specimen thickness
CMOD	Crack mouth opening displacement
CTOD	Crack tip opening displacement
D	Specimen diameter
E	Young's modulus
FPZ	Fracture process zone
F_C	Load at evaluation point
F_{MAX}	Maximum load
G	Strain energy release rate or crack driving force
G_I	Strain energy release rate for mode I
G^C_{CB}	Crack extension resistance in terms of energy release rate
J	J-integral
J_{IC}	Critical value of J-integral
I	Moment of inertia
K	Stress intensity factor
K_C	Critical value of stress intensity factor
K_I	Stress intensity factor for mode I
K_{IC}	Fracture toughness for mode I
K_I^{DIN}	Dynamic stress intensity factor
K_{Ia}^{DIN}	Dynamic stress intensity factor at arrest
K_{ia}^{STAT}	Static stress intensity factor at arrest
K_{ID}	Dynamic facture toughness
K_{CB}	Fracture toughness for mode I
K^C_{CB}	Critical value of fracture toughness for mode I
LEFM	Linear elastic fracture mechanics

LVDT Linear variable differential transducer

LPD Load point displacement

M_a Bending moment

p Non-linearity correction factor

P Applied force

P_0 Pore pressure

P_Q Critical applied load

PPZ Plastic process zone

P_5 Critical load corresponding to the 25% offset secant line

P_{max} Maximum load

Q_f Tensile fracture surface energy

Q_s Thermodynamic surface energy

r Distance measured from the crack tip

s_i The slope of linear part of the P-CMOD curve

SSY Small scale yielding

U Potential energy of the system

W Strain energy density

W^f_{CB} Total work of fracture

w Thickness of specimen

Greek Symbols

σ_U Ultimate stress

σ_{flow} Flow stress

σ_Y Tensile stress normal to the crack surface

ν Poisson's ratio

INTRODUCTION

The formation of deep underground openings in rock causes redistribution of the stress, which can interact with the exposed rock causing it to fracture. The degree and orientation of fracturing within the immediate vicinity of mine openings are the determining factors in designing support systems for safe and economic mining operations.

While the rock mass is of primary importance in engineering rock mechanic design problems, the rock material itself becomes important in fragmentation processes such as drilling, blasting, tunnel boring, cutting or crushing. However, the two are closely related and consequently fracture mechanics concepts have, despite being primarily concerned with rock material, made important contributions to practical rock engineering [14]. In recent years, these concepts have received an increasing amount of interest, both through analytical studies and in the area of fracture toughness testing of rock [12].

In spite of extensive research undertaken worldwide, very little is known about the mechanism of fracturing in rock. Traditionally, the fracturing around mine openings has been a subject of rock engineering. Current studies, however, tend to indicate that basic theories of Fracture Mechanics can be used to describe at least some of the modes, such as extension fracturing.

One of the important material parameters used in Fracture Mechanics is the fracture toughness. The fracture toughness parameter for fracturing in tension is called

Mode I (K_{IC}). The value of K_{IC} for rock types encountered in South African mining conditions is not known (with exception of Quartzite, investigated from Middlemass, MSc, Wits, 1991).

The quantity K_{IC} has been shown to be an important and useful parameter in rock engineering and is a property of a rock indicating its fracture resistance to crack propagation. A higher value of K_{IC} means increased fracture resistance of crack extension. K_{IC} can only be determined by testing a properly prepared specimen with a crack in it. The crack may be either pre-existing or pre-fabricated. So far, numerous testing methods employing various specimen geometries have been used to derive K_{IC} for rocks.

With the development of the fracture toughness methodology based on J, various methods for experimentally determining J from a load versus load point displacement test have been proposed. The goal of these proposed methods is to simplify the experimental procedure and the data analysis in a J_{IC} fracture toughness test. This dissertation describes an experimental program conducted to evaluate the accuracy of these estimation methods. Comparison between the values of K_{IC} as calculated by the energy rate definition and those calculated by the estimation technique for three-point bend specimens are made.

This dissertation presents the results from a series of tests carried out to determine the mode I fracture toughness and J-integral studies of four different rock types dominant in South African mining, namely Quartzite, Norite, Sandstone and Coal. The tests were conducted using a servo-controlled testing machine with a specifically developed mode I testing fixture.

II. FRACTURE MECHANICS

Fracture mechanics is an engineering discipline where the aim is to give a quantitative description of the transformation by crack growth of an intact structural component into a broken one. In its most basic form it relates the maximum permissible stress to the size and location of the crack. It can also predict the rate at which cracks grow to a critical size, by environmental influences or by varying loads (fatigue). Further it can determine the conditions of rapid propagation and arrest of moving cracks [7].

As part of the introduction to the subject fracture mechanics concepts are given here under the following headings: *crack tip displacement modes, stress intensity analysis, fracture initiation and propagation, J integral, crack extension laws, process zone, crack tip opening displacement, crack arrest factor, dynamic fracture and evaluation of fracture mechanics parameters for specific crack systems.*

II.1 Crack Tip Displacement Modes

There are three basic modes of fracture mechanics (Fig.II.1).

A. *Mode I*, which is also known as the opening mode, is so called because the crack tip is subject to a normal stress and the crack faces separate symmetrically with respect to the crack front so that the displacements of the crack surfaces are perpendicular to the crack plane.

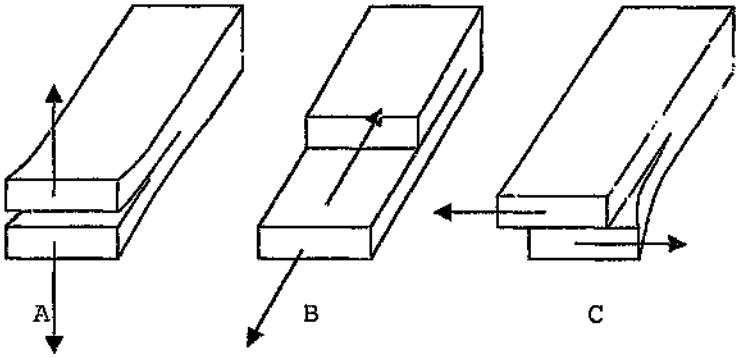

Figure II.1. Schematic drawing illustrating the three fundamental modes of fracture. A: mode I, tensile or opening mode; B: mode II, in-plane shear or sliding mode; C: mode III, anti-plane shear or tearing mode [32]

B. *Mode II* is the edge sliding (or in-plane shearing) mode where the crack tip is subjected to an in-plane shear stress and the crack faces slide relative to each other so that the displacements of the crack surfaces are in the crack plane and perpendicular to the crack front (or leading edge).

C. *Mode III* is also called the tearing mode or anti-plane mode and, in this case, the crack tip is subject to an anti-plane (or out-of-plane) shear stress.

The crack faces move relative to each other so that the displacements of the crack surfaces are in the crack plane but parallel to the crack front [1].

II.2 **Stress Intensity Analysis**

The stress distribution in the crack tip region is analysed on the assumption of McClintock and Irwin (1965) that classical linear theory of elasticity applies. This is valid provided that any region of non-linear behaviour is negligibly small compared with the length of the crack and the dimensions of the cracked body. It is recognised, however, that non-elastic effects are involved at c[illegible] tits in many materials.

The *K* value for mode I can be further defined as

$$K_I = \lim [\sigma_y (2\pi r)^{1/2}] \qquad \text{II.1}$$

where σ_y is the tensile stress normal to the crack surface. Lawn and Wilshaw, (1975) have given a completely general expression for the near field stress distribution for any mode as

$$\sigma_{ij} = K_L (2\pi r)^{1/2} f_{ij}(\theta) \qquad \text{II.2}$$

where $f_{ij}(\theta)$ is a well defined function of θ and depends upon the loading mode, and K_L is the stress intensity factor which embodies the loading configurations of the crack system. The subscript *L* to *K* denotes the mode of loading, *L* = I, II, III.

II.3 Fracture Initiation and Propagation

Instead of considering crack tip stress, an alternative fracture mechanics approach to crack extension is to examine the crack extension force, *G*. The crack extension force, or strain energy release rate, is the loss of energy per unit of new crack separation area formed during an increment of crack extension. In geomaterials such as rock and concrete, Hardy, 1973; Hoagland et al., 1973; Schmidt 1980; etc.,[32] this region is called the crack tip microcraking zone. It is so called because this microcraking zone is largely formed by the initiation and propagation of the microckracks near the crack tip, which makes the material in this region behave plastically.

Irwin and Barenblett, 1948 [32] defined a small region around the crack tip, in which the material behaves plastically rather than elastically as usual assumed for the treatment of fracture mechanics problems. This small region is referred to as the crack plastic zone in metallic materials.

Both the plastic zone in metals and the microcracking zone in rock-line materials are discriminately called the crack tip inelastic zone. Because *G* is calculated for infinitesimal increments of new separation area it can be applied to both stationary and running cracks. The strain energy release rate is a rate with respect to crack length and not with respect to time.

II.4 *J* Integral

In recent years a considerable effort has been expanded on the development of a methodology for J-integral to characterize the fracture behavior of structural materials employed at temperatures where they exhibit elastic-plastic behavior. This effort has focused, to a large extend, on the J-integral, first proposed by Rice [40, 41] and later advanced as a failure criterion by Begley and Landes [42, 43]. Subsequently other analyses have evolved [44, 48].

Although being accepted for metals, the use of J as a fracture parameter in the nonlinear range is now for rock material. Some work has been reported by Wilkening [49], and Schmidt and Lutz [50] where the J-integral is determined by an energy rate interpretation.

Thus, J is equivalent to the potential energy release rate. It is most widely used, however, for the characterization of crack tip conditions in the case of large scale yielding. In such applications the crack tip is assumed to be nearly stationary, strains are assumed to increase monotonically with time during loading, and the stress field energy density is assumed to be the same as it would be if the stress-strain behaviour were reversible.

However, the optimum procedures of analyses have yet to be conclusively defined and standardised.

II.7 **Crack Extension Laws**

Griffith in 1924, [8] and Irwin in 1960, [13], defined that there are two types of crack extension laws in fracture mechanics.

(a) *Equilibrium laws*, which specify that cracks may extend stable or unstable at some critical value of a fracture mechanics parameter. This is because various energy dissipation processes operate at crack tips in many solids, other than those processes associated purely with new surface formation (Atkinson [1]). These additional processes include crack tip micro plasticity and acoustic emission, and they are included in the calculation of the fracture surface energy.

(b) *Kinetic laws*, in which, at certain subcritical values of fracture mechanics parameters, a crack can extend.

Evans, 1972 [6], mentioned that this values are assumed from experimental results and Landes and Begley, 1973 [38] from physicochemical theories regarding the assumed crack tip weakening processes.

Rice (1978) [26] has re-examined the thermodynamics of Griffith-type crack growth, however, and shown that it is governed by

$$(G-2Q_s)v \geq 0 \qquad \text{(II.3)}$$

where Q_s is the ideal or thermodynamic surface energy.

Chemically active environments can reduce the thermodynamic threshold for crack growth so as to allow subcritical crack growth by influencing Q_s.

Lawn (1983) [15] has also shown that fracture mechanics can be extended to cover the growth of atomically sharp brittle cracks by the sequential rupture of bonds through various detailed microscopic mechanisms.

II.6 **Process Zone**

Lawn, 1983 [15] deals with a single, ideal sharp crack. This is a suitable representation for single crystals or at a microscopic level in polycrystalline materials. In these cases extensive electron optical studies have supported the assertion that brittle cracks are atomically sharp and propagate by the sequential rupture of bonds.

At a more macroscopic level of study, rocks and ceramics, show more complex behaviour. On loading the blunt, machined notch in Fig.II.2 a few isolated micro cracks are formed, but the system behaviour remains linear. On further loading the intensity of micro cracking increases and behaviour in the crack tip region becomes non-linear. Finally, macro crack extension occurs because of the linking of micro cracks in this non-linear zone, known as the process zone. The macro crack propagates by taking with it a cloud of damage contained in the process zone.

The use of the term process zone is linked above to the development of crack tip micro cracking. In the fracture mechanics literature, however, it is given a more general meaning as any zone of non-linear behaviour at a crack tip. Plasticity, instead of micro cracking, could be the means by which the non-linearity is obtained.

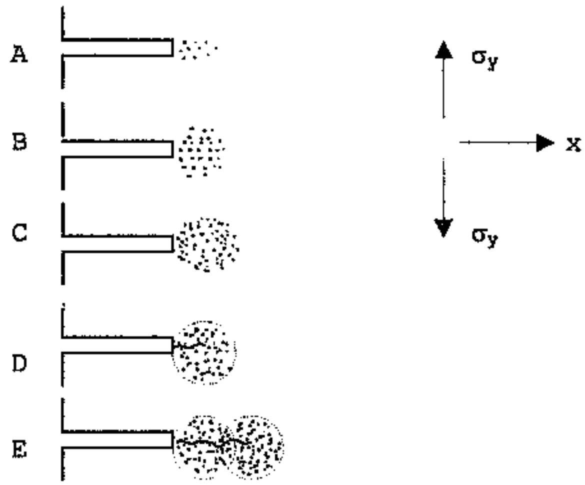

Figure II.2 Schematic drawings illust·ating the development of a process zone and its influence on macro crack growth. Simple tensile deformation occurs across the plane *y=0*. Stress increases through drawings A to E. (A) Machined notch with a few isolated micro cracks induced by machining. (B) Micro cracking begins. Micro cracks mostly isolated and linear elastic behaviour is still observed. (C) Micro cracking becomes more intense. Some micro cracks link up. N -linear behaviour is observed. (D) Within the now fully

Schmidt and Lutz, 1979 [8] defined that for a large process (micro cracking or plasticity) zone the material behaves as if it has a slightly longer macro crack than is actually measured. *K* and *G* determinations can be extended to include a process zone adjustment in the calculation of an effective crack length.

Problems do arise with materials such as ice, some rocks and concrete with no well defined yield stress (Goodman, 1980; Labuz et al., 1985) [7,15] and here different and more complex schemes for estimating the process zone size are required.

II.7 **Crack Tip Opening Displacement (CTOD)**

The crack tip opening displacement, is given approximately by the crack opening at the intersection of the boundary to a non-linear crack tip region (plastic or micro cracked) with the crack surface.

The direct measurement of crack tip opening displacement (CTOD) has been attempted in past using double notch specimen technique [4], infiltration method [5], etc. It is, however, not practicable to measure CTOD directly in fatigue cracked specimens. The clip gauge method [6] is used to measure the crack mouth opening displacement (CMOD) in the fatigue cracked specimens and the CTOD is evaluated from the measured CMOD values at the original crack tip [7]. Wells [8] converted CMOD into CTOD by using plastic hinge model. DD 19 [9] provides the necessary relation for the above conversion using a nondimensional limiting value of elastic clip gauge displacement. Some ambiguity with the elastic clip gauge displacement values has been reported in the recent past [10]. New draft for CTOD evaluation has been proposed based on Daves work [11] through BS 5762 [12] which uses deep crack SEN bending specimen.

The current method for CTOD evaluation thus heavily depend on the method of extrapolation of CMOD to the physical crack tip with the help of rotation factor. The effect of specimen and loading geometry on rotation factor is not well documented. A reliable method for CTOD evaluation is available only for deeply notched SEN bending specimens. For other geometries large variation in the CTOD values is expected depending upon the method used for evaluation of rotation factor [51, 52].

II.8 Crack Arrest Factor

For a running and arresting crack, the dynamic stress intensity factor K_I^{din} is given as a function of time, and is compared with the corresponding value K_I^{din} resulting from the static formulas. Kalthoff, Beinert and Winkler [53] in 1981 defined influence of dynamic effects on crack arrest in compact-specimens.

The value of the stress intensity factor at arrest, K_{Ia}^{din}, in principle, could be measured directly by use of experimental stress analysis techniques. These methods, however, in general, are too complicated for standard engineering testing procedures. In order to simplify the measurement procedure, two different concepts have been developed in the past.

Crosley and Ripling [54-58] introduced a purely static concept. The dynamic effects are neglected and the static value of the stress intensity factor at arrest, K_{Ia}^{din}, is determined using static formulas. This value is lower than with dynamic effect, but the error is tolerated because of the simplicity of the procedure.

Hahn, Kannien et al. [59-63] take the dynamic effects into consideration by application of a theoretical-numerical analysis of the run-arrest process. The computation result in the so-called Reference-Curves, which are used to determine the crack velocity V and the dynamic fracture toughness K_{ID} for the running crack. In general, K_{ID} depends on the crack velocity. The autors assume that the crack arrests when K_{ID} attains its minimum value K_{IM} which, consequently, represents the crack arrest toughness.

II.9 **Dynamic Fracture**

In practice, running cracks can accelerate to significant fractions of the velocity of sound. From purely inertial considerations the crack velocity cannot be greater than the speed of Raleigh waves (approximately 0.9 of the transverse sound wave velocity). In real solids, limiting crack velocities observed commonly range from 0.1 to 0.6 of the sound wave velocity (Irwin, 1960) [13]. An increase in crack driving force (*G* or *K*) beyond that necessary to drive the crack at the limiting speed results in crack branching and hackle formation on the crack surfaces.

II.10 **Evaluation of Fracture Mechanics Parameters for Specific Crack Systems**

Two distinct methods are used to evaluate fracture mechanics parameters for specific crack systems: (a) *stress analysis*, and (b) *direct measurement* using compliance calibrations (Atkinson [1]).

For metals, certain well defined standards, such as ASTM E399 and E561, have existed for a number of years. The fact that the same approach has only recently been applied to fracture in rocks has hindered the wider use of fracture mechanics in geophysics. Limitations to rock fracture mechanics experimental methods are discussed by Atkinson [2] and Ouchterlony [20]. Ouchterlony has chaired a working group of the Commission on Testing Methods of the International Society for Rock Mechanics (ISRM) that has recently recommended the use of chevron-notched core specimens as the standard method for determining the fracture toughness of rock (ISRM, 1988) [12].

III. MODE I FRACTURE TOUGHNESS TESTING

III.1 Mode I fracture toughness (K_{IC})

Representative value of the fracture toughness of material for mode I cracking (i.e. K_{IC}) can be obtained from fracture mechanics testing. A higher value of K_{IC} means increased fracture resistance to crack extension. K_{IC} can only be determined by testing a properly prepared specimen with a crack in it. The crack may be either self-produced (e.g. the indentation method and the modified ring test) [31] or pre-fabricated. So far, numerous testing methods employing various specimen geometries have been used to derive K_{IC} for rocks.

Some tests methods require the introduction of a V shaped chevron notch, which causes crack propagation to initiate at the tip on the V shape. Fracture propagation is in the notch plane along the rod axis and has stable manner until the load reaches its maximum value P_{max}. Then unstable crack propagation takes place.

III.2 Fracture toughness testing methods

III.2.1 The Chevron Notched Short Rod (SR)

The SR method was introduced by Barker, 1977, [32] (Appendix 1) and to determine fracture toughness of rock. This specimen is core-based one with a mechanical notch along the load axis. The external load is applied to the notch mouth to split the specimen into two identical halves.

When this geometry was introduced for determining fracture toughness, he provided an explicit expression for the stress intensity factor K_I based on the relationship between strain energy release rate to compliance and to stress intensity factor.

III.2.2 **The Chevron Edge Notched Round Bar in Bending Short Rod (CB)**

The CB specimen was developed by the Ouchterlony and co-worker (Ouchterlony, 1980; Ouchterlony and Sun, 1983) [32] (Appendix 2), who used this geometrical shape in three point bending to determine fracture toughness of rocks. The chevron notch in CB causes crack propagation to start at the tip of the V and proceed in the chevron notch plane in a stable manner until the applied load reaches its maximum value, which is used to evaluate the level I fracture toughness.

III.2.3 **The Brazil Disk in diametral compression**

The Brazilian disk test has been often used to determine the indirect tensile strength in the laboratory (Brown, 1981) [32] (Appendix 1). The tensile stress in the disk results from the applied diametrical compressive load (Timoshenko and Goodier, 1951; Hondros, 1959). It has significant potential for application in fracture toughness testing of rocks (Sun et.al., 1990).

There are various methods to derive fracture toughness by using the Brazilian disk with diametrically orientated crack cut in different ways, i.e. central straight-through crack, central through chevron notch, single edge crack, double edge cracks.

III.2.4 **Radial cracked ring test (RCRT)**

The ring is another method for determining tensile strength of brittle materials (Choi et.al., 1988) [32] (Appendix 1). It was proposed by Shiryaev and Kotkis (1982) to determine fracture toughness.

III.2.5 **Modified ring test (MRT)**

A modification to the RCRT has been made by Thiercelin and Roegiers (1986) (Appendix 1). This test is more like the grooved disk containing an edge crack proposed by Szendi-Horvath (1980). It has been used to determine fracture toughness of rocks by Thiercelin and co-worker (Thiercelin and Roegiers, 1986; Thiercelin, 1987, 1989) [32].

It is essentially based on a hollow Brazilian disk with two diametrically opposite flat loading surfaces. One of the main features of this method is that when the diametric compression is increased, two diametrically opposite cracks will be initiated at the inner hole, which propagate along the loading axis until reaching the loading surfaces.

III.2.6 Single edge cracked half disc specimen in three point bending (HDB)

This test was developed by Chong and Kuruppu (1984) [32] (Appendix 1). This is suitable for compact specimens requiring duplicate samples to investigate various parameters such as strain rate, moisture content and temperature, etc (Karfakis et al., 1986). It is suitable to study the effects of anisotropy on the fracture toughness of rocks (Chong et al., 1987). They have developed a formula for K_{IC} by using both the strain energy release rate method (Dixon and Strannigan, 1972) and the elliptical displacement approach (Woo and Kuruppu, 1982). Both methods have yielded close results.

III.2.7 Round compact disc in tension (RCT)

This is a standard method in E399 for metallic materials. Sun (1983) and Ouchterlony (1986) (Appendix 1) have adopted this method to determine fracture toughness of rocks with the CMOD increased at a rate of 0.06 m/s during loading in their tests, where the direct tensile load is applied to split the specimen [32].

III.3 **Specimen size requirements**

III.3.1 **Relevance of crack tip non-linear region**

Earlier rock fracture toughness tests followed the ASTM-E399 [65] standard method suggested for metallic materials. The size requirements to ensure the measurements of fracture toughness in the plane strain condition (K_{IC}) are for specimens with large plastic zone sizes. The secant method of the ASTM (E399-74) for linear-elastic fracture mechanics evaluation cannot be applied directly at rock fracture mechanics. Sinse the plane strain fracture toughness is a parameter of LEFM, it requires that the crack tip non-linear region is sufficiently small in comparison with the smallest dimension of the specimen being considered, that is, the condition of small scale yielding (SSY) must be satisfied.

III.3.2 **Fracture toughness dependency on specimen size**

ASTM - E399 [65] has been shown that the fracture parameter K_{IC} is specimen-size dependent, which can be well explained from the formation of the crack tip non-linear region. In order to ensure that measured values of fracture toughness for a metallic material are a constant, the plane strain fracture toughness, the characteristic dimensions of the specimens, namely, crack length, specimen thickness and the uncracked ligament must be sufficiently large [32].

Costin [67] have estimated the value of fracture toughness coefficients of oil shale according specimen size (specimen length l, according specimen width W). For example, for specimen size of 4W in MPa/m they are between 0.86 and 0.99; for specimen size of 2W they are between 0.57 and 0.94; for specimen size of W they are between 0.54 and 1.0.

III.3.3 **Plane stress and plane strain: influence of test specimen**

For rocks, however, the specimen thickness seems to be a less important factor affecting fracture toughness than for metallic materials (Ingreffea and Schmidt) [10]. This is possibly mainly because of the distinct difference between the Fracture Process Zone (FPZ) in rocks and the Plastic Process Zone (PPZ) in metallic materials. In metallic materials a specimen which is too thin is shown to fracture under plane stress instead of the plane strain state, which leads to a larger plastic zone size and causes a greater value of fracture toughness.

Schmidt [28] has been shown that in rock materials, however, the FPZ is independent of whether the crack is under plane strain or plane stress state, and hence the size and shape of FPZ will not change whether the FPZ is located on the specimen's free surface or deep in the specimen.

III.3.4 **Criticality of rock specimen thickness**

Barton [3] pointed out that the thickness of a rock specimen is not critical but must not be smaller than the width of the FPZ. The size requirements for a valid representative value of fracture toughness for a rock specimen depend on the tensile strength and critical size of the fracture process zone.

III.3.5 **Minimum crack length**

Sun and Ouchterlony [21] inferred, for Stripa granite, that the minimum required specimen dimensions (suppose H) for plane strain fracture toughness testing can be found by measuring the apparent fracture toughness, K_Q. For specimens with constant other specimen dimensions, but with different H values to determine the point from which K_Q is independent of H. Schmidt and Ingraffea [10] found minimum crack length of a_{min}=50 mm and minimum specimen thickness of W_{min}=100 mm for Indiana limestone.

Number of investigators have shown that the factor of 2.5 (specimen thickness over crack length) for the minimum required is somewhat conservative and a factor of less than 2.5 has been found for most rocks. Chong and Kruppu (1985) determined fracture toughness of oil shale by using a specimen configuration of a half disc and proposed a factor of 2.0 for the minimum size requirements.

Ouchterlony [68] have calculated Young's modulus values variations with respect to notch depth. The E-values from

33 valid tests, where $0<a/D<0.35$ given as a $mean_{No\ tests} \mp$ standard deviation, the results are

$$E = 87.20_{9} \mp 3.01 \text{ GPa when } a/D = 0$$

$$E = [illegible].02_{11} \mp 2.63 \text{ GPa when } 0.1<a/D<0.2$$

$$E = 85.60_{13} \mp 2.72 \text{ GPa when } 0.2<a/D<0.3.$$

III.3.6 **Crack tip FPZ and rock grain size**

Nolen-Hoeksema and Gordon [19] have shown that the FPZ is as large as 20-40 grain diameters in Stockbridge dolomite. The minimum specimen dimension must be at least 20-40 times the grain diameter in order to obtain a valid K_{IC} value for the rock.

Traditionally in rock mechanics studies, a ratio of smallest specimen dimension to grain size of 10:1 has been considered to be sufficient to ensure that all the measurements have been representative of the material. When the influence of the crack tip FPZ is taken into account, the simple ratio of 10:1 for the measurements of fracture parameters of rock materials may not be sufficient.

III.4 **Specimen Precracking Requirements**

III.4.1 **Basic requirements**

ASTM - E399 [65] standard method was used from Brown, Peng and Johnson [4,24] but with narrow saw-cut notches without precracking to measure plane strain fracture toughness for various rock materials. The results, which were obtained, were too low. The fracture toughness results from subsequent tests were again found to be too low and furthermore dependent on notch depth. Even though specimen preparation and test procedure were much simpler, the fracture toughness results were again found to be too low and furthermore dependent on notch depth, indicating an R-curve behaviour.

The requirements of specimen precracking essentially aim at achieving a "natural crack", which is geometrically well defined and sufficiently sharp and is free from the effects of residual stress, specimen boundaries and the pre-fabricated notches.

III.4.2 Crack closure in concrete

Swartz and co-workers [30] used both pre-notched and pre-cracked concrete beams to determine fracture toughness. They found that the naturally cracked beams yielded higher failure loads and fracture toughness values than notched beams with the same crack lengths. For example, the average K_{IC} values for pre-cracked beams were approximately 38%, 77% and 96% higher than those for pre-notched beams for dimensionless crack lengths a/W of 0.3, 0.5 and 0.7 respectively.

Another explanation for this given by Sih and Gdoutos [29] is that since crack tips are in crystal grains which usually resist crack propagation, more energy is required to cause cross-grain (transgranular) crack propagation. On the other hand, wide notch tips contain structural weakness like grain boundaries and crack propagation is usually along the grain boundaries to form intergranular crack propagation.

III.4.3 Specimen precracking

At ASTM, E399 [65] the preckraking was done with a sinusoidal tension - tension loading. Specimen precracking is notoriously cumbersome since it usually requires expensive and sophisticated loading machines to accurately monitor the load and displacement in order to arrest any further propagation of the crack after it has been initiated.

Travers and Tharp [31] in order to avoid this, adopted a layer of thin and highly compliant material (paper) between the specimen and loading platen to precrack the three-point bending specimen. The layer of paper produced a distributed load on the bottom of the specimen during loading and hence could reduce the degree of risk of unstable crack propagation.

III.4.4 Chevron-notched specimens

The fundamental principle of this method is that a V-shaped chevron-notch is used instead of a straight-through notch and hence the length of the crack front is generally increased as the crack propagates (Fig.III.1).

The test with chevron-notched specimens requires neither crack length nor complicated fracture toughness calculation techniques, but just the recording of the maximum applied load and load point displacement (LPD) [12].

(a) A chevron-notched specimen

(b) Linear elastic or non-linear

(c) Non-linear

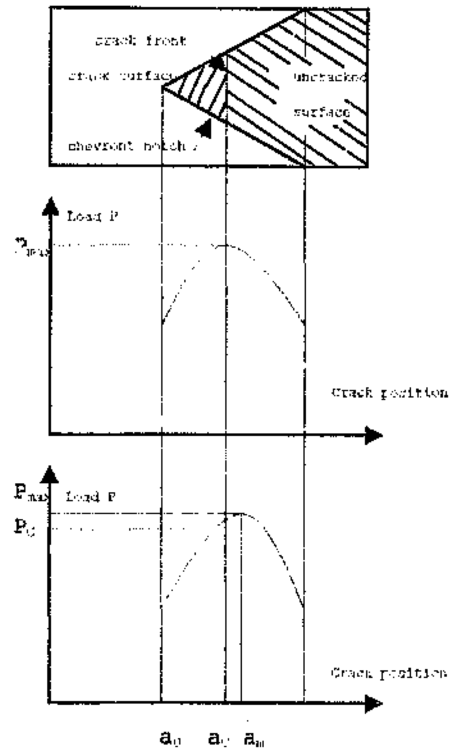

Figure III.1 Schematic interpretation of a chevron-notched specimen showing relationship between load and crack front position and linear and non-linear behaviour [32].

In E399 [65], there are other requirements for precracking. These requirements are mainly related to crack geometry, such as crack front straightness, crack plane tilt and final crack length. But these requirements have been shown to be unimportant in rock fracture toughness tests and hence have been ignored in such tests.

III.5 Testing Requirements

III.5.1 Crack displacement monitoring

The standard testing method for metallic specimens requires that experimental results should be recorded as a plot of the applied load *P* against the Crack Mouth Opening Displacement (CMOD). Such a plot is used to determine the critical load, P_Q, which is then required in the derivation of the apparent fracture toughness, K_Q.

Ouchterlony [23] has alternatively used *P* versus load point displacement (LPD) curves in his three-point bending tests using round bar specimens with significant success. In some cases where the load is not applied at the crack mouth, such as bending tests, *P* versus Load Point Displacement (LPD) is recorded, which is usually used to directly determine the energy-related fracture parameters by measuring the area under the curve of load-point displacement versus load. These parameters include the strain energy release rate, the *J*-integral and the fracture resistance curve (*R*-curve).

III.5.2 Loading rate

ASTM-E399 [65] requires for testing of metallic specimen, the loading rate K_I must be within the rate of 0.55 to 2.75 MPa$\sqrt{m}$/s. For metallic specimens tested at such a high loading rate, test duration is usually of the order of one minute. For rock specimens also tested at such high loading rates, however, the test could be finished within one second, since the apparent fracture toughness for most rocks is much lower than that for metals. Usually it is not more than 3 MPa$\sqrt{m}$/s.

Joyce and Gudas [69] calculated fracture toughness coefficients on different kind of metals, used in US Navy industry. They are as follow: for HY-130, K_{IC}=213 MPa$\sqrt{m}$, for 10 Ni_{steel}, K_{IC}=174 MPa$\sqrt{m}$, for 17-4PH_{steel}, K_{IC}=157 MPa$\sqrt{m}$, for Ti-7Al-2Cb-1Ta, K_{IC}=97 MPa$\sqrt{m}$, for Ti-6Al-4V, K_{IC}=78 MPa$\sqrt{m}$. Zhe-Ming [70] calculated fracture toughness coefficients of metals. They are as follow: for No.45 steel, K_{IC}=71.9 MPa$\sqrt{m}$, for 45MnCiV, K_{IC}=83.7 MPa$\sqrt{m}$, for 34CrNi3Mo, K_{IC}=121-138 MPa$\sqrt{m}$.

Number of rock fracture investigators have followed the E399 [65] recommended rates, most rock fracture researchers have used much lower rates resulting in the fracture test duration of approximately one minute. Schmidt [28] used loading rate of K_{IC} = 0.022 MPa$\sqrt{m}$/s in his three-point loading tests of Indiana limestone. Ingreffea and Schmidt [10] used an even lower loading rate of K_{IC} = 0.011 MPa$\sqrt{m}$/s for Indiana limestone. Schmidt and Lutz [27] used a wide range of loading rates of K_{IC} = 0.01 - 0.03 MPa$\sqrt{m}$/s in their fracture toughness tests of Westerly granite.

III.6 Fracture Toughness Calculation

III.6.1 Dependency of stress intensity factor

Swartz, Hu and Fartash [30] noted that for an infinite cracked body the stress intensity factor is dependent on the crack geometry and the applied stress, i.e. $K_I = \sigma/\pi a$. For the experimental tests they used appropriately cracked specimens of finite size. In most cases, for a given applied load the stress intensity factor is usually a function of the dimensionless crack length, a/W, where W is specimen width or some other characteristic specimen dimension which is equivalent to the specimen width.

Landes and Begly [34] mentioned that the calculation of the critical stress intensity factor (usually termed as the apparent fracture toughness before the validity is verified and denoted by K_Q) requires the critical applied load, P_Q, and the corresponding critical crack length, i.e. the crack length at failure, a_c.

III.6.2 Determination of the critical applied load

In E399 the test results should be reported as a plot of load versus CMOD.

The procedures for determining P_0 are as follows:

(1) A tangent, OA, to the original linear part of the P versus CMOD curve is drawn.

(2) A second line, OB, with a slope of 5% less than the slope of the tangent OA is drawn. The intersection point of OB with the *P* versus CMOD curve is defined as P_5, which corresponds to a 2% crack growth from the initial pre-cracked crack tip induced by the crack tip non-linearity behaviour.

(3) The determination of P_Q depends on the types of *P* versus CMOD curves:

a) If P_5 precedes the maximum load P_{max} as shown in Fig. III.2(a), P_Q is then defined as P_5. Most rocks are of this type of P versus CMOD records.

b) If pop-in (at some stage of loading, CMOD increases rapidly while the load maintains at the same level) occurs during the testing [see Fig. III.2(b)], P_Q is also defined as P_5 . Pop-in rock specimens are known to rarely take place.

c) If P_{max} precedes P_5 as shown in Fig. III.2(c), P_Q is equal to P_{max} . A number of rock specimens are known to have this type of P versus CMOD records.

d) If a local maximum load P^I_{max} instead of the overall maximum load P_{max} precedes P_5, then P_Q is defined as P^I_{max}. Rocks rarely have this type of P versus CMOD behaviour.

(4) Two horizontal lines are drawn at P_Q and 0.85 of P_Q respectively [See Fig. III.2(a)]. The distance between the tangent OA and the P versus CMOD curve at P_Q and $0.85P_Q$ are δ and δ_I respectively, where δ and δ_I correspond to the deviations from the linearity at P_Q and $0.85 P_Q$ respectively. In E399 it is required that δ_I should not be greater than 25% of δ , i.e. $\delta_I < 0.25\delta$. This requirement pertains to the crack tip non-linearity

and ensures that the condition of SSY is satisfied. If $\delta_I > 0.25\delta$, then the effect of non-linearity must be take- into account and a correction factor for non-linearity should be introduced.

Another restriction in E399 for a valid P_Q value is that the ratio P_{max}/P_Q must not exceed 1.1, i.e. $P_{max} < 1.1P_Q$. If this requirement is not satisfied, there is a possibility that K_Q may not bear sufficient relation to K_{IC} for the test, or the material is extremely ductile.

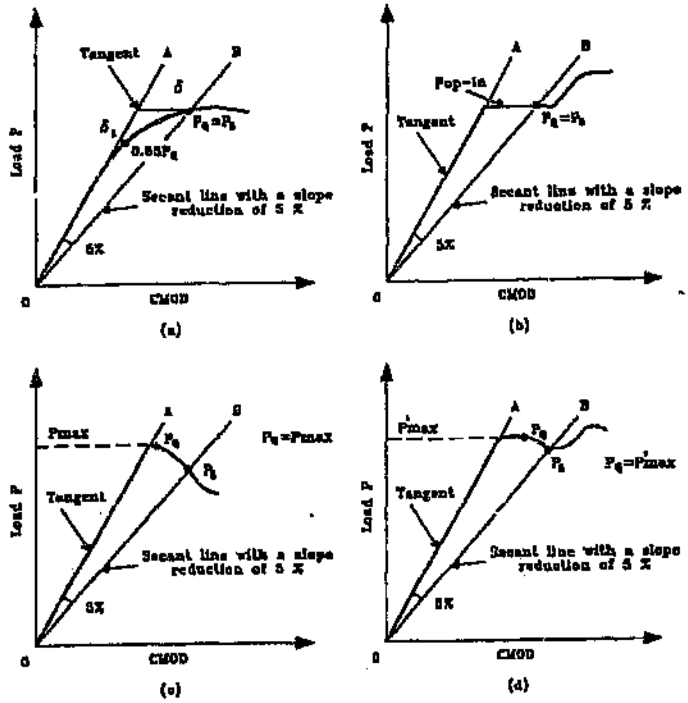

Figure III.2 Load versus CMOD records used to determine the critical load to failure, PQ [32]

This approach has been known as the 5% second approach and has frequently been used by most rock fracture mechanics investigators. For small specimens, however, this 5% second procedure gives a specimen size effect on K_{IC} even though LEFM conditions are satisfied.

Munz [18] accordingly proposed a variable secant, which has a slope adjusted to the specimen size, to determine P_Q.

III.7 K_{IC} Determination

Ouchterlony [20] mentioned that K_Q by itself has no physical importance and cannot be considered as a fracture property of a brittle material since its measurement does not take into account the effects of the crack tip non-linearity behaviour inherently existing at the crack tip upon unloading. When K_Q is compared with K_{IC}, it is an interesting parameter since the degree of influence of the crack tip non-linearity can be examined.

III.8.3 Compatibility of fracture toughness values

In order to show the compatibility of the fracture toughness values determined by different methods, Meredith [17] has performed a series of SR and double torsion (DT) tests to evaluate the fracture toughness values for a variety of rocks.

It must be emphasised that this method can well explain the phenomenon of increasing K_Q with crack length and specimen size, since the non-linearity correction factor p is always in the range $0 < p < 1$, which leads to $K_Q <$

K_{IC}. However, in ASTM - E399, K_Q can be either larger or smaller than K_{IC}. The former is the case for thin specimens where a plane stress state prevails.
Since p is dimensionless, this nonlinearity correction only requires the displacement measurement equipment to be linear, not calibrated absolutely. Large variations in p between the specimens in a test sample or a negative value is probably an indication of unacceptable errors in the evaluation procedure. In rocks, there is evidence that $p < 0$ and hence $K_Q > K_{IC}$ [10]. This method has been mostly used in the chevron-notched round bar and short rod tests in which the crack tip plane strain state always prevails and the non-linearity correction factor $p > 0$, which leads $K_Q < K_{IC}$. For $p = 0$ corresponds to linear elastic behaviour where there are no residual displacements upon unloading, i.e. $\delta_i = 0$.

III.9 ISRM Suggested Methods

Two suggested methods for determining the fracture toughness of rock material in the form of core specimens are described [12]. Core specimens were chosen because rock is readily available in the form of core pieces which then require little machining.

Method I uses a bend specimen with a notch cut perpendicular to the core axis. The specimen rests on two support rollers and a compressive load is applied to press apart the notch sides. This causes transverse splitting of the specimen by crack growth in the ligament, i.e. in the unnotched part, of the notched cross section during the test.

Method II uses a specimen, called the short rod, which has a notch cut parallel to the core axis. A tensile load is applied to the specimen to pull apart the notch sides. This causes lengthwise splitting of it by crack growth in the ligament of the notched section during the test.

Both methods offer two test levels. Level I testing can be made with portable equipment and it requires only the registration of maximum load during the test.

Level II testing requires continuous load and displacement measurements to be made during the test. Level II testing is clearly laboratory oriented and relatively complicated to perform.

IV LOADING EQUIPMENT AND FIXTURE

IV.1 MTS - 815 rock and concrete testing system

MTS rock and concrete mechanics testing systems [64] are designed for laboratory experiments on materials ranging from soft sandstone to high strength brittle rock. The high-capacity, high-stiffness design of the load frames coupled with high-response servo-hydraulics, digital control technology, application software and complete accessory packages provide an extremely versatile tool for investigation of the complete deformation behaviour of rock over a wide range of testing conditions.

A basic system includes a load frame assembly, an hydraulic performance package, the TestStar II digital controller, and complete system service.

IV.1.1 Model 315 load frame assembly

The Model 315 load frame assembly is designed specifically for uniaxial and triaxial rock testing with particular attention to studies on post failure behaviour. The assembly consists of a fixed crosshead mounted on two rectangular columns which result in an extremely rigid, yet free standing frame. Integrated into the base plate is a single-ended, double acting actuator. This arangment provides a high loading capacity in a stiff, compact frame. Two feedback transducers are included in a frame assembly. One is a differential pressure (P) transducer, which monitors the difference in pressure on each side of the actuator piston and is calibrated to represent the force output of the actuator. The other is an internal linear variable differential transformer (LVDT) which provides control and measurement of the actuator displacement during testing and specimen positioning.

IV.1.2 **Hydraulic performance package**

These hydraulic performance packages represent the most commonly used packages for testing soft and hard rock. Each package consists of an hydraulic power supply, an actuator manifold, servo valves and hydraulic hoses.

- An hydraulic power supply (HPS) is the fluid-power source for servo hydraulic testing systems. It is important that the fluid-power source has a high degree of pressure stability, cleanliness, and safety. MTS hydraulic power supplies are designed to meet these criteria, along with providing quiet, trouble free operation with long life and minimum maintenance.

- An actuator manifold functions as the mounting block between the servo valve and the hydraulic actuator. It provides flexibility by offering a selection of pressure controls, close-coupled accumulators, single- or dual-servo valve mounting and optional fluid filtration in a compact package. The servo valve functions as the final control element in a servo hydraulic test system by regulating the direction and rate of flow of the hydraulic fluid to the actuator. It is important that the servo valve has a high frequency response and low contamination sensitivity to provide a wide range of trouble-free testing capabilities.

- The TestStar II controller provides high speed servo control of the loading system. The TestStar II workstation consists of three major parts: the PC Workstation, the Digital Controller and the Load Unit Cont Panel. These work together as an integrated stem to spend more time testing and less time setting up.

IV.2 **Fracture toughness configuration**

The Fracture Toughness configuration (Figure IV.1) uses: a Bend Fixture, a Force Transducer, spacers and a strain measurement kit. The fatigue-rated force transducer is sized for the testing requirements. In addition to the mechanical fixture for fracture toughness testing, the model 790.63 Fracture toughness for Rock software is provided to execute some of the most common fracture toughness tests and analyse the resulting data.

The complete fracture toughness package includes:

- A Model 642.10 3-Point Bend Fixture (1a - Figure IV.1).
  The Model 642.10 Fracture Toughness Fixture is designed to accurately locate strain and displacement transducers on the specimen in order to obtain accurate, repeatable results when conducting Method 1 type Fracture Toughness tests on rock. A

Mo' l 642.10 includes alignment hardware to ac ately locate the clip-on displacement gauge and dual LVDTs on the specimen, and correctly orient the specimen on the fixture.

- A selected Series 661 Force Transducer - calibrated 2 ranges (2a - Figure IV.1).
  The Model 661 Force Transducers are designed to resist the extraneous forces and moments inherent in testing rock and concrete specimens. Its fatigue rated tension /compression transducers are designed for through zero and monotonic testing applications making them ideal for both indirect tension and direct tension tests.

- An attachment kit to attach the fixture to the load frame (3a - Figure IV.1).
  The fixture and specimen aligned tools ensure proper and consistent mounting of the specimen in the bend fixture and correct position displacement measurement fixture on the specimen.

- A Model 632.02 Clip-on Gage - calibrated in 2 ranges (1b - Figure IV.1).
  The Model 632.02 Clip-on Displacement Gauge is a double - cantilevered, displacement-type gauge used in fracture mechanics studies. The Clip-on Displacement Gauge senses crack-opening displacements and can monitor crack growth during fracture mechanics tests. The gauge uses precision, resistance type strain gauges bonded to the cantilever arms to form a Wheatstone bridge circuit. The arms of the Clip-on Gauge are mounted between

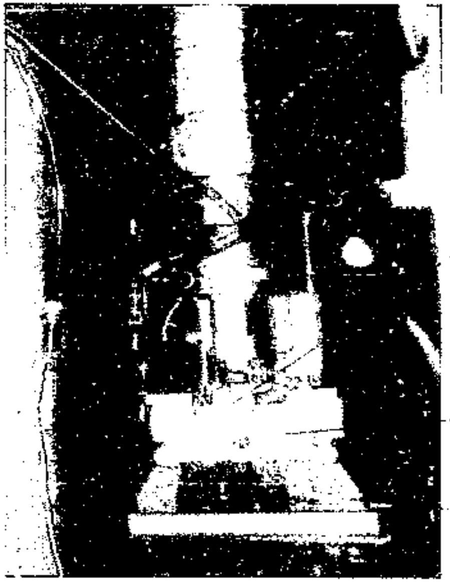

2b - An LVDT monitoring fixture

1a - Force transducer

3b - Dual LVDT's

3a - Attachment kit

1b - Clip-on gage

1a - 3-point bend fixture

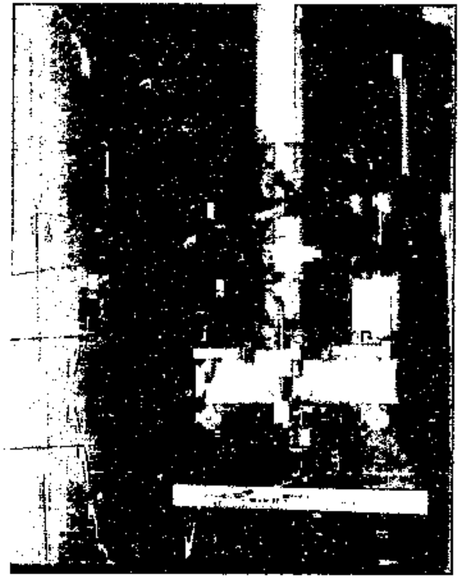

Figure IV.1-a
Specimen alignment of the
3 point bending fixture

Figure IV.1-b
Fracture toughness configuration
In the time of testing

Figure IV.1

Fracture toughness configuration

two knife edges attached to the specimen. Deflection of the specimen at the crack mouth causes movement at the ends of the arms. This movement causes the arms to bend, straining the bonded gauges, changing their resistance. This change in resistance unbalances the Wheatstone bridge circuit causing a change in electrical output that is proportional to the displacement of the cantilever arms.

- Two knife edge sets which are attached to the specimen for monitoring the model 632.02 Clip-on Gauge to the specimen (Figure IV.2).

- An LVDT monitoring fixture and alignment tools for fixture and specimen alignment (2b - Figure IV.1).

- Dual LVDTs (linear variable differential transformers) with averaged output for load point displacement measurement - calibrated in 2 ranges (3b - Figure IV.1).

- Four signal conditioners.

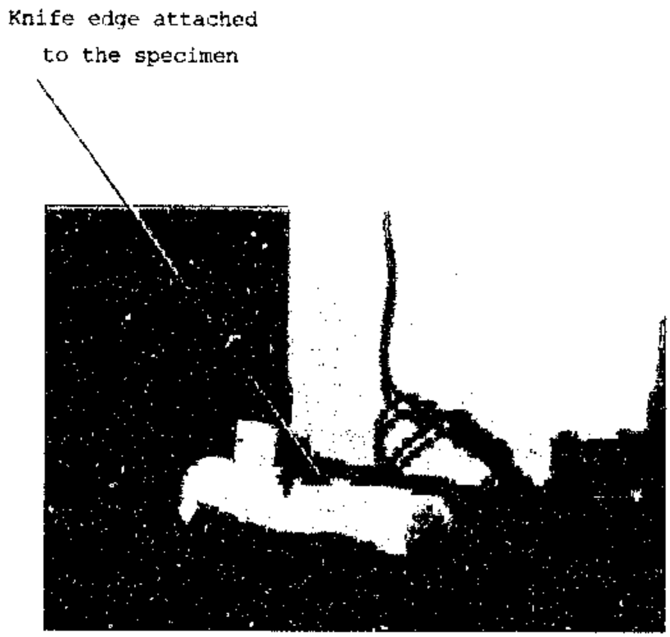

Figure IV.2
Specimen preparation

V EXPERIMENTAL METHODOLOGY

V.1 Estimating parameters of V shaped notch

For a better understanding of events and processing in three point bending specimen the first task was to establish the parameters of the V shaped notch from cylindrical specimens. The different investigators used different shaped specimens in practice for Fracture Toughness tests. According to the "Suggested Methods for Fracture Toughness" of ISRM cylindrical specimens with established parameters of V shape must be used. The parameters of a V shape are related to the diameter's size (Appendix 2). So, for different diameters there will have different sizes of a V shape. In the present work all Fracture Toughness tests used specimen diameters of 53 mm for Quartzite and Norite, and 54 mm for Sandstone and Coal. The following chapters will establish centroid and moments of inertia of the V shaped cross section.

The V shaped cross section was divided into two parts, with form of triangle (at the bottom) and form of circular segment (at the top) and is symmetric with respect to the z axis. Then the moment of inertia of the cross-sectional area with respect to y axis is the sum of these two parts. The neutral axis passes through the centroid of the cross section. Then, the moment of inertia of the cross sectional area with respect to the y axis is

$$I = \int z^2 dA \qquad \text{(V.1)}$$

The normal stress in the specimen can be related to the bending moment from applied load from the expression for σ_y yielding

$$\sigma_y = \frac{Mz}{I} \qquad \text{(V.2)}$$

This equation shows that the stresses are proportional to the bending moment *M* and inversely to proportional to the moment of inertia. The normal stresses calculated from this formula are called bending stresses.

The maximum tensile and compressive stresses in the specimen occur at points located farthest from the neutral axis. Let c_1 and c_2 denote the distances from the neutral axis to the extreme elements in the positive and negative z directions, respectively (Figure V.1).

Then the maximum normal stresses are

$$\sigma_1 = \frac{Mc_1}{I} = \frac{M}{S_1} \qquad \text{(V.3)}$$

and

$$\sigma_2 = \frac{Mc_2}{I} = \frac{M}{S_2} \qquad \text{(V.4)}$$

in which

$$S_1 = \frac{I}{c_1} \wedge S_2 = \frac{I}{c_2} \qquad \text{(V.5)}$$

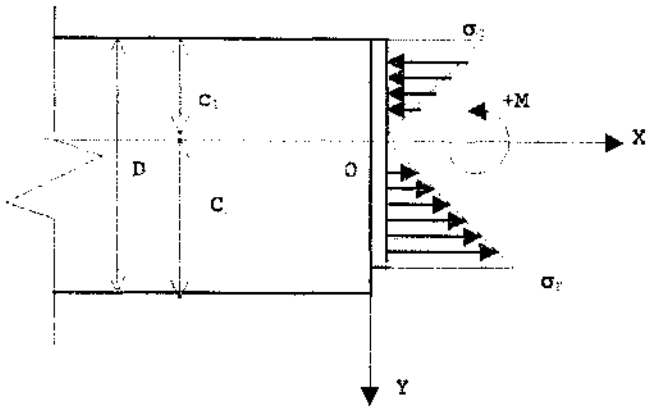

Figure V.1 Relationship between signs of bending moments and signs of normal stresses [39]

V.2 Determination of Tensile Stress

The other common feature of the Level I Fracture Toughness test is the ability to calculate tensile stress and determinate the tensile strength of specimens. The ap, lied cross section of the specimen was divided into two parts - triangle and circular segment (calculation of inertial moment of figure can be seen in Appendix 4).

The first task was to establish the physical parameters of the V shaped notch for a better understanding of events and processes in three point bending specimens from cylindrical specimens. The different investigators of fracture toughness used different types of specimen shapes. Cylindrical specimens with fixed parameters of the V shape must be used according to "Suggested Methods for Fracture Toughness" of ISRM. The parameters of the V shape depend on the size of the specimen's diameter (Appendix 2). Obviously, different diameters will give different sizes of V shapes. The centroid and moment of inertia of the cross section of V shaped specimens was established and can be seen in Appendix 4. The tensile stress of the specimen σ_T, is calculated by the following general formula:

$$\sigma_T = \frac{14{,}34.P}{D^2}$$

Where P is the load (N) and D is the diameter of the test specimen (m). The resultant tensile strength is in Pa.

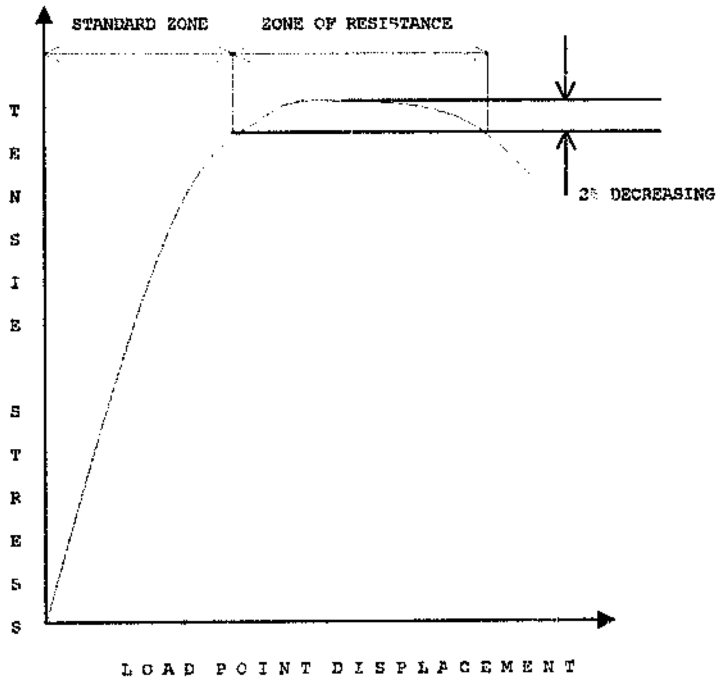

Figure V.2

Methodology for determination of "Peak Resistance zone".

The graphs created using the above equation can be divided into three parts. The first part is from the beginning of loading to the onset of yielding and consists of elastic behaviour. The second part is from the yielding point to the 2% offset before ultimate stress and includes plastic behaviour. The third part is from 2% offset before ultimate stress to its 2 % decrease in post-peak region (Figure V.2).

In the following Chapter VII.2 will be present a more detailed analysis of the tests regarding tensile strength under different loading rates.

V.3 **Establishing of J_{IC} value from J-integral studies**

The J-integral proposed by Rice as an analytical tool for elastic-plastic crack tip field analysis has been successfully used by Begley and Landes [33,34] as an elastic-plastic fracture criterion. The method developed by Rice [26] for measuring J on bend-type specimens offered the simplest single specimen technique for measuring J. For this technique a bend-type specimen is loaded to the distance of interest and J is determined as a function of displacement from the expression,

$$J = \frac{2A}{bB} \qquad (V.6)$$

where A is the area under the load-displacement curve taken at the displacement of interest, B is the thickness, and b is the uncracked ligament. Critical values of J were labelled J_{IC} and taken when crack extension was first encountered. This method for determining a critical J value was patterned after the K_{IC} measurement technique.

V.3.1 **Experimental procedure**

Specimens were tested in an MTS servo-controlled testing machine where loading displacement was controlled. Load vs CMOD and LPD was measured from clip-gauge and LVDT sensors and monitored on real time plots on the screen. Specimens were loaded to the desired axial LVDT displacement and then unloaded. This is shown schematically in Figure V.3.

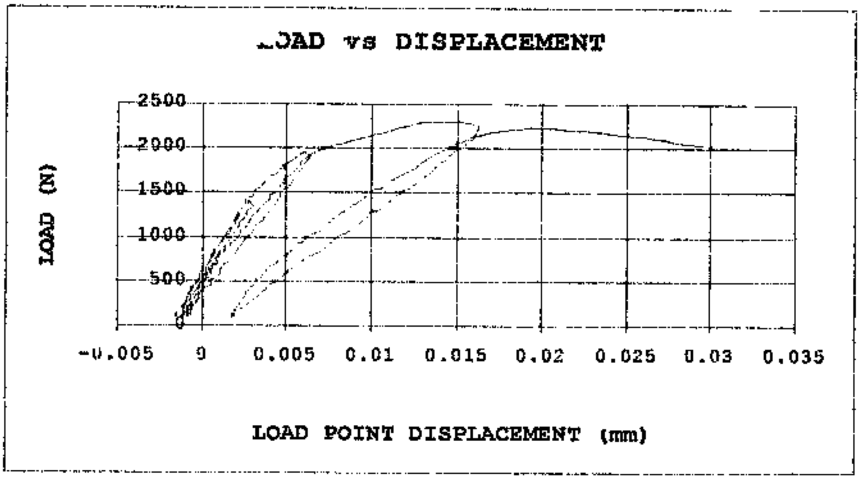

Figure V.3 Description of the graphical evaluation of J from Load vs LPD record

Specimens were subsequently cut after unloading, so that the fracture surface could be examined. The crack extension on the fracture surface was measured under a binocular microscope with magnification of x50. The specimens were loaded with the same loading rate under the same conditions. Crack extension was taken from the tip of a V shape to the end of the crack. Maximum extension generally occurred about mid-thickness.

V.3.2 **Analysis Techniques**

The data was analysed by plotting the value of J as a function of crack extension. During investigation a series of different methods were used for determining of J values, in order to choose the most appropriate value for different rock types. J should always be overestimated as a result of the area under the load displacement curve being overestimated. Consider the case where the non-linear part of the load displacement curve is caused only by crack extension (no plastic deformation), Figure V.4. The nonlinear curve has an original crack length of a_1. On loading to the point shown, assume that the crack extends to length a_2. The actual J value corresponding to the displacement shown at crack length a_2 should be a function of the area under the linear curve in equation V.6. The calculated value of J will correspond to the area under the nonlinear curve. The area between these two curves is a measure of the overestimate in J. Figure V.4 shows the same problem for the case with crack growth from a_3 to a_4, where nonlinearity is caused by the crack growth and plasticity. The curve on the left has the advancing crack and is originally steeper with more nonlinearity at the load. The curve at the right shows what the curve should be with no crack extension. Hence, the area under this corresponds to the actual J value, and the area between the curves corresponds to the overestimate in J.

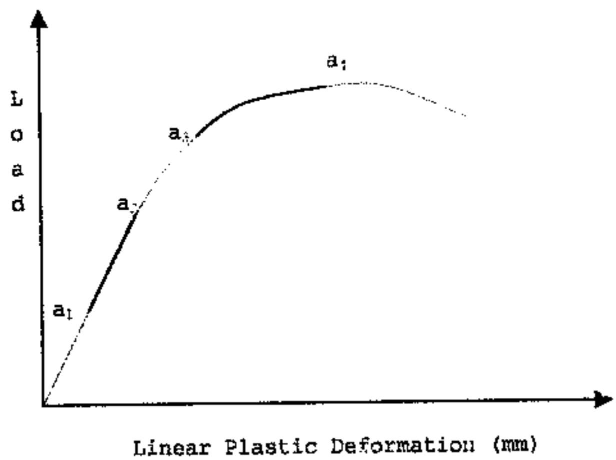

Figure V.4 Description of the crack growing [35]

The data were plotted in the form of an R-curve by plotting vs measured LPD.

VI CALCULATIONS

VI.1 Calculations for Fracture Toughness of the rock type tested

All calculations in this chapter are based on "Suggested Methods for Determining the Fracture Toughness of Rock" of ISRM (Commission on testing methods) [12].

VI.1.1 Calculation of loading rate

The displacement rate in displacement controlled testing, which is referred to as Level I and Level II, exceeds the following calculated limit value:

$$CMOD > 0.006\,K_{CB}/(E\sqrt{D})\,m/\sec \qquad \text{(VI.1)}$$

Here K_{CB} is the fracture toughness defined for Level I testing and E is the Young's modulus of the material. The prefactor 0.006 in above the equation has the dimensions *m/sec* since it contains the minimum required crack speed 0.001 *m/sec* as a factor. If it is more convenient to express CMOD or Axial LVDT in *mm/sec*, for example, then the prefactor 6.0 should be used instead.

VI.1.2 **Calculation of slope values**

The slope of a straight line, s, is defined as

$$s = \tan(\text{angle between line and CMOD axis}). \qquad (VI.2)$$

The initial tangent slope of the load vs CMOD record is the slope of a straight line through the origin at zero load which is tangent to the curve (Fig.VI.1b).

VI.1.3 **Calculation of Fracture Toughness**

For Level I testing, the fracture toughness of the specimen shall be calculated by the following formula:

$$K_{CB} = A_{min} F_{max} / D^{1.5} \qquad (VI.3)$$

where

$$A_{min} = [1.835 + 7.15 a_0/D + 9.85(a_0/D)^2] S/D \qquad (VI.4)$$

With the failure load, F_{max}, in kN and the specimen diameter, D, in cm the fracture toughness will be in Mpa$\sqrt{m}$ or $MN/m^{1.5}$. The factor A_{min} is dimensionless. A notch angle value within the tolerance limits must be less than 1% variation in the computed K_{CB} value.

VI.1.4. **Correction of fracture toughness for nonlinearity**

a) For Level II testing, the evaluation starts by calculating the fracture toughness as in 3 above. Then a nonlinearity correction factor shall be evaluated in the load vs CMOD record according to the graphical construction methods shown in figures.VI.1a-c.

b) Draw a straight line for each unloading-reloading cycle, in the sense specified below. Each line is defined by two points, H and L. The high point (H) is where CMOD starts to decrease on the unloading part of the cycle and the corresponding load is denoted by F_H (Fig.VI.1a). The low point (L) lies on the reloading part of the cycle and is defined by the load level:

$$F_L = 0.5 F_H \qquad \text{(VI.5)}$$

An initial straight line shall then be drawn through H and L.

c) The extent of hysteresis centred about F_L in the unloading-reloading cycle is defined by the vertical distance ΔF (Fig.VI.1a). The final straight line for each cycle shall then be obtained by translating the initial line vertically downwards by an amount 0.5 ΔF. It shall intersect the CMOD axis.

d) The slope of each final line is then computed. Find the two lines whose slope values most closely span the value:

$$s_c = [1.05 - 2.1\,a_0/D + 4.21(a_0/D)^2]\, s_{initial\text{-}tangent} \qquad \text{(VI.6)}$$

The po ˆ corresponding to the unloading slope s_c on the load vs CMOD curve is where the fracture toughness should be evaluated.

If the final linearized unloading lines do not span the evaluation point, further testing of specimens from the same sub-sample should be accompanied by more unloading-reloading cycles so that the final lines do span the evaluation point.

The evaluation point can still be obtained. Should it lie before the final lines, then the initial tangent line and the first final line shall be chosen as the two lines which span it and the calculations proceed accordingly. In this case F_e in equation (11) will be the interpolation between F_1' and F_2.

e) Thethese two chosen linearized unloading lines define the residual displacements in the unloaded state, δ_1 and δ_2, and the horizontal distance (Fig.VI.1b);

$$x_u = \delta_2 - \delta_1 \qquad \text{(VI.7)}$$

A smooth approximation of the load vs CMOD curve is drawn between these unloading lines, ignoring the unloading-reloading dips. Next find the intersection points between the unloading lines and the smoothed curve. Denote their loads by F_1 and F_2, the average load is found to be

$$F^* = (F_1 + F_2)/2 \qquad \text{(VI.8)}$$

If the unloading lines span F_{max}, then the greatest of F_1 and F_2 shell be replaced by F_{max}. Then draw a horizontal load line at this level (Fig.VI.1b). This defines displacements of two matching loaded states along the linearized unloaded lines. The difference between these displacements is designated x_1. Then let the displacement ratio

$$p = x_u / x_l \qquad \text{(VI.9)}$$

define the "degree of nonlinearity", p.

f) If the two chosen unloading lines span the evaluation point and if F* is not less than $0.98F_{max}$ then the nonlinearity corrected facture toughness value shall be calculated as

$$K^c_{CB} = \sqrt{[(1+p)/(1-p)]}\, K_{CB} \qquad \text{(VI.10)}$$

The superscript (c) denotes a corrected fracture toughness value.

g) If the two chosen unloading lines do not span the evaluation point, or if F* is less then $0.98F_{max}$, then by

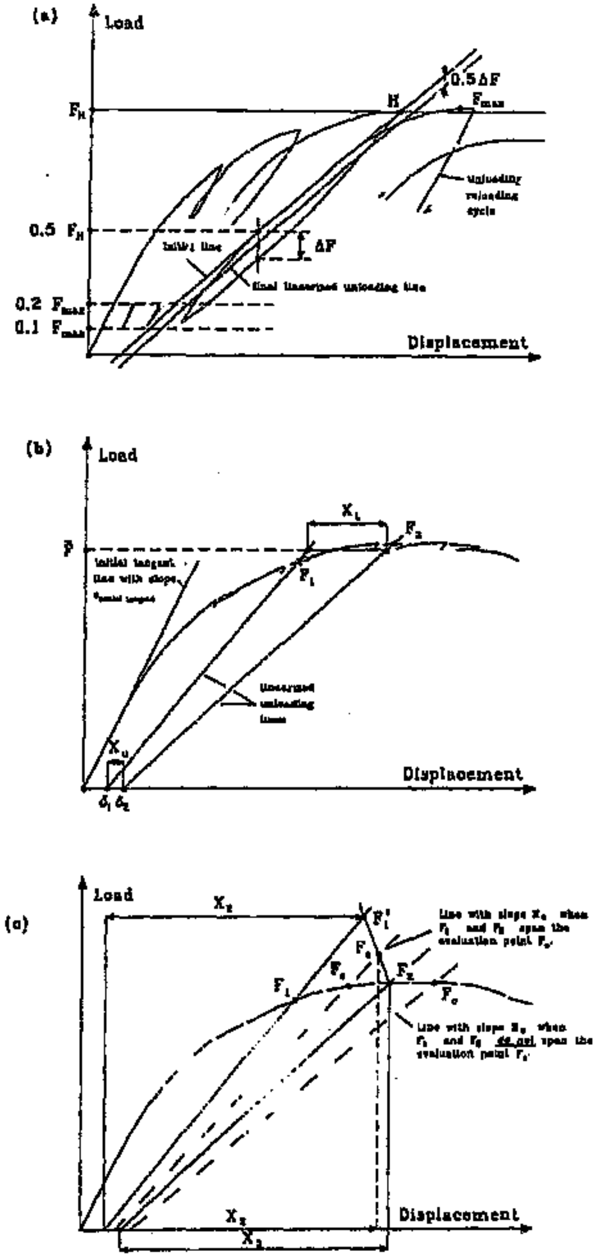

Figure VI.1

The principles of nonlinearity correction of either K_{ca} in load vs LPD record (Method I)

(a) Construction of linearized unloading line;

(b) Derivation of degree of nonlinearity, p;

(c) Derivation of load at evaluation point, F_c.

linear interpolation or extrapolation draw the unloading line with slope s_c. The procedure shall be based on a constant amount of recovered displacement (CMOD), i.e. the horizontal distance x_2 (Fig.VI.1c).

h) First, along the unloading line through F_1, find the point F_1' which has the same amount of displacement recovery upon unloading as an unloading from F_2 along the second unloading line, i.e. the amount x_2. Then draw a straight line through F_1' and F_2 and find the point on this line whose load is

$$F_e = s_c x_2, \qquad \text{(VI.11)}$$

Next draw a straight line through this point which leads to a recovered displacement x_2 upon unloading. Its slope will then by definition be s_c. Finally, find the load at the evaluation point, F_c , as the intersection between this line and calculated as

$$K^c_{CB} = \sqrt{(p+1)(p-1)}\, F_c / F_{max} K_{CB} \qquad \text{(VI.12)}$$

This correction of $_s$ does not require the material to be isotropic.

VI.1.5 **Calculation of additional quantities**

VI.1.5.1 **Calculation of Young's modulus**

If the initial tangent slope is known in absolute terms then the Young's modulus in bending of the specimen material, E, may be calculated by using the following equation

$$E = g_0 s_{initial\text{-}tangent} D \qquad \text{(VI.13)}$$

where

$$g_0 = 20.8 + 19.4 a_0 D + 142.3 (a_0 D)^2 \qquad \text{(VI.14)}$$

With $s_{initial\ tangent}$ given in kN/mm and D in mm the resulting Young's modulus value can will be in GPa which is the recommended unit. A support span variation within the tolerance limits will cause less than 2% variation in the computed E value.

VI.1.5.2 **Calculation of energy release rate**

If the Poisson's ratio of the specimen material, v, is also known, it is possible to convert the fracture toughness value in stress intensity terms, $MPa\sqrt{m}$ to crack extension resistance in terms of energy release rate:

$$G^c_{CB} = (1 - \nu^2)(K^c_{CB})^2 / E \qquad \text{(VI.15)}$$

The recommended unit of $G_{CB}{}^{c}$ is J/m^2. The ν-value is not essential. Since ν is less then 0.3 for most competent rock, it may either be guessed with sufficient accuracy or assumed to be zero if this is stated clearly.

VI.1.5.3 **Calculation of total work**

If the load vs CMOD recording is followed through until the specimen has virtually no residual strength, then the total work of fracture $W_{CB}{}^{f}$, which is required to separate

$$W^f_{CB} = \int_0^\infty F d(CMOD) \qquad \text{(VI.16)}$$

the notched specimen into two halves may be calculated as Relating $W_{CB}{}^{f}$ to the ligament area of the notched specimen, A, one then obtains the specific work of fracture :

$$R^* = W^f_{CB} / A. \qquad \text{(VI.17)}$$

The dimension of $R_{CB}{}^{*}$ is J/m^2 and its value should correlate closely with that of $G_{CB}{}^{c}$.

The (projected) ligament area of the chevron bend specimen is given by

$$A = 0.25[\arcsin\beta + \beta(1-2a_0/D)]D^2 \qquad \text{(VI.18)}$$

where

$$\beta = 0.5[1-2a_0/D+\sqrt{(1+4a_0/D-4(a_0/D)^2)}] \qquad \text{(VI.19)}$$

VI.2 **Calculations for J-integral**

Different approximate equations were developed to determine J from one load-displacement curve [35]. For compact specimens these equations are as follows.

1. Landes and Begley [34]:

$$J = \frac{2U}{Bb} \qquad \text{(VI.20)}$$

where:

U = deformation energy

Equation VI.20 can be rewritten into the form most often used to estimate the value of *J* for bend type specimens

$$J = \frac{2A}{Bb} \qquad \text{(VI.21)}$$

where A is the area under the load versus load point displacement curve.

A number of authors have reported that problems exist when using equation VI.21 for bend specimens.

Srawley [66] shows that there is a considerable difference when using the total energy as compared with the energy due to the presence of a crack. To further illustrate this point, the estimation equation VI.21 was compared with the strain energy release rate G_I in the elastic regime. In order to demonstrate this comparison, the constant 2 in equation VI.22 is replaced by the variable β. For a one-to-one comparison between J and G in the elastic region, β will be 2.0.

The values of β for three-point bend specimens with a span to width ratio of 4 are listed in Table 3 and are plotted in Figure 4 of "Evaluation on Estimation Procedures Used in J-integral Testing" [35].

2. Merkel and Corten simplified [36]:

Critical J-integral data were determined by the J-resistance curve technique [37] with the Merkel-Corten correction factors for the compact specimen geometry. Using guidelines recommended by ASTM on Elastic-Plastic

Fracture Mechanics Terminology, the J-integral data were reduced using

$$J = \alpha_1 \frac{2A}{Bb} + \alpha_2 \frac{2P\delta}{Bb} \qquad \text{(VI.22)}$$

where

α_1, α_2 = Merkel-Corten coefficients,

A = the area under the load vs load-line displacement curve,

B = thickness,

b = remaining ligament,

P = final load value, and

δ = final displacement value.

In the above equation, Merkel-Corten's coefficients are;

$$\alpha_1 = \frac{(1+\alpha)}{(1+\alpha^2)} - \frac{\alpha(1-2\alpha-\alpha^2)}{(1+\alpha^2)^2} \qquad \text{(VI.23)}$$

$$\alpha_2 = \frac{\alpha(1-2\alpha-\alpha^2)}{(1+\alpha^2)^2} \qquad \text{(VI.24)}$$

where

$$\alpha = 2\sqrt{(a/b)^2 + (a/b) + 0.5} - 2(a/b + 0.5)$$

where

a = crack length

b = uncracked ligament

To determinate the total work done on the specimen the actual area, A, under the load versus load-line displacement curve, was modified slightly to account for the energy stored at zero load due to crack closure. Since crack closure prevents a complete relaxation of stress from occurring, the actual area used is in the shaded area of Figure VI.3.

VI.3 **Defining of J_{Ic}**

The progress of fracture beginning from a sharp crack [71] is separable into four regimes: (1) crack-opening stretch or crack tip blunting by plastic flow at the crack tip, (2) crack growth initiation, (3) stable crack growth by material separation at the crack tip, and (4) unstable crack propagation. These four events determine the shape of the R-curve. Of these four regimes, crack tip blunting and stable crack extension predominate during the fracture process described by an R-curve. Crack initiation occurs over a short interval and unstable crack propagation usually begins at some point beyond where the useful R-curve terminates (Figure VI.2)

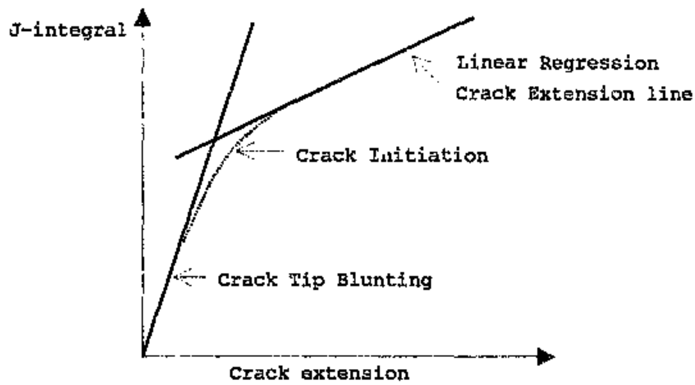

Figure VI.2

Schematic representation of crack extension

during the initiation regime

To establish a J_{IC} measurement point [38] it is desirable to pick a point where crack extension has taken place by actual material separation rather than by crack front geometry change. Under consideration is taken an absolute amount of crack extension but not a relative amount of crack extension as in the K_{IC} test. An obvious point would be where the curve from crack extension intersects the stretch zone line (blunting line) $J = 2\ \sigma_{flow}\ \Delta a$, which is linear function of applied stress and crack extension. This point has several drawbacks. At this point no actual crack extension due to material separation has occurred. Also the stretch zone may not develop strictly as a function of $J\ /\ \sigma_{flow}$, where

$$\sigma_{flow} = \frac{1}{2}(\sigma_y + \sigma_u) \qquad \text{(VI 26)}$$

Δa - crack extension

σ_{flow} - flow stress

σ_y - 0.2 percent offset yield stress

σ_u - ultimate stress

The J_{IC} measurement point will be where a best fit line to the crack extension points intersects the line $J = 2 \sigma_{flow} \Delta a$. Using this technique J_{IC} will be calculated for each specimen.

1. Calculate J values from the load versus LPD using $J = 2A/bB$, where A is the area under the curve up to the point of unloading (Fig.VI.3a), b is the uncracked ligament measured from the end of the fatigue crack and B is specimen thickness. In measuring the area under the curve do not subtract out the area due to elastic unloading. The right-hand side of the area measured should be a vertical line at the unloading displacement.

2. Plot J versus crack extension, Fig.VI.3c.

3. Construct the line $J = 2 \sigma_{flow} \Delta a$ (Fig.3c) as calculated above (Equation VI.26).

4. Draw best fit line to the J versus crack extension points, Fig.VI.3c. Include only the points where actual crack extension appears. As a stretch zone the points should fall along the line $J = 2 \sigma_{flow} \Delta a$.

5. Mark J_{IC} at the intersection of the lines constructed

in Steps 3 and 4, Fig.VI.3c.

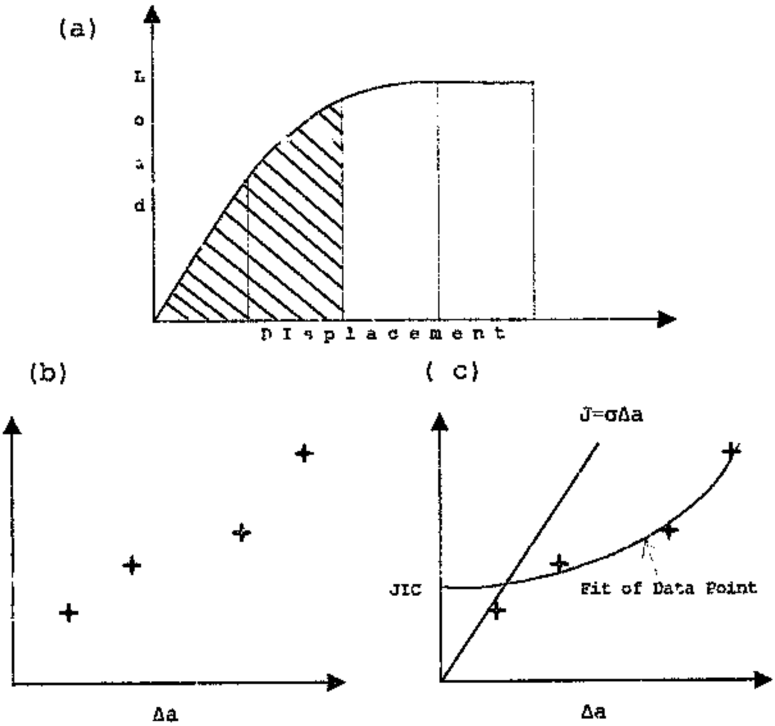

Figure VI.3 Procedure for JIC measurement

(a)Load specimens to various displacements, (b)Calculate J for each specimen and plot area vs a, (c)Construct two curves for JIC measurement.

When linear elastic behaviour predominates, J_{IC} is

$$J_{IC} = \frac{(1-\nu^2)}{E} K_R^2 \qquad \text{(VI.27)}$$

or

$$K_{IC} = \sqrt{\frac{J_{IC} E}{1 - \nu^2}} \qquad \text{(VI.28)}$$

With this mind, (equation VI.28) values will present in table for comparison with average K_{IC} values from the compact specimen. Stress intensity factor will be calculated with following equation proposed by R. Singh and B. Whittaker [32].

$$K_I = 1.12\sigma\sqrt{\pi a} \qquad \text{(VI.29)}$$

A single value of J_{IC} was determined for each specimen from a curve such as Fig.VI.3c.

VII **RESULTS**

VII.1 **Tests for Fracture Toughness**

The tested specimens were of diameter 53 mm and length 212 mm for quartzite and norite and of diameter 54 mm and length 216 mm for coal and sandstone. The V shaped notch was 7.9 mm deep and 1 mm wide.

VII.1.1 **Quartzite**

The Level I Fracture Toughness tests were run under loading rate 0.01, 0.005 and 0.001 mm/sec and reached loads were between 2250 and 2170 N. Average maximum load F_{max} was calculated to be equal of 2208 N with standard deviation of 28.56. The corresponding duration of failing for these loading rates were between 13 and 119 sec. A loading rate of 0.01 mm/sec was chosen for Quartzite specimens.

A test template was used with a final value of 100 N during the Level I tests, as the specimens failed between 2250 and 2170 N. The limit load was set to 50 N to prevent specimens from fracturing. The initial tangents had values between 7.906E+04 N/mm (for specimen Q3L1) and 6.766E+04 N/mm (for specimen Q1L1). The Young's modulus was calculated on this basis, and were between 40.5 GPa and 52.2 GPa. Average level I fracture toughness coefficient of K_{CB}=1.886 MPa$\sqrt{m}$ was calculated.

The axial displacement for the level II fracture toughness tests were 0.023, 0.046, 0.069, 0.092, 0.115,

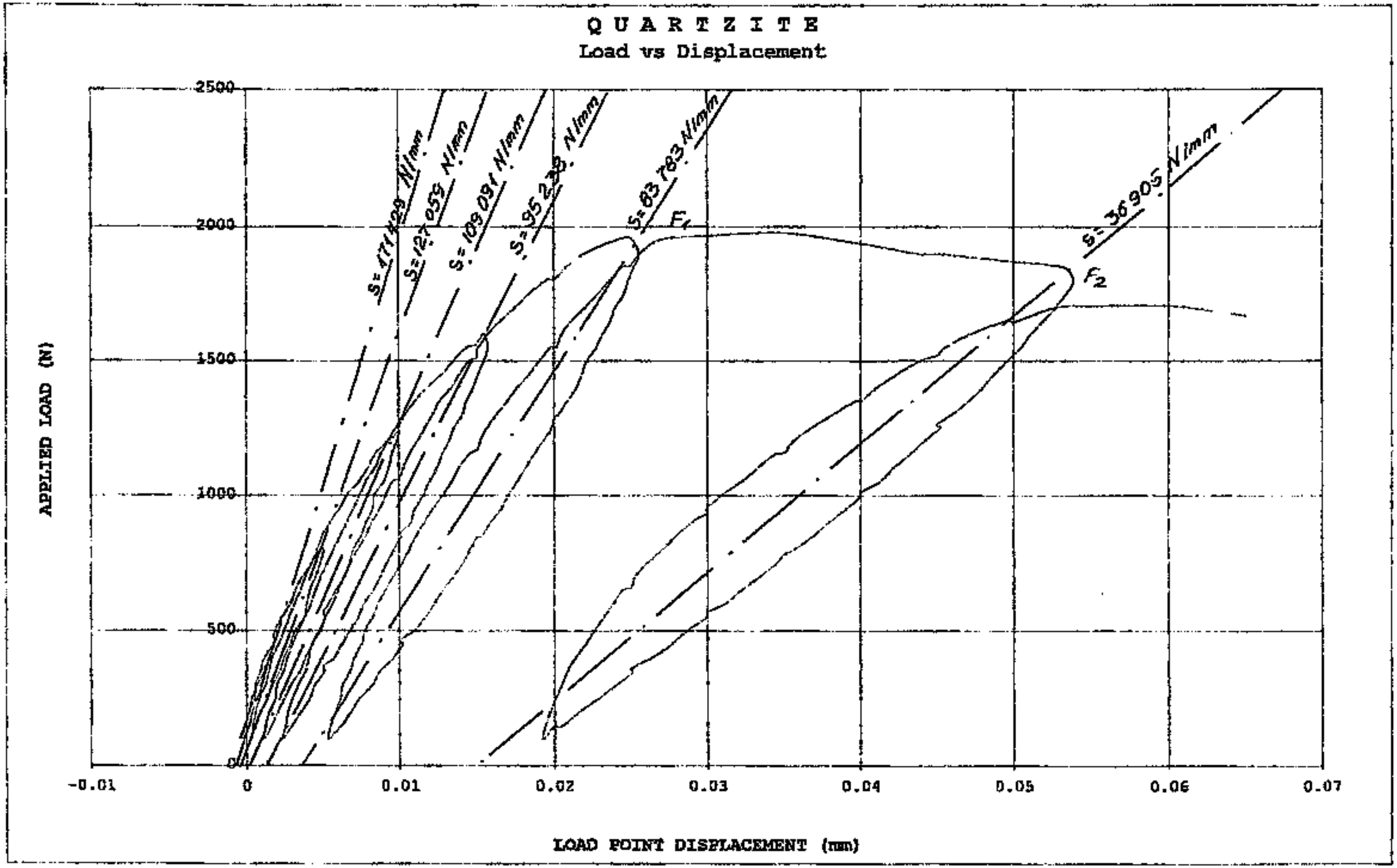

Figure VII.1

Load vs LPD displacement record of specimen Q3L2

0.138 mm. The final displacement was 0.161 mm. The loading rate was 0.001 mm/sec. The maximum load reached was between 1800 and 2018 N (from specimens Q5L2 and Q2L2) giving a stress intensity factor between 2.09 and 2.52 MPa/m. The duration of the tests were between 409 and 730 sec. The initial tangents values obtained from the tests were between 1.01E+05 N/mm and 8.52E+04 N/mm. The calculated displacement ratio was between 0.14 and 0.18. The calculated values of fracture toughness coefficients can be seen in Table.1, Appendix 3.

Quartzite Level II fracture toughness tests remained elastic during first or second cycles (load between 600 and 800 N and stress intensity factor of 0.678 MPa$\sqrt{m}$, which is 30% - 35% from maximum load). Calculated slope values s_c (average s_c = 7.71E+04 with standard deviation of 0.93) were between the lines of the fourth and the fifth cycles. Some of the fracture toughness coefficients, calculated from the Level II tests, were when the differences between the peak loads of the cycles enclosing the s_c line were within 98% from the maximum loads (for example specimen Q3L2, Fig. VII.1). The fracturing began when the applied load was about 200 N. From this load Quartzite began to lose its elasticity and plastic behaviour started appearing.

The estimated average fracture toughness coefficients are with standard deviation of 0.043 and average Young's modulus values (standard deviation of 2.73 for Quartzite specimens are as follows:

Fracture Toughness K_{Ic} (MPa$\sqrt{m}$): 2.20

Young's Modulus E (GPa): 49.63

All other calculated values are shown in Table 1 (a and b), Appendix 3.

VII.1.2 **Norite**

The Level I Fracture Toughness tests were run under a loading rate of 0.01, 0.005 and 0.001 mm/sec and reached loads from 2200 N to 2721 N (specimens N3L1 and N5L1). The stress intensity factor was 2.34 MPa$\sqrt{m}$. The times of failure of specimens under the above loading rates in seconds were between 5 and 10 sec. A loading rate of 0.01 mm/sec was chosen for Norite specimens. The load limit in the test template was 50 N.

The Level I test template used a final value of 100 N. The initial tangents had values between 1.598E+05 N/mm (spec. N4L1) and 1.672E+05 N/mm (spec. N5L1). The calculated average maximum load of failing F_{max} was 2310 N with standard deviation of 78.17. Level I fracture toughness coefficient of K_{CB}=1.974 MPa$\sqrt{m}$ was calculated.

The axial loading displacements were determined on the basis of the results from Level I tests. The final values, estimated for each loading cycle, were as follows: 0.02, 0.04, 0.06, 0.08, 0.10, 0.12, 0.14 mm. The loading rate was 0.001 mm/sec. The maximum loads reached were between 2150 N and 2450 with stress intensity factor of 2.35 MPa$\sqrt{m}$ and initial tangents s_{it} between 1.73E+05 and 1.92E+05 N/mm.

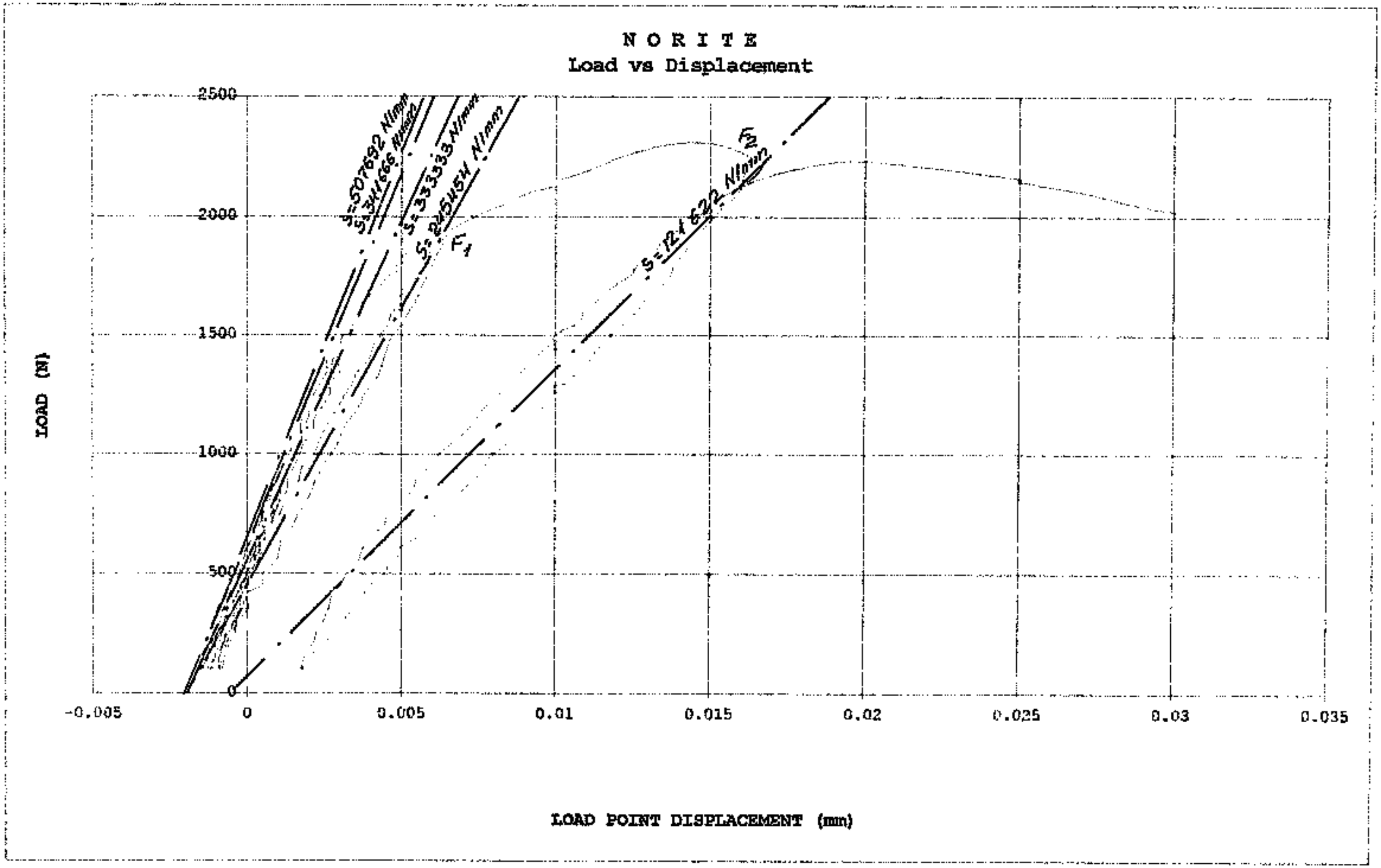

Figure VII.2

Load vs LPD displacement record of specimen N7I.2

The first two or three cycles (for which the load was about 1250 N), all Norite Level II tests are very close to the initial tangent. From these loads Norite began to lose its elasticity and started to show plastic behaviour.

The slope of each final line was calculated and two lines were found. The slope with average value of s_c = 1.53E+05 N/m (standard deviation of 0.066) was calculated. Slope values were between the lines of the fifth and the sixth cycles around the maximum load. Calculated load F_c is beyond maximum load F_{max}, which can be seen from Figure VII.2. Equation VI.12 was used to calculate Fracture Toughness values, which can be seen in Table.2, Appendix 3.

The estimated average fracture toughness coefficient was with standard deviation of 0.094 and average Young's modulus values (standard deviation of 3.05) for Norite are as follows:

Fracture Toughness K_{Ic} ($MPa\sqrt{m}$): 2.29
Young's Modulus E (GPa): 93.31

All other calculated values can be seen in Table.2, Appendix 3.

VII.1.3 **Sandstone**

The Level I Fracture Toughness tests for Sandstone were run under a loading rate of 0.02 mm/sec and reached load 1000 N or stress intensity factor of 0.56 MPa$\sqrt{m}$ (the other results of sandstone Level I tests are given in the chapter on tension stress analyses). The times of failing on rocks were between 6 to 10 sec. Level I test template used a final value of 40 N, because the specimen failed under a maximum load of 1000 N and the limit load was 40 N. The initial tangent had a value of 2.699E+04 N/mm. Calculated average maximum load of failing for level I fracture toughness tests was F_{max}=990 N with standar deviation of 41.83. Fracture toughness coefficient which was calculated, had value of K_{CB}=1.40 MPa$\sqrt{m}$.

Level II Fracture Toughness tests had following axial displacements for each loading cycles: 0.026, 0.052, 0.078, 0.104, 0.130, 0.156 mm and a final loading 0.182 mm. The loading rate was 0.001 mm/sec. Maximum loads between 684 N (spec. SST5l2) and 918 N (spec. SST7L2) were reached. Duration of the tests was between 319 sec (spec. SST5L2) and 543 sec (spec. SST7L2) with stress intensity factor of 1.62 MPa$\sqrt{m}$. Initial tangents on tests were between 7.82E+04 N/mm (spec. SST5L2) and 8.42E+04 N/mm (spec. SST6L2) with Young's modulus between 39.71 GPa and 42.75 GPa (average E = 41.06 GPa with standard deviation of 1.36). The displacement ratio was 0.1.

Sandstone fracture toughness tests kept elasticity during the first and second cycles. The calculated slope value, s_c (average s_c = 6.72 N/mm with standard deviation of 0.24) gave the most span lines between the first and

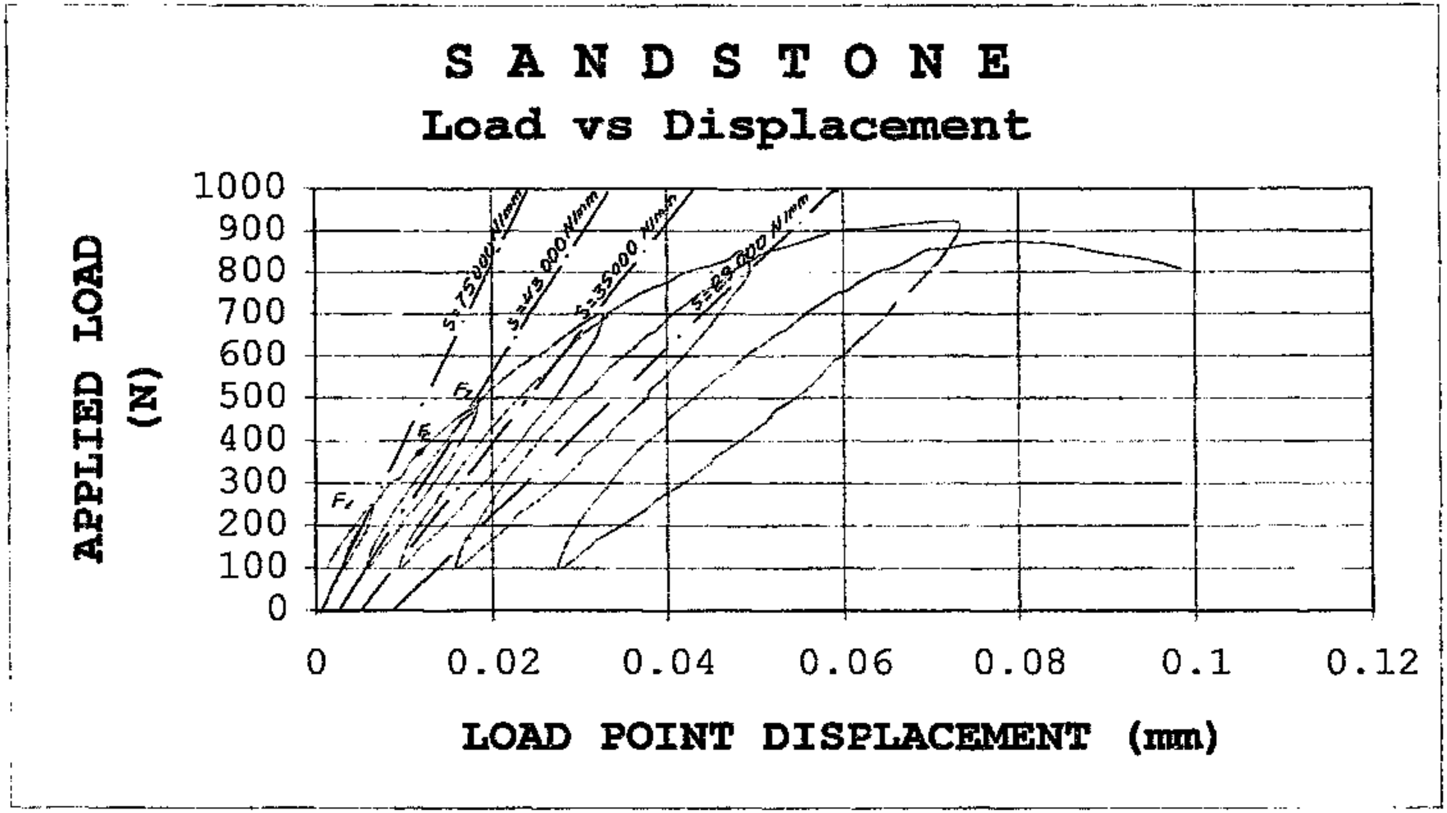

Figure VII.3

Load vs LPD displacement record of specimen SST7L2 second loading. For calculations, equation VI.12 was used because F_c appeared to be between the maximum values of first and second cycles (Fig.VII.3). The fracturing began at an applied load about 200 N. From this load Sandstone began to lose its elasticity and started appearing to behave plastically.

The estimated average fracture toughness with standard deviation of 0.037 and Young's modulus values for Sandstone are as follow:

Fracture Toughness K_{IC} ($MPa\sqrt{m}$):	0.34
Young's Modulus E (GPa):	41.06

All other calculated values can be seen in Table 3, Appendix 3.

VII.1.4 **Coal**

Fracture Toughness Level I tests were run under a loading rate of 0.015 mm/sec. and reached loads of 121 N - 150 N. The times of failure of the specimens were between 8 and 10 sec. The load limit pod in the template was fixed at 20 N and a final value of 40 N. These values were chosen mainly for two reasons. The first was on the basis of structural cracks in the specimens. The other reason was the maximum load of failing (about 140 N).

Axial loading displacements for level II tests were determined on the basis of results from the Level I test. The final values were estimated for each loading cycle, which were as follows in mm: 0.035, 0.070, 0.105, 0.140,

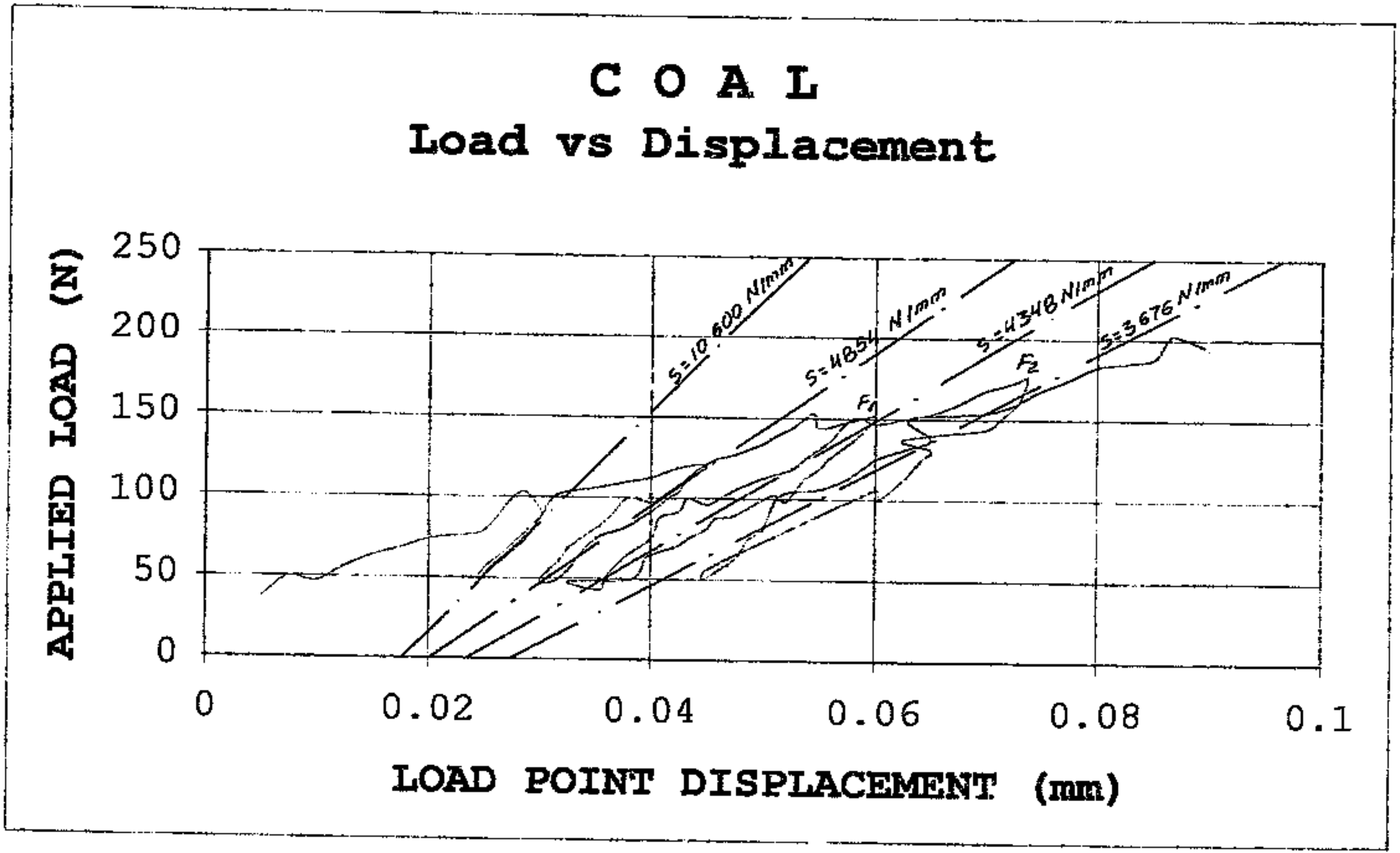

Figure VII.4

Load vs LPD displacement record of specimen C2L2

0.175, 0.210 and a final loading of 0.245. The loading rate was 0.001 mm/sec and maximum loads were reached at 170 N (spec. C3L2), 175 N for specimen C2L2 (Fig.VII.4) and 202 N (spec. C1L2). Tests duration were between 338 sec and 433 sec and displacement ratios were between 0.27 and 0.30.

Initial tangents values were between 2.44E+04 N/mm and 2.56E+04 N/mm. Fracture toughness coefficients were calculated at between 0.134 MPa/m and 0.150 MPa/m with standard deviation of 0.007 and average Young's modulus of E = 2.72 GPa with standard deviation of 0.26.

The slope values were calculated for each loading-unloading cycle. Calculated slope value s_c mostly span lines between the third and fourth loading cycles and have average value of s_c=7.98E+04 N/mm with standard deviation of 1.231. The methodology applied for the calculation of fracture toughness was the same as for sandstone, shown above.

The estimated average Fracture Toughness and Young's modulus values for Coal are as follows:

Fracture Toughness K_{Ic} (MPa/m): 0.143
Young's Modulus (GPa): 2.72

All other calculated values can be seen in Table.4, Appendix 3.

VII.1.5 **Fractography**

The fracture surfaces were studied using a Nikon shine microscope. Selected photos can be seen in Appendix 6. There appear to be big differences between fatigue crack growth of the investigated brittle rocks (Quartzite and Norite) and Sandstone, which will be discussed in this chapter. The fatigue region shows more evidence of intergranular cracking and grain pull-out, and the quartz grains appear dulled, possibly by crack working.

VII 1.5.1 **Fracturing in Quartzite**

Fracturing in Quartzite specimens begins with individual cracks at the tip of the V shape (Appendix 6, Pictures Q-1,2). A common feature is the position of the main crack. It begins from one of the sides of the V shape tip, where the concentration of the stress has the largest value. The fracture propagation has a split form in this zone. Fractures with straight linear forms, according direction of mine crack, can be observed.

In general, the main crack maintains a straight direction in the curve of the specimen. The crack, which can be seen on pictures Q-3 to 11, occurs throughout the boundary of the quartz grains. This crack creates secondary fracturing (as a result of the tensile stress) to a different degree in quartz grains.

For example, in picture Q-5 the crack comes from the top through the boundary of the grains and joins the tip of the grain at the centre of the picture. Then it splits again and joins when passing the grain.

Table VII.1

Picture No:	Description and angle of secondary fracturing
Q-3	30°,parallel - grain in top left part of the picture; 45° - grain in central right part of the picture.
Q-4	45° - grain in middle top part of the picture; 45°,90° - grain in central part of the picture.
Q-5	45° - grain in top left side of the crack; 30° - grain in top right side of the crack.
Q-6	45° - crack in top part of the picture; 90°,45° - crack in central part of the picture; 45° - crack in bottom part of the picture.
Q-7	30°,45° - crack in central part of the picture.
Q-8	30°,45° - grain in left side of the crack; 45°,90° - grain in right side of the crack.
Q-9	45° - grain in middle right part of the picture.
Q-10	45° - grain in right side of the crack.
Q-11	45° - grain in top part of the picture; 35°,40° - grain in central part of the picture.
Q-12	70° - grain in top part of the picture; 45° - grain in central part of the picture.
Q-13	45°,90° - grain in right part of the picture.
Q-14	45°,90° - grain in bottom half of the picture.

In picture Q-6 it can be seen that the crack comes from the top of the picture, in the centre it turns left around the other grain and continues in the previous direction. In the bottom left side of the picture it can be seen to be in the process of meeting on the grain. The reaction is passed on to this grain, first right, then left and in the end through the grain. This can be estimated on the basis of the contrast of colours. In the picture Q-11, the main crack comes from the top, and goes inside of grain. Then it jumps to the right and continues through the boundary of the quartz. This behaviour can be seen in picture Q-14 as well. Here the crack comes from the top, goes inside the quartz breaking up the corner of the grain, jumps to the right and continues through the boundary of grain. The angles of secondary fracturing of quartz grains are given in Table VII.1. The main crack can be seen in pictures Q-12 to 14 going through the grains of quartz. In this case, the crack also creates secondary fracturing and the angles of secondary fracturing of quartz grains are given in Table VII.1.

VII.1.5.2 **Fracturing in Norite**

Fracturing in Norite specimens begins with a clear fracture processing zone (Appendix 6, Pictures N-1,2). The fracture propagation has a chaotic distribution in this zone. Fractures with circular and linear forms according to the direction of main crack can be observed.

This zone exists around the whole tip of the V shape and creates two cracks, which go in the core of specimen.

In general, the crack does not keep a straight direction in the core of specimen. The main crack, which can be seen in pictures N-3 to 8, runs throughout the boundary of the grains. This crack creates secondary fracturing (as a result of the tensile stress) to a different degree in the quartz grains. The angles of secondary fracturing of quartz grains are given in Table VII.2.

Table VII.2

Picture No:	Description and angle of secondary fracturing
N-3	20^0 - grain in middle top part of the picture; 40^0 and 60^0 - grain in middle part of the picture.
N-4	60^0 - grain in top left part of the picture; 90^0 - grain in middle right side of the picture; 80^0 - grain in bottom left half of the picture.
N-5	80^0 90^0 - grain in top left corner of the picture; 60^0 - grain in centre of the picture.
N-6	60^0 - grains in top and bottom left parts of the picture; 90^0 and parallel - grain in right side of the picture.
N-7	80^0,90^0 - grain in middle left part of the picture; 90^0,parallel - grain in central part of the picture; 80^0 - grain in bottom left part of the picture.
N-8	90^0 - grain in top half of the picture; 80^0,parallel - grain in central and bottom part of the picture.
N-9	80^0 - grain in top half of the picture; parallel - grain in bottom left of the picture.
N-10	90^0,parallel - grain in bottom left part of the picture.
N-11	80^0 - grain in top half of the picture; 60^0 - grain in bottom half of the picture.
N-12	80^0 - grain in middle right of the picture.

The main crack, which can be seen on pictures N-9 to 12, runs throughout the grains of quartz. In this case, the crack also creates secondary fracturing and the angles of secondary fracturing of quartz grains are given in Table VII.2.

VII.1.5.3 **Fracturing in Sandstone**

Fracturing in Sandstone begins with a fracture process zo. , but to determine this is very difficult, because Sandstone is a sedimentary rock and connection between the grains is very slight. This zone can be seen in pictures S-1 and 2. The fracture propagation starts from there as bundle. This can be seen in pictures S-3 to S-6 (Appendix 6).

VII.2 **Estimation of Tensile Stress**

One of the difficulties in comparing the results from each rock type is the difference between the slopes of the initial tangents. This results coming from differences in the distribution of grains, their size and formation of micro cracks in specimens. To eliminate this the length of LPD from the beginning of loading till 2% offset before load of failing was used. As a comparison, a length of LPD from the 2% offset befor tensile strength until 2 % decrease of tensile stress after peak, which can be named "peak resistance zone" was used.

The value of 2% was chosen because the tensile stress is a linear function of the load. This tensile stress reached the maximum value in the Level I tests (Norite specimens) of about 2500 N - 2700 N. The test template recorded load values on every 50 N, which is about 2 % from load of failing.

VII.2.1 **Quartzite**

The tensile strength of quartzite specimens was estimated after using three different loading rates, as shown in Figure VII.5. The first loading rate was 0.01 mm/sec, where a value of loading was suggested by ISRM that failing must occur within 10 sec and the necessary crack velocity of 0.001 m/sec. The other loading rates were 0.005 and 0.001 mm/sec.

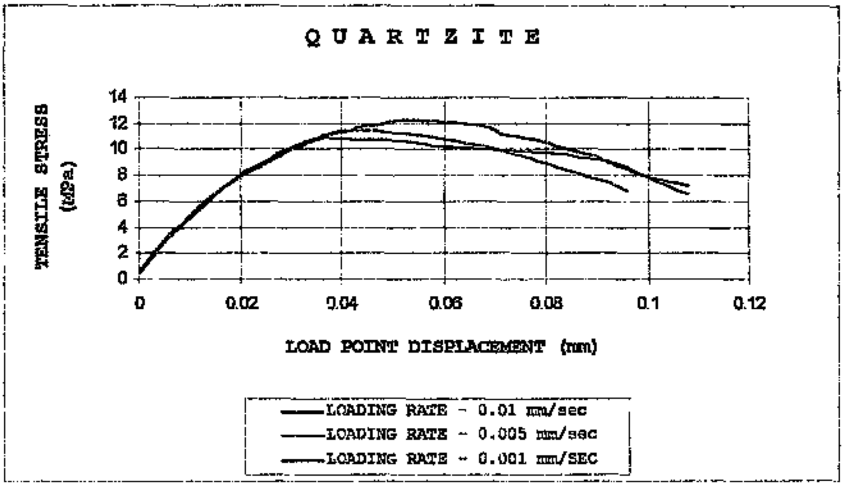

Figure VII.5
Estimating of Tensile stress on Quartzite specimens

The first part of a graph for each loading rate is a straight line, where specimens keep elasticity. From this part yield stress can be defined, which is about 5 MPa (42% from tensile strength). Differences between the graph with a loading rate of 0.01 mm/sec (which was taken as standard) and others in this part are from +14 % to - 11 %. This can be seen on Figure VII.6. This event results from the grains in the tip of a V shape, where fracturing starts. The differences decrease after initial loading. For the LPD value of 0.01 mm and tensile stress of 5.2 MPa (which is yield tensile stress), the differences between the specimens under different loading rates are between -2 and -5%. From this point, the tensile stress starts to curve. The differences of the values in plastic behaviour of specimens were within 0 to -2 %. The ultimate tensile stress (tensile strength) was calculated at the load of failure (Fig.VII.5 and Fig.VII.6). The differences increase in value around the failure load till 13 to 16%. The determined tensile strength was between 10.7 MPa and 12.2 MPa (average 11.56 MPa), calculated from the above formula. These values were compared with the results from the Brazilian disk tests. The results received for tensile strength have average value of 11.45 GPa, which has of 1 % difference.

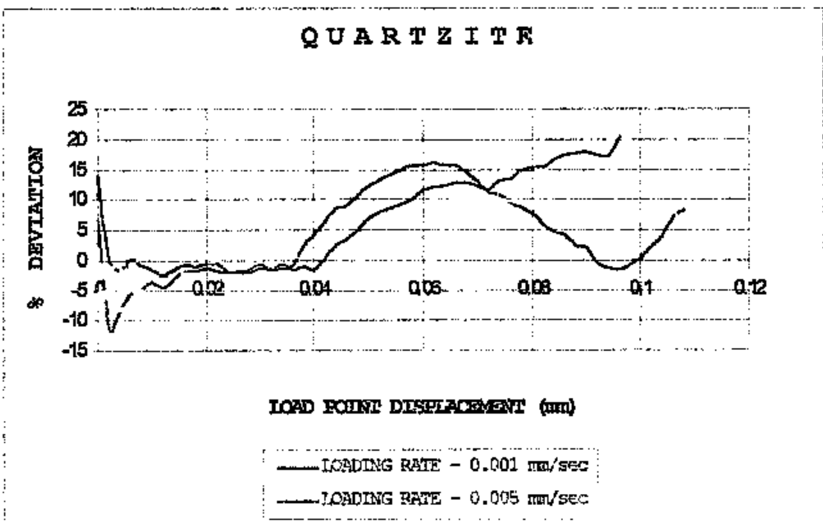

Figure VII.6

Tensile stress deviation from stress in test with loading rate 0.01 mm/sec

The "peak resistance zones" show different behaviour under the different loading rates. The LPD standard values for different loading rates are as follows:

Loading rate 0.010 mm/sec - LPD 0.0481 mm
Loading rate 0.005 mm/sec - LPD 0.0378 mm
Loading rate 0.001 mm/sec - LPD 0.0334 mm

The specimen, which was loaded with a loadi _ te 0.01 mm/sec, has a resistance zone with length 1..6E-02 mm (32.5% from a standard). After this with increasing LPD, tensile stress reduces. The specimen, under a loading rate of 0.005 mm/sec, has a resistance zone with length of about 1.41E-02 mm (37.2% from a standard) before failing. The specimen, under a loading rate of 0.001 mm/sec has resistance zone with length of about 1.34E-02 mm (40.2% from a standard) before dropping down.

VII.2.2 **Norite**

The tensile strength of Norite specimens was estimated after using four different loading rates, as shown in Figure VII.7. The first loading rate was 0.01 mm/sec, where the value of loading was as suggested by ISRM so that failure occurs within 10 sec and crack velocity is 0.001 m/sec. The other rates were 0.015, 0.005 and 0.001 mm/sec. For easier analysis, the average results from loading rates 0.01, 0.005 and 0.001 mm/sec were plotted on Figure VII.8. The graphs with loading rate of 0.015 and the last with loading rate of 0.005 mm/sec are excluded from the analysis because the first has too high

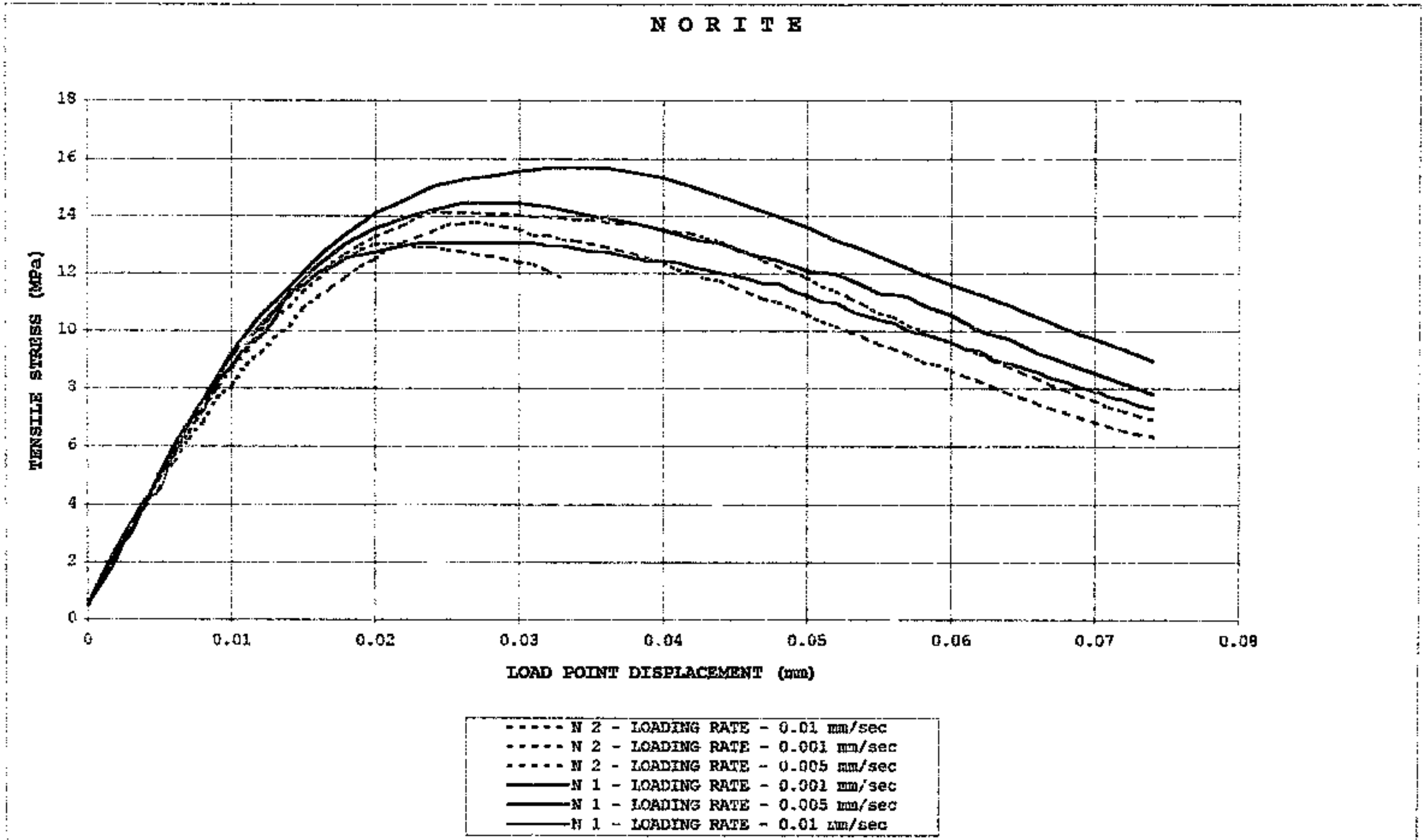

Figure VII.7

Estimating on tensile stress of Norite specimens under different loading rates a loading rate and the second has preliminary loading till 400 N. This is the reason for the low value of tensile strength and the long resistance zone.

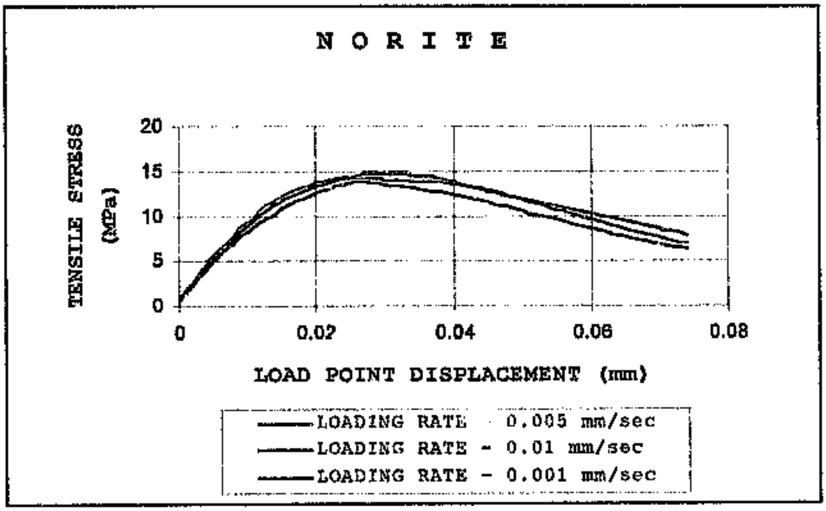

Figure VII.8
Estimating of Tensile stress on Norite specimens

The first part of the graph for each loading rate is a straight line, where specimens maintain elastic behaviour. Yield stress can be defined, which is about 7 MPa (50% from tensile strength). The difference between the graph with loading rate 0.01 mm/sec (which I take as standard) and others in this part is from -5 % to -9 %. This can be seen in Figure VII.9. The differences decreased in value until 0 to 14 % after initial loading. The differences between specimens under loading rates 0.005 mm/sec and 0.001 mm/sec are between 7% and 2% in the value of LPD - 0.01 mm and tensile stress 7 MPa (which can be defined as yield tensile stress). From this point, the tensile stress starts to curve, which maintains the same tendency even post peak. The differences were within 2% and 7% between the values under different loading rates (Fig.VII.8 and Fig.VII.9). The peak values of tensile stress (tensile strength), calculated from the above formula, were between 13.82 MPa and 14.43 MPa (average 14.13 MPa). These values were compared with results from the Brazilian disk tests. The results received for tensile strength from this test had an average value of 13.44 GPa, which is a 4% difference.

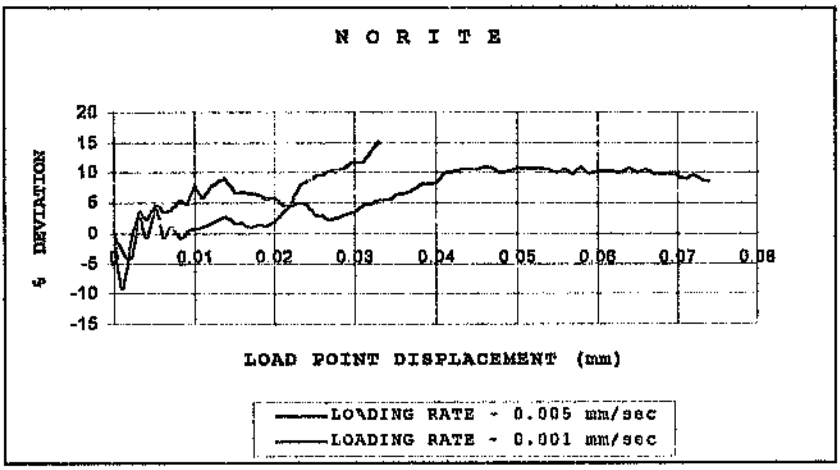

Figure VII.9
Tensile stress deviation from stress in test with loading rate 0.01 mm/sec

The peak tensile stress shows different behaviour under the different loading rates. The LPD standard values of series one and two (two kind of sandstone blocks) for different loading rates are as follows:

Series - 1

Loading rate 0.010 mm/sec - LPD 0.0273 mm

Loading rate 0.005 mm/sec - LPD 0.0238 mm

Loading rate 0.001 mm/sec - LPD 0.0216 mm

Series - 2

Loading rate 0.010 mm/sec - LPD 0.0238 mm

Loading rate 0.005 mm/sec - LPD 0.0229 mm

Loading rate 0.001 mm/sec - LPD 0.0197 mm

The specimens, which were loaded with loading rate 0.01 mm/sec, have resistance zone with a length of Series 1 - 1.3E-02 mm (48.1% from a standard) and 1.1E-02 mm (47.8% from a standard) of Series - 2. After this with increasing LPD, tensile stress decreases. The specimens under a loading rate 0.005 mm/sec, have a resistance zone of Series - 1 with length of 1.1E-02 mm (47.8% from a standard) and 8.6E-03 mm (39.1% from a standard) of Series - 2, before failing. The specimens, under a loading rate of 0.001 mm/sec, have a resistance zone of Series - 1 with length of about 9.25E-03 mm (42.9% from a standard) and Series - 2 of 6.36E-03 mm (33.5% from a standard) before decreasing.

VII.2.3 **Sandstone**

The tensile strength of sandstone specimens were estimated after using three diffelent kinds of sandstone. The loading rates and graphs are shown in Figure VII.10, where they are marked with numbers 1, 2 and 3. The loading rate of sandstone No 1 was 0.02 mm/sec, where a

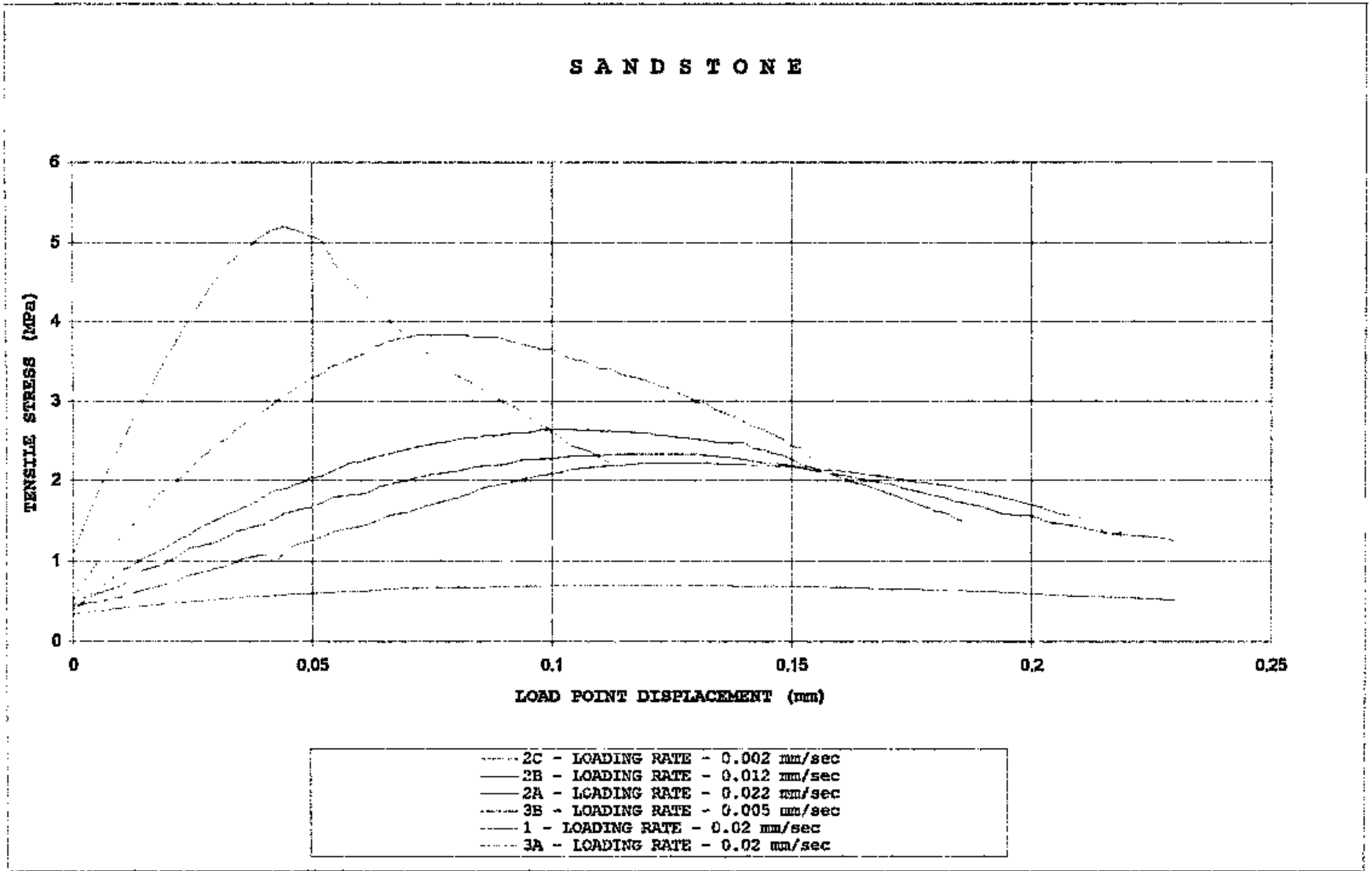

Figure VII.10

Estimating on tensile stress of Sandstone specimens under different loading rates value of loading is as suggested by ISRM so that failure occurs within 10 sec and crack velocity is 0.001 m/sec. For sandstone No 2, loading rates 0.022, 0.012 and 0.002 mm/sec (Fig.VII.10) were applied. For sandstone No 3 loading rates of 0.02 and 0.005 mm/sec (Fig.VII.10) were used. The results from rock No 2 (Figure VII.11) were used for analysing the sandstone tensile stress.

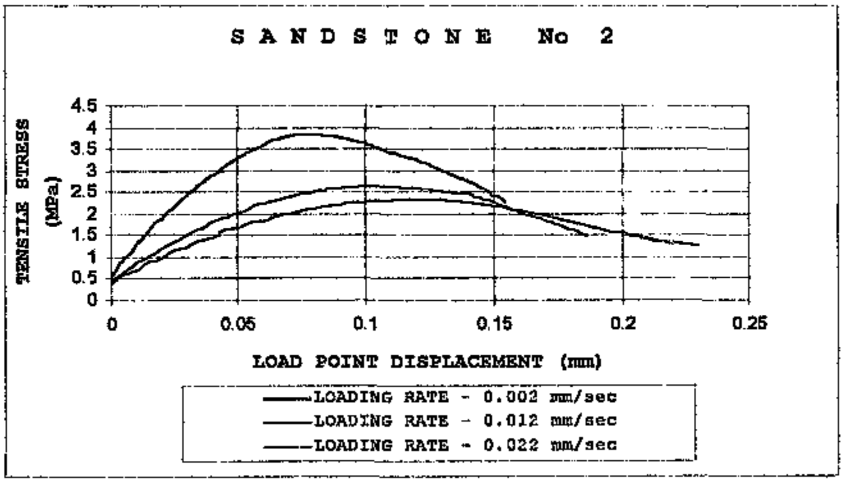

Figure VII.11
Estimating of Tensile stress on Sandstone specimens

The first part of the graph for each loading rate is a straight line, with specimens maintaining their elastic behaviour. Yield stress can be defined, which is about 1.75 MPa (40% from tensile strength) for a loading rate of 0.002 mm/sec and about 1 MPa for loading rates of 0.012 and 0.022 mm/sec. The differences between the graph with loading rate 0.022 mm/sec (which is taken as standard) and others in this part were from -20 % for loading rate 0.012 mm/sec to -95 % for loading rate 0.002 mm/sec. This can be seen in Figure VII.12.

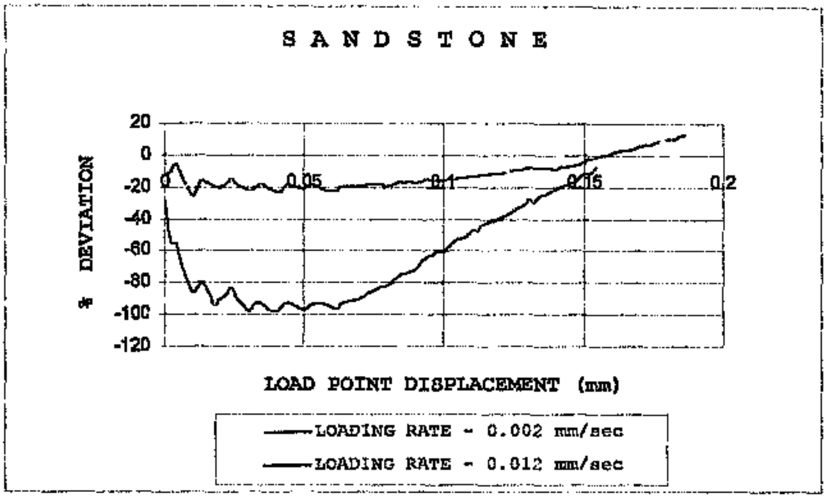

Figure VII.12
Tensile stress deviation from stress in test with loading rate 0.01 mm/sec

The differences decrease after initial loading. The second part of the graphs start from the value of LPD 0.06 mm and tensile stress 2 MPa. The differences between different loading rates decrease until -20% for loading rate 0.012 mm/sec and -100% for loading rate - 0.002 mm/sec. The peak values of tensile stress (tensile strength) in the third part, calculated from the above formula, are between 3.80 MPa and 2.35 MPa (average 3.5 MPa). The average value was estimated including the other tested specimen, of which the tensile strength value was 5.24 MPa and loading rate 0.02 mm/sec, drilled from sandstone block No 1 and those from block No 3. These values were compared with results from Brazilian disk tests, from which results were obtained for tensile strength with a value of 4.24 MPa, which has 14 % difference.

The LPD standard values for different loading rates in the third part of the graphs are as follows:

Loading rate 0.022 mm/sec - LPD 0.1144 mm
Loading rate 0.012 mm/sec - LPD 0.0880 mm
Loading rate 0.002 mm/sec - LPD 0.0669 mm

The specimen, which was loaded with a loading rate of 0.002 mm/sec, has peak resistance zone with length of 2.68E-02 mm (40.1% from a standard) and after this with increasing LPD, tensile stress decreases. The specimen, under loading rate of 0.012 mm/sec, has a resistance zone with length of 3.22E-02 mm (36.6% from a standard) before failing. The specimen under a loading rate of 0.022 mm/sec has a resistance zone with length of 3.65E-02 mm (31.9% from a standard) before decreasing.

VII.2.4 **Coal**

The tensile stress for Coal was estimated using a loading rate of 0.015 mm/sec. On the basis of the Level I Coal test (C4L1), tensile stress was plotted versus LPD (Fig.VII.13). The curve starts from the beginning of axes and goes straight to about 0.32 MPa, which is about 53% from the ultimate tensile stress or 0.014 mm LPD, which is about 22% from LPD of ultimate stress. On this basis yield stress with a value 0.32 MPa can be defined. Compared to that of Sandstone, Coal's ultimate tensile strength is not very clear to determine from the graphs. The graph shows that the tensile strength of Coal is 0.58 MPa.

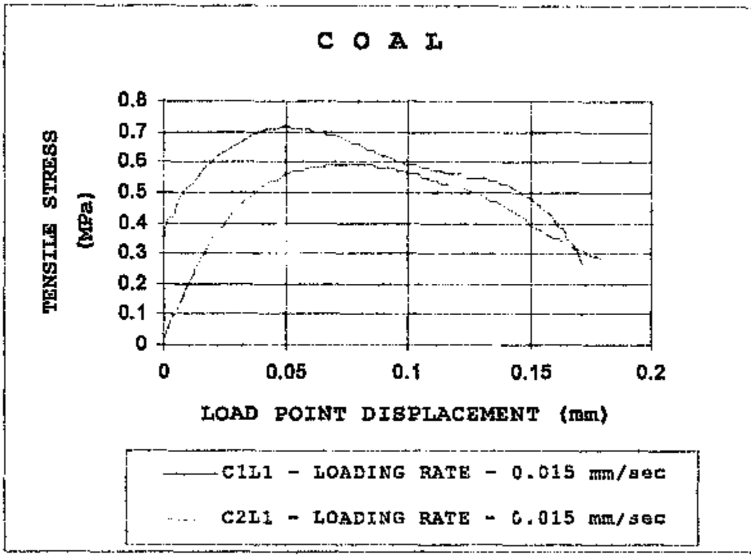

Figure VII.13
Estimating of Tensile stress of Coal specimens

As the basis of the analysis on post peak behaviour of the tensile stress, the value of LPD from the beginning of loading till the point of failure, was used as a standard,

Loading rate 0.015 mm/sec - LPD 0.0145 mm,

and for the stress, a 2% decrease. The specimen, which was loaded with a loading rate of 0.015 mm/sec, has a resistance zone with length of about 1.45[illegible] mm (19%

from etalon). After this as LPD r?ases, tensile stress decreases.

VII.3 **J-integral studies**

Critical J-integral data were determined using the J-resistance curve technique. The analysis shows the results from the three kind of rocks (quartzite, norite and sandstone). Guidelines recommended by the ASTM Subcommittee E24.08 on Elastic-Plastic Fracture Mechanics Terminology were used. The areas were estimated on the basis of load vs LPD displacement for these kinds of rocks. To determine the total work done on the specimen the actual area A, under the load vs LPD, the displacement curve was modified slightly to account for the energy stored at zero load due to crack closure. The energy values for each area of t rocks were plotted against the corresponding crack length value, using equation by Landes and Bergly (equation VI.21), the equation by Landes and Bergly with Srawley's correction (β - Chapter VI, p.59) and the Merkle-Corten (equation VI.22). This can be seen on figures VII.14-16. Equations for the best fitted curvature parts from the graphs are listed in table VII.1.

The slope of "blunting line" was estimated according to equation VI.26 and the values are as follows;

For quartzite specimens: - 16.46E+06 (N/m)

For norite specimens: - 20.99E+06 (N/m)

For sandstone specimens: - 4.5E+06 (N/m)

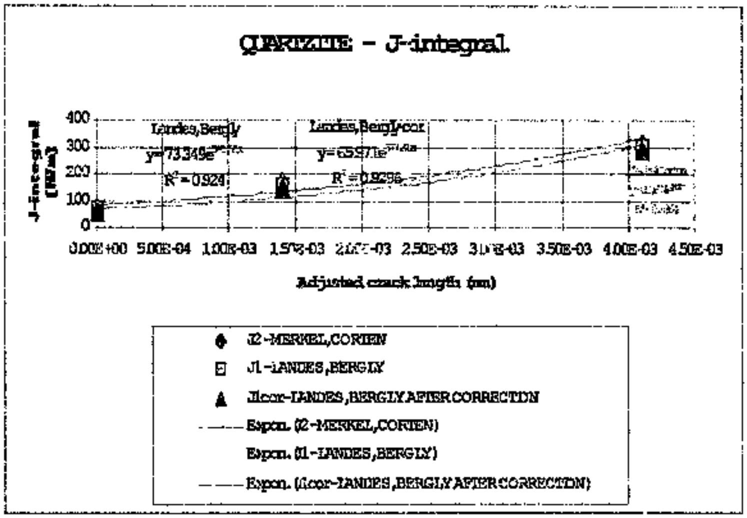

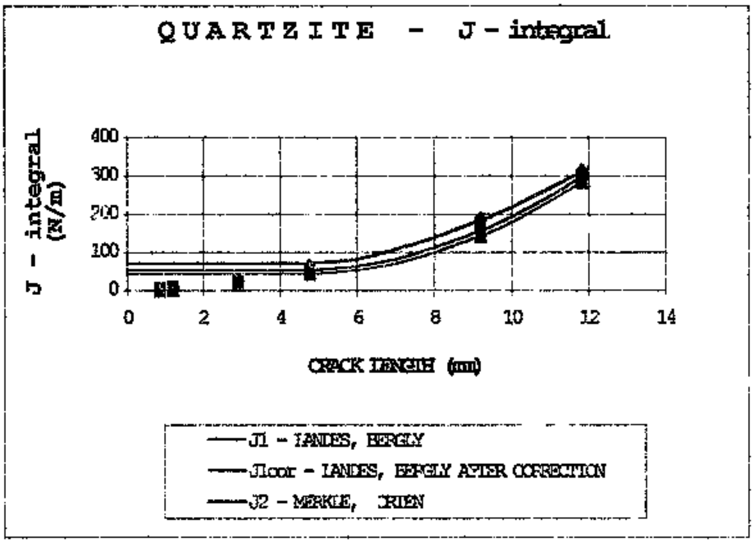

Figure VII.14
Estimating equation on curvature and critical value J_{IC} of J-integral of Quartzite specimens

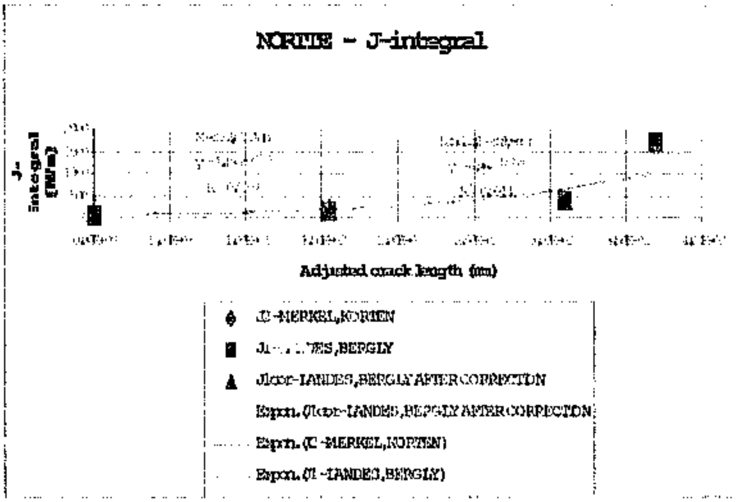

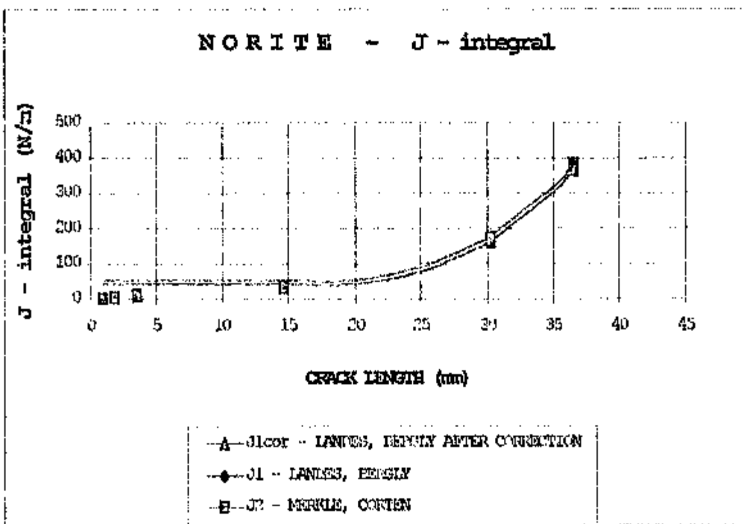

Figure VII.15
Estimating equation on curvature and critical value J_{Ic} of J-integral of Norite specimens

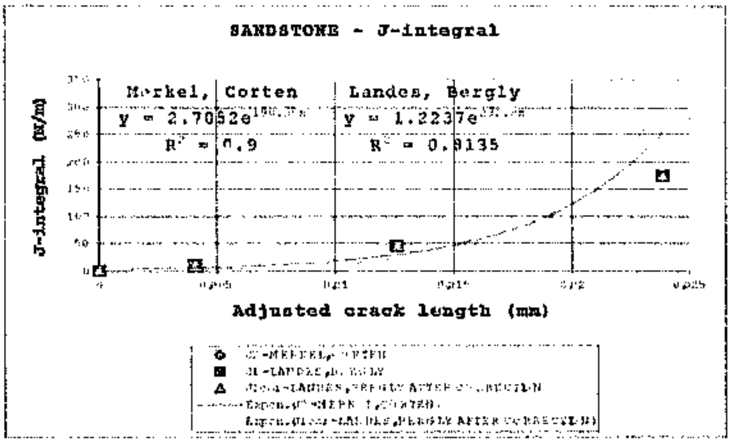

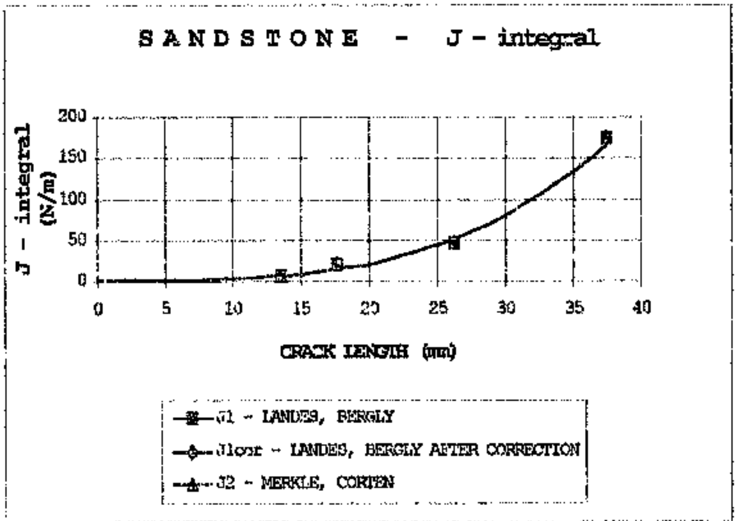

Figure VII.16
Estimating equation on curvature and critical value J_{IC} of J-integral of Sandstone specimens

Table VII.1

Results calculated from equation of	Equation of exponential line	Square deviation R^2
QUARTZITE		
Merkle and Corten	$Y=82.674*e^{[illegible]}$	0.9364
Landes and Bergly	$Y=73.349*e^{[illegible]}$	0.9296
Landes and Bergly after correction	$Y=73.349*e^{[illegible]}$	0.924
NORITE		
Merkle and Corten	$Y=51.49*e^{[illegible]}$	0.9107
Landes and Bergly	$Y=36.98*e^{[illegible]}$	0.9015
Landes and Bergly after correction	$Y=36.98*e^{[illegible]}$	0.9007
SANDSTONE		
Merkle and Corten	$Y=2.7052*e^{[illegible]}$	0.9000
Landes and Bergly	$Y=1.2237*e^{[illegible]}$	0.8135
Landes and Bergly after correction	$Y=1.2237*e^{[illegible]}$	0.8135

The values for yield and ultimate stresses were taken from the previous chapter. For all practical purposes the blunting line for these tests can be considered as a vertical line and J_{IC} is then J-integral extrapolated to the zero growth condition. The crack growth resulting from a single loading cycle was determined from the crack lengths calculated on the basis of the compliance of that loading cycle and the cycle immediately following.

Crack growth that may occur during the unloading portion of each cycle is included here as necessary but, since the J_{IC} point is the value extrapolated to infinitesimal crack growth, the only consequence would be a change in the scale of the crack growth axis with little effect on J_{IC}. A single values of J_{IC} which ware determined for each kind of rocks on the basis of equation VI.21, equation VI.21 with Srawley's correction and equation VI.22 as was mentioned in Chapter VI.3 (Figure VII.14-16) are listed bellow.

Quartzite - J_{IC} = 82.06 N/m

Norite - J_{IC} = 50.8 N/m

Sandstone - J_{IC} = 2.65 N/m

The initial J estimation used methods by Landes and Bergly, the equation by Landes and Bergly with Srawley's correction and the Merkle-Corten are compared in Figure VII.17 in a non-dimensional form with the value of J as calculated by the energy rate definition. It can be seen that equation VI.22 most closely approximates the value of J derived by equation VI.21.

The fracture toughness coefficients, K_{IC}, were calculated by equation VI.28 and compared with results, which were obtained from Chapter VII.1. The comparison of K_{IC}, calculated from fracture toughness tests and from J_{IC} can be seen in Table VII.2

Table VII.2

Kind of rock	Number of data points	Average K_{IC}, MPa/m	$Kic = \sqrt{\frac{J_{IC} \cdot E}{1-\nu^2}}$ MPa/m	Percent Difference
Quartzite	6	2.20	2.11	-4.1
Norite	6	2.29	2.20	+3.9
Sandstone	4	0.34	0.32	-5.9

All other values for the J-integral calculation can be seen in Tables 1 - 3 (Appendix 5).

VIII. **DISCUSSION**

VIII.1 **Fracture toughness tests**

VIII.1.1 **Testing procedure**

Fracture toughness tests as were shown in the previous chapters were divided into two levels.

Level I tests were run under load control until the specimen failed. The loading rate during the tests was increased gradually till failure occurred within 10 seconds of the initial load application or reached crack velocity of 0.001 mm/sec. The average stress intensity rate during the tests was not less then 0.25 MPa m/sec. When the suggested speed of failing was reached, axial LVDT was plotted versus applied load for estimating conditions to Level II tests.

Level II Fracture Toughness tests were ran under axial displacement (LVDT) control. Tempates containing procedures were set up for different stages of testing. The test template for Level II tests contains seven loading-unloading cycles, which are sufficient according to the ISRM suggestion that Level II tests should have a minimum of 3 loading-unloading cycles before and 1 loading-unloading cycle after failing of specimens. The five cycles before and two cycles after the load of failing were used. All fracture toughness tests were ran on room temperature (20^0C).

The estimated fracture toughness coefficients used values of displacement ratio - p as follow. For quartzite, between 0.14 and 0.18 (average value of 0.16 with standard deviation of 0.014); for norite, between 0.14 and 0.25 (average value of 0.18 with standard deviation of 0.036); for sandstone, 0.1 and for coal specimens - 0.1. They are close enough to the suggested from ISRM value of 0.2 for rock specimens. The condition, related to the size of grains and specimen diameter (more than 1:10) is acceptable.

VIII.1.2 **Quartzite**

For calculation of fracture toughness coefficients two cases were used. First when the two chosen lines span the evaluation point and F* is not less than $0.98F_{max}$ (specimens Q2L2, Q3L2, Q6L2 and Q6-5) and second when the two chosen unloading lines do not span the evaluation point and F* is less than $0.98F_{max}$ (specimens Q1L2, Q4L2, Q5L2 and Q6-4).

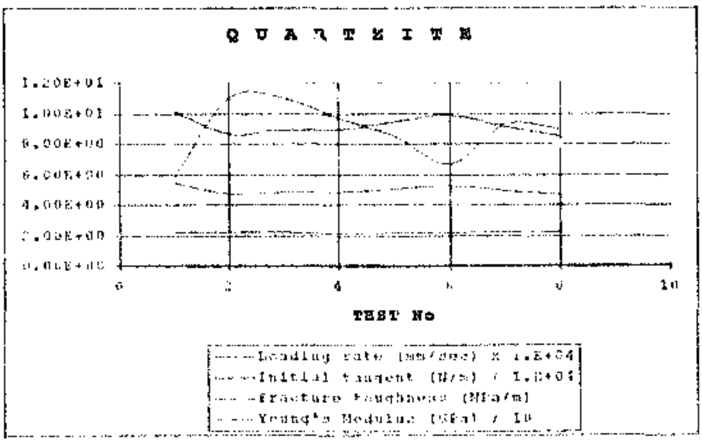

Figure VIII.1

Loading rate, initial tangent, fracture toughness coefficient and Young's modulus variations of quartzite specimens

As can be seen from the figure VIII.1, the relation is inverse proportional between loading rate and initial tangent, ch is involve in calculation on Young's modulus. Higher initial tangent value correspond to lower loading rate and vice versa, on lower initial tangent value correspond higher loading rate. From there is coming a difference in calculation of Young's modulus, which using a linear function in its estimating. Fracture toughness calculations have smaller influence on loading rate and al tangent, which can be seen from above mentione are. Consequently, applied loading rate is acceptable for fracture toughness estimating, but not for formal Young's modulus calculation. The fracture toughness and Young's modulus variation of quartzite specimens can be seen on Figure VIII.2.

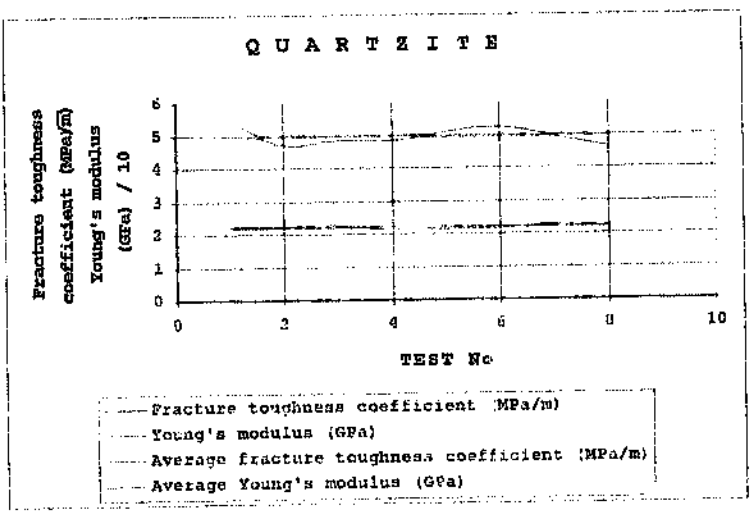

Figure VIII.2
Fracture toughness coefficients and Young's modulus compared to average values of quartzite specimens

The average results from Level II tests (contains results from 8 Level II tests) were compared with average results from Level I tests (contains results from 4 Level I tests). The average values are shown in Figure VIII.3. The applied loads from Level I are 10 to 12 % higher than those of Level II. This means that the Quartzite as a rock is more stable on static loading while losing stability under fatigue loading with about 10 %. The differences of the LPD values are higher from those of the CMOD values (Figure VIII.4). The biggest differences between LPD and CMOD from Level II tests appeared at the beginning of the tests. In the elastic phase (excluding initial loading) the differences between LPD and CMOD is within 11 - 15 % (Figure VIII.4). After this, the differences increase in the plastic phase to 20 - 25 %.

Fractographic studies shows that the quartzite as a rock forms a split crack in one of the both ends of the tip of the V shape. The crack in the core of quartzite specimen keeps straight direction. When the crack meets grains of quartz in Quartzite specimens it is trying to pass through the boundary of the grain. In other cases, the crack passes the grain's boundary. The average angle of secondary fracturing is 48^0 (mainly the angle is between 30^0 and 45^0) in the quartz grains of quartzite specimens.

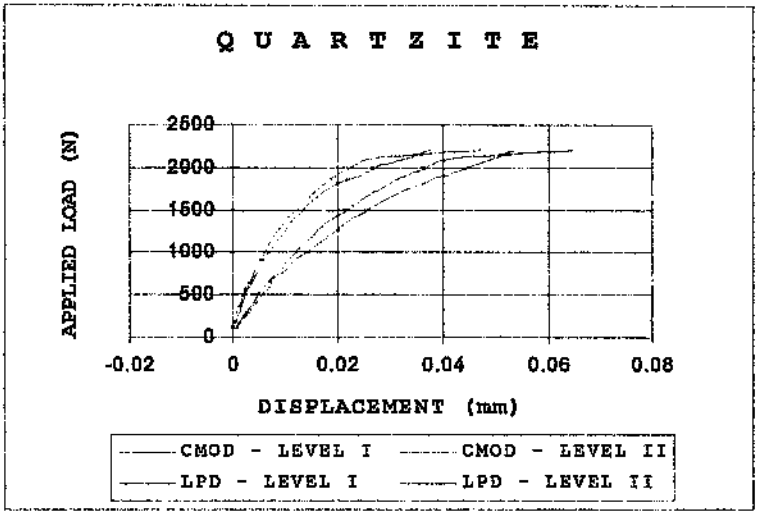

Figure VIII.3
Average displacement results of Level I and Level II tests

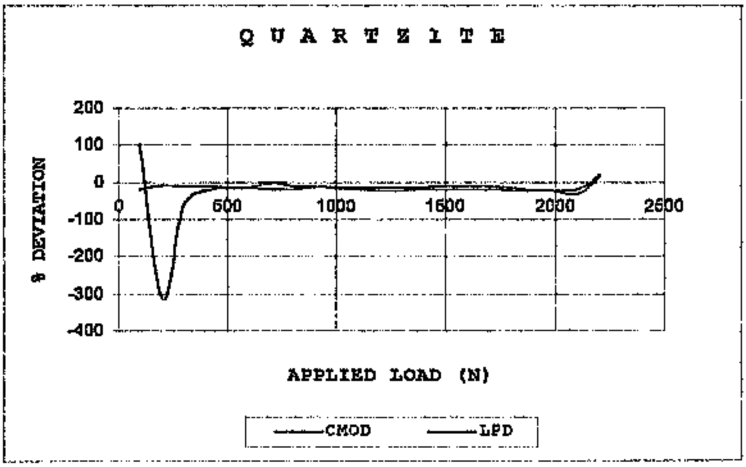

Figure VIII.4
Percent displacement of Level II tests

VIII.1.3 **Norite**

For calculation of fracture toughness coefficients two cases were used. First when the two chosen lines span the evaluation point and F* is not less than $0.98F_{max}$ (specimens N6L2 and N7-4) and second when the two chosen unloading lines do not span the evaluation point and F* is less than $0.98F_{max}$ (specimens N1L2, N3L2, N4L2, N5L2, N7L2 and N7-5).

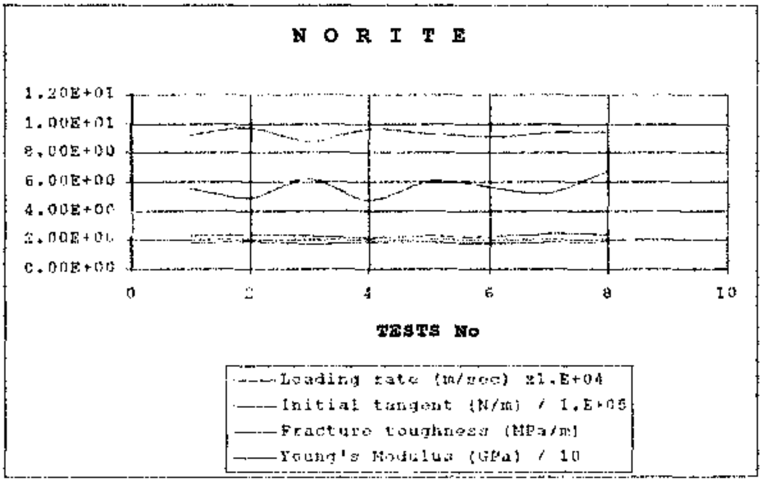

Figure VIII.5
Loading rate, initial tangent, fracture toughness coefficient and Young's modulus variations of norite specimens

As can be seen from the figure VIII.5, the relation is inverse proportional, between loading rate and initial tangent, the same as quartzite tests, which is involve in calculation on Young's modulus. Higher initial tangent value correspond to lower loading rate and vice versa, on lower initial tangent value correspond higher loading rate. From there is coming a difference in calculation of Young's modulus. Fracture toughness calculations have smaller influence on loading rate and initial tangent, which can be seen from above mentioned figure. Consequently, applied loading rate is acceptable for fracture toughness estimating, but not for formal Young's modulus calculation, which gives lover results. The variation of fracture toughness and Young's modulus norite specimens can be seen on Figure VIII.6.

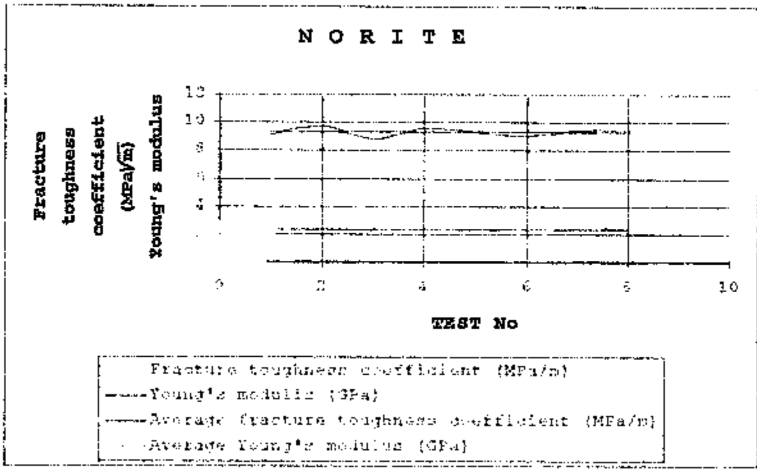

Figure VIII.6
Fracture toughness coefficients and Young's modulus compared to average values of norite specimens

The average results from Level II tests (contains results from 14 Level II tests) were compared with the average results from Level I tests (contains results from seven Level I tests). The average values are shown in Figure VIII.7. The applied loads from Level I are 12 to 15 % higher from those of Level II. This means that the Norite as a rock is more stable on static loading and loses stability under fatigue loading by about 15 %. The differences on the CMOD values are higher for this LPD (Figure VIII.8). The biggest differences on LPD and CMOD from Level II tests appeared at the beginning of the tests. In elastic state (excluding initial loading) the differences between LPD's are within 0 - 5 % and between CMOD's are within 11 to -20 % (Figure VIII.8).

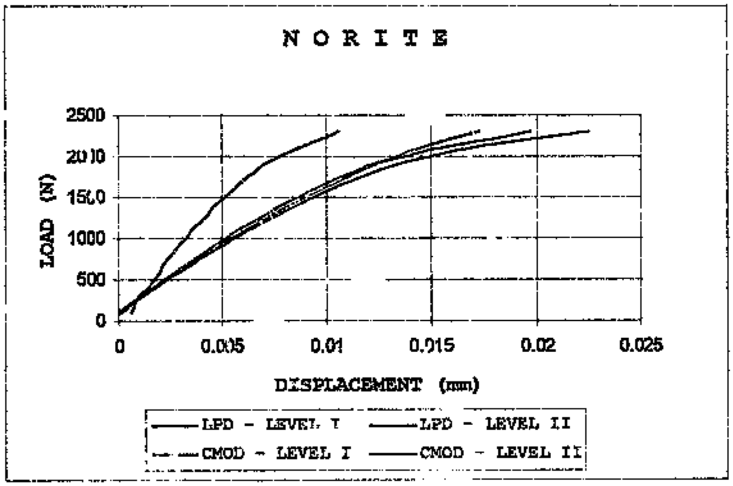

Figure VIII.7
Average displacement results of Level I and Level II tests

After this, the differences increase their values in plastic state for LPD to 15 - 20 % and CMOD to 60 - 80 %. From Figure VIII.7 and Figure VIII.8 it can be seen that LPD maintains the tendency to increase the difference permanently, but in a very small interval. The CMOD gauge also increases its differences in the elastic region from +80 to -65 % and in the plastic region from -65 to -80 %.

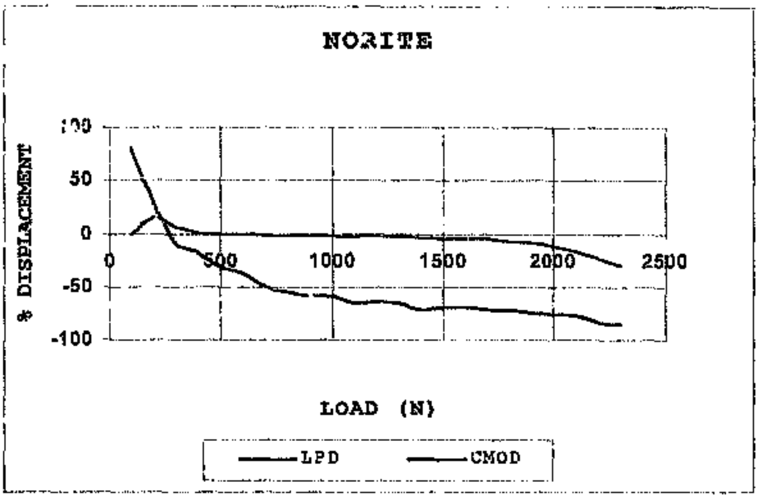

Figure VIII.6
Percent displacement deviation of Level II tests

Fractographic study shows presentation on fracture processing zone in the tip of the V shape. The crack does not keep straight direction in a core of norite specimens. The crack crosses the grains of quartz at the time of meeting, without changing the direction of fracture propagation. The average angle is 75^0 (mainly the angle is between 70^0 and 90^0) of the secondary fracturing in the quartz grains of norite specimens.

VIII.1.4 **Sandstone**

For calculation of fracture toughness coefficients was used the case, when the two chosen unloading lines do not span the evaluation point and F* is less than $0.98F_{max}$.

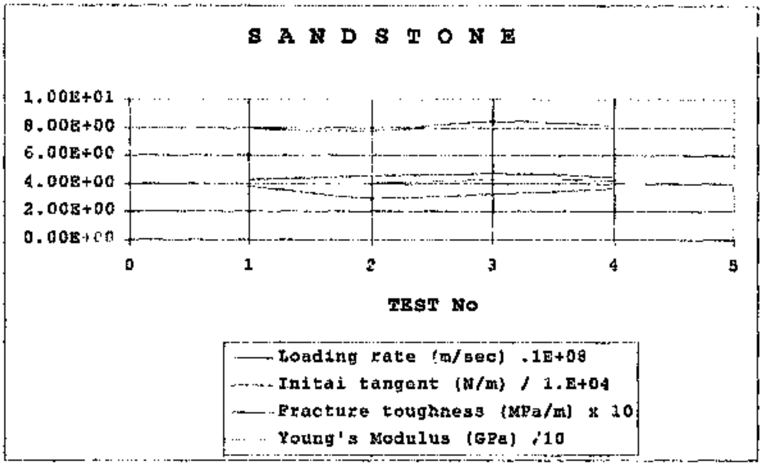

Figure VIII.9
Loading rate, initial tangent fracture toughness coefficient and Young's modulus variations of sandstone specimens

As can be seen from the figure VIII.9, the relation is proportional between loading rate and initial tangent, which is involve in calculation on Young's modulus. Higher initial tangent value corresponds to higher loading rate. Young's modulus follows the same tendency. Fracture toughness calculations have smaller influence of loading rate and initial tangent, which can be seen from above mentioned figure. In tests with higher loading rate and initial tangent, calculated fracture toughness has lower value. Applied loading rate is acceptable for fracture toughness estimating and for Young's modulus calculation. The variation of fracture toughness and Young's modulus of sandstone specimens can be seen on Figure VIII.10.

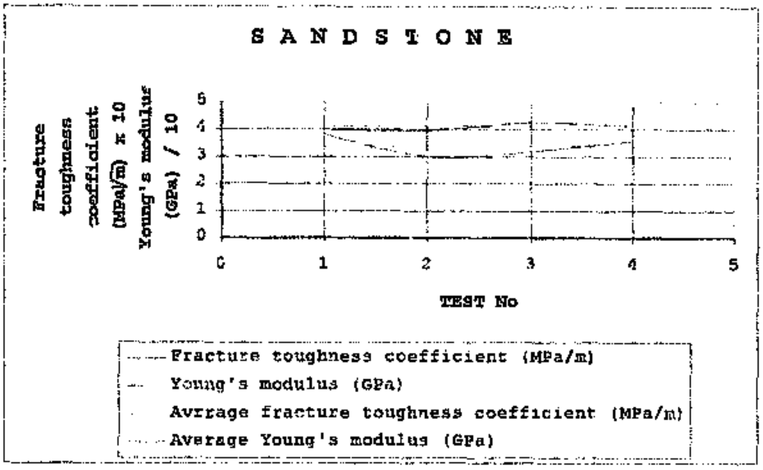

Figure VIII.10
Fracture touganess coefficients and Young's modulus compared to average values of sandstone specimens

The average results from Level II tests (contains results from eight Level II tests) were compared with the average results from Level I test (contains results from six Level I tests). The average values are shown in Figure VIII.11. The applied loads from Level I are from 15 to 20 % higher then those from of Level II. This means that the sandstone as rock is more stable on static loading and loses its stability under fatigue loading by about 18 %. The differences in the LPD values are higher then those of CMOD (Figure VIII.12). The biggest differences between LPD and CMOD of Level II tests appeared at the beginning of the tests. In the elastic state (excluding initial loading) the difference of LPD is between -95 and -150 % and CMOD is between 25 - 40 % (Figure VIII.12). After this, in the plastic state the differences of LPD tend to be a stable, permanent value of about -160 %. The different CMOD values decrease their values in plastic situation from 25 to 15%.

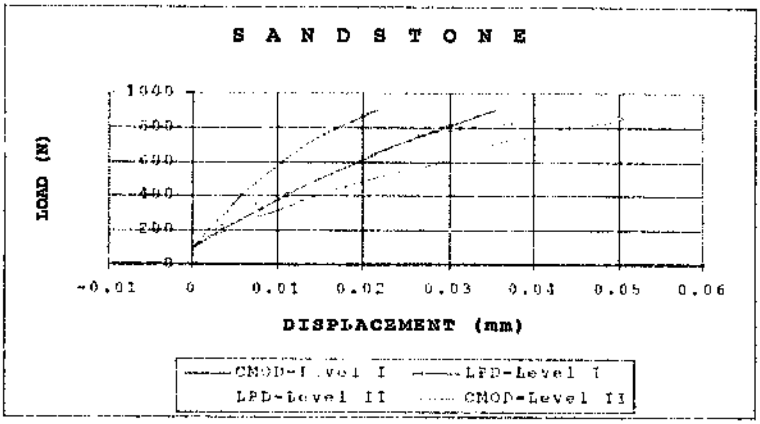

Figure VIII.11
Average displacement results of Level I and Level II tests

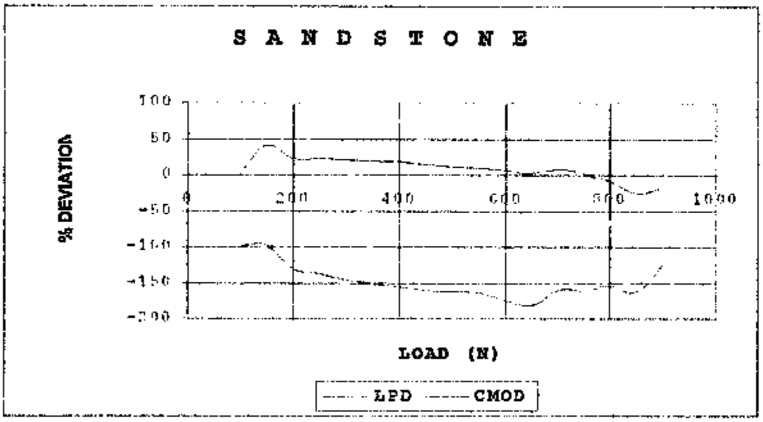

Figure VIII.12
Percent displacement deviation of Level II tests

VIII.1.5 **Coal**

For calculation of fracture toughness coefficients was used the case, when the two chosen unloading lines do not span the evaluation point and F* is less than $0.98F_{max}$.

As can be seen from the figure VIII.13, the initial tangent for coal specimens, which is involves in calculation on Young's modulus, is independent from loading rate. For different ranges of loading rate, initial tangent staying very stable (figure VIII.13). From there Young's modulus follows the same tendency without any significant differences.

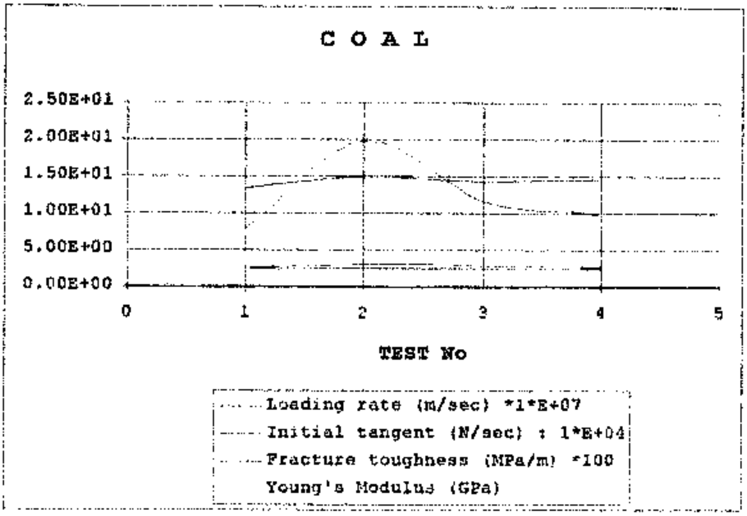

Figure VIII.13
Loading rate, initial tangent, fracture toughness coefficient and Young's modulus variations of coal specimens

This can be seen from figure VIII.14. Fracture toughness calculations have smaller influence of loading rate and initial tangent, which can be seen from above mentioned figures. Applied loading rate is acceptable for fracture toughness estimating and for Young's modulus calculation. The variation of fracture toughness and Young's modulus of sandstone specimens can be seen on Figure VIII.14.

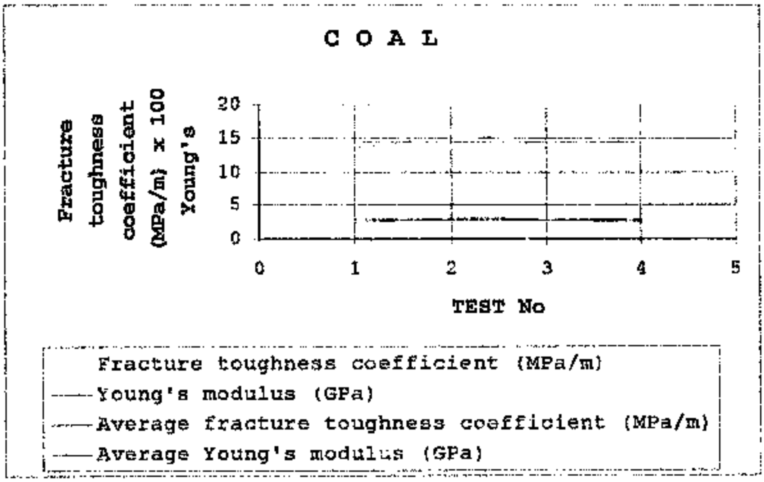

Figure VIII.14
Fracture toughness coefficients and Young's modulus compared to average values of sandstone specimens

The average results from the Level II tests (contains results of 3 Level II tests) were compared with the average results of the Level I tests (contains results of 3 Level I tests). The average values are shown in Figure VIII.15. The applied loads in Level I were 50 % lower then those of Level II (averages maximum load 120 N for Level I and 230 N for Level II). This means that the Coal as a rock is more stable on fatigue loading and loses its stability under static loading. The differences of LPD values are lower than CMOD (Figure VIII.16). In the elastic region the difference of LPD is between 70 and 10 % and of CMOD is between 11 to -40 %. In the plastic region, the differences of LPD and CMOD increased their values to about -50 % (LPD) and -160 % (CMOD).

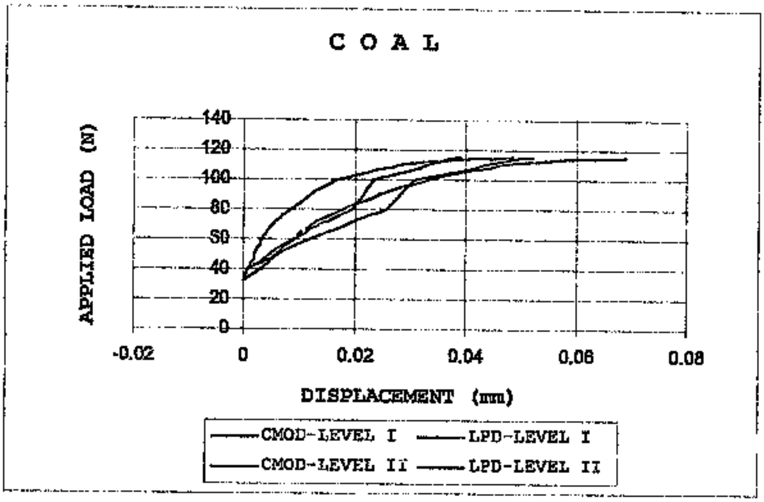

Figure VIII.15
Average displacement results of Level I and Level II tests

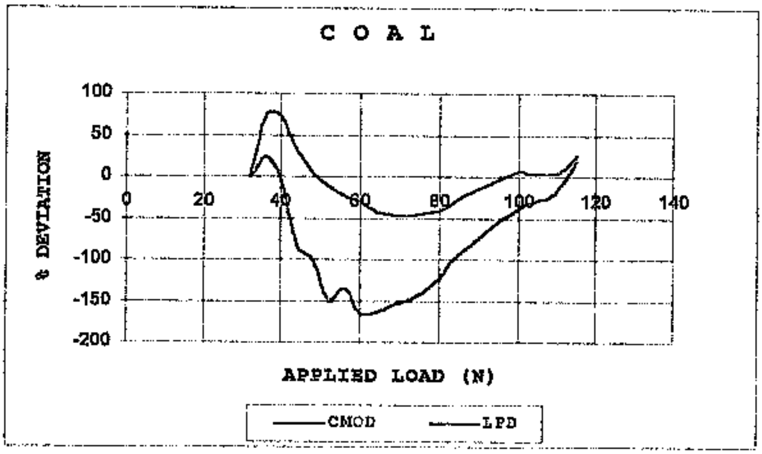

Figure VIII.16
Percent displacement deviation of Level II tests

VIII.2 **Tensile stress and strength**

The applied methodology for estimating of tensile stress and strength of different rock specimens shows satisfactory results. The differences which were obtained from Brazilian disk testing showed 1% deviation for quartzite specimens, 8% deviation for norite specimens and 14% deviation for sandstone specimens. The bigger deviation for sandstone specimens results from the suggested crack velocity - 0.001 m/sec of ISRM for Level I fracture toughness experiments. The tendency, which can be seen from tensile stress calculation, is that with increasing loading rate the tensile strength also increases in value for quartzite and norite, which are brittle rocks (Fig.VIII.17).

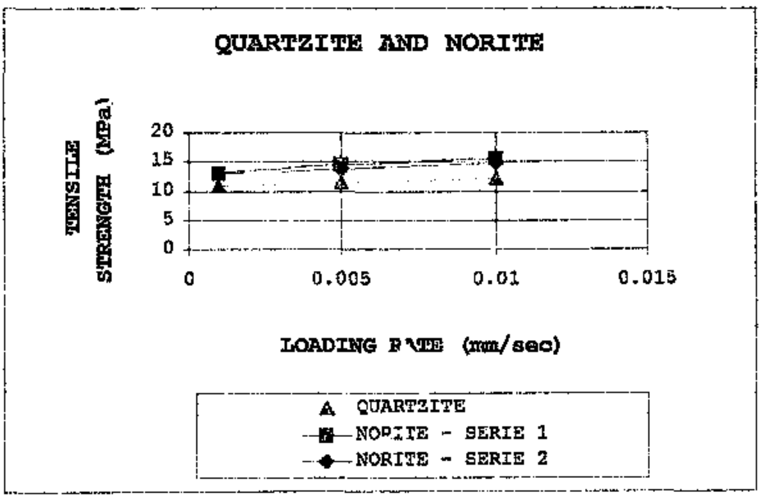

Figure VIII.17
Tensile strength tendency of investigated Quartzite and Norite specimens

Sandstone specimens have a totally different tendency. With increasing loading rate, the tensile strength decreases. This can be seen on Figure VIII.18.

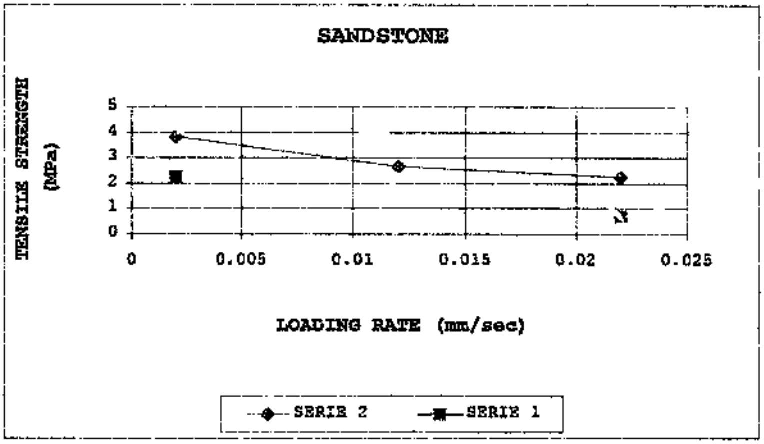

Figure VIII.18
Tensile strength tendency of investigated Sandstone specimens

The comparison of brittle rocks and sandstone specimens under static and dynamic loading shows that they are more stable on static loading. Coal behaviour is different. Coal specimens are more stable under dynamic loading and lose stability under static loading. This can be seen from the load of fail of Level I tests of specimens C1L1 - 140 N; C2L1 - 120 N and Level II tests of specimens C1L2 - 225 N; C2L2 - 200 N and C3L2 - 210 N.

The feature of the tensile stress is the post peak behaviour of the tested rock specimens. All tested specimens show behaviour of decreasing of the resistance zone with the increase of the loading rate (Figure VIII.3 and 4). This can be proved by the five test series done, which means test specimens from different block of rocks (1 block for Quartzite, 2 blocks for Norite and 2 for Sandstone), under three different loading rates. When comparing the highest and lowest loading rates of all 14 tests of the different kind of rocks, it can be seen that the peak resistance zone maintains this tendency.

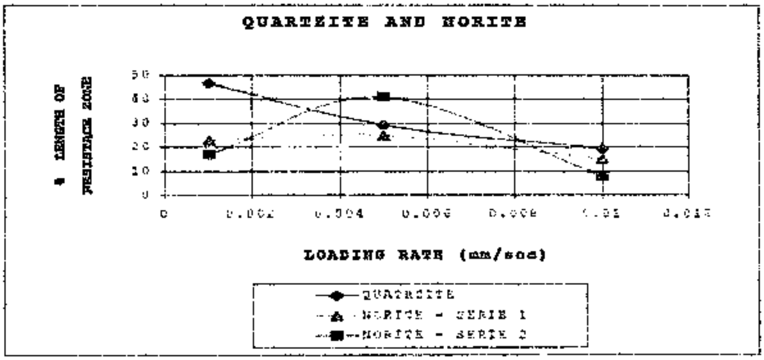

Figure VIII.19
Length of post peak resistance zone of Quartzite and Norite specimens

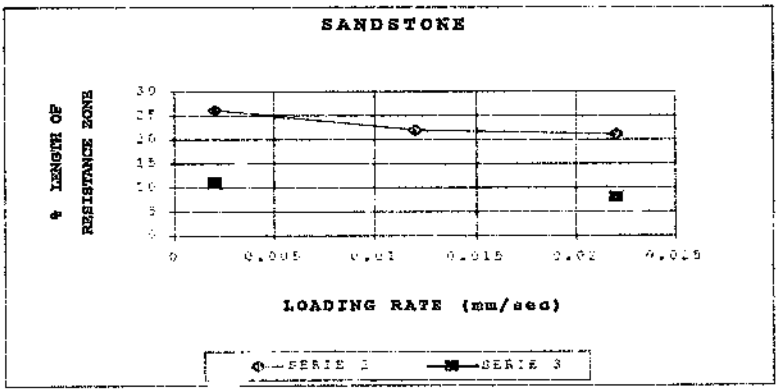

Figure VIII.20
Length of post peak resistance zone of Sandstone specimens

VIII.3 **J-integral studies**

The values of J for the three point bending specimens were calculated from the expression proposed by Merkel/Corten that is presently recommended by ASTM, from equation of Landes/Begley and from equation of Landes/Begley, after Srawley's correction. J-integral results calculated from investigated three kinds of rocks (Appendix 5, tables 1-3), shows that in an elastic region, where is calculate fracture toughness coefficient, the equation of Landes/Begley (eq.VI.20,21) and equation of Merkel/Corten (eq.VI.22) have similar and higher value, compared to the equation of Landes/Begley after Srawley's correction. Srawley's correction is mostly applicable for brittle isotropic materials, but not for rocks. R.A. Schmidt and T.J. Lutz also had been used Merkel/Corten equation for estimating of K_{IC} and J_{IC} of Westerly granite [27,28].

The other discussion element in J-integral studies, use of "blunting line" for estimating of J_{IC} is not applicable for purposes of rock mechanics. Results, which were calculated for estimation on slope of "blunting line" shows that their values are very high and the lines are very steep. Without any serious mistakes they can be approximate as vertical lines, coincide with the Y axis of figures VII.14-16.

From figure VIII.21 can be seen that with increasing of the crack length in investigating kind of rocks, the apparent fracture toughness increases in value and reach its critical value when the material separation begins. As was mentioned in Chapter VI.3 critical value of J-integral is in a point from where begins real material separation in a form of crack. Slope value that was calculated from fracture toughness tests for different kind of rocks best-fit slope lines of quartzite specimen between fourth and fifth cycles, for norite specimen between fifth and sixth cycles and for sandstone specimens between first and second cycles. In a previous cycles missing real material separation and calculated J values are not included in J_{IC} estimated graphs because they belong to crack tip blunting zone. This points have steeper slope in the graphs of figure VIII.21.

Applied methodology can be used when the necessary results are in term of work done or applied energy.

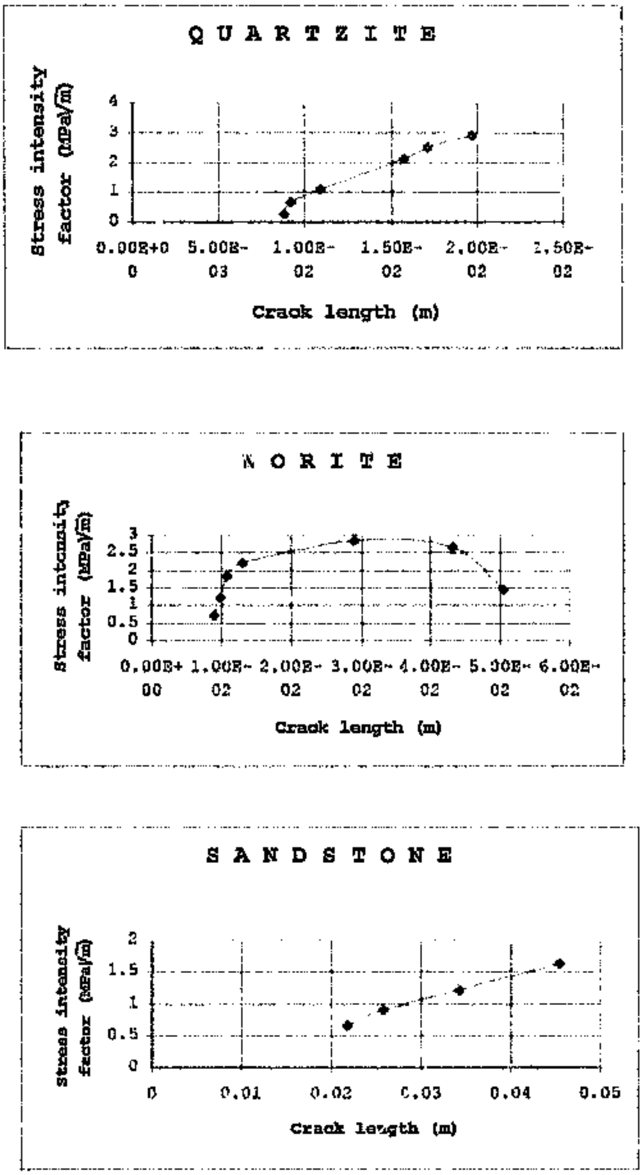

Figure VIII.21

Variation of stress intensity factor according to crack length in Quartzite, Norite and Sandstone specimens

IX CONCLUSIONS

IX.1 Fracture toughness tests

The following conclusions can be made from the estimated values of fracture toughness tests.

1. Calculated value for Mode I fracture toughness coefficient is K_{IC} = 2.20 MPa/m for Quartzite, K_{IC} = 2.29 MPa/m for Norite, K_{IC} = 0.34 MPa/m for Sandstone and K_{IC} = 0.14 MPa/m for Coal.
2. Calculated value for Young's modulus of Quartzite is E = 49.6 GPa, for Norite E = 93 GPa, for Sandstone E = 41 GPa and for Coal E = 2.72 GPa.
3. The appropriate loading rate for Level I tests for Quartzite is 0.01 mm/sec, for Norite - 0.01 mm/sec, for Sandstone - 0.02 mm/sec and for Coal - 0.015 mm/sec.
4. The appropriate loading rate for Level II tests for Quartzite, Norite and Sandstone is 0.001 mm/sec. For Coal - 0.015 mm/sec.
5. The maximum loads which were reached from Level I tests, compared with those from Level II tests, for Quartzite were within 10 - 12 % higher, for Norite - within 12 - 15 % higher and for Sandstone within 10 - 15 % higher. This means that these rocks are more brittle under dynamic loading, compared to static loading.
6. The maximum loads which were reached from Coal Level I tests are 45 % lower than those from Level II tests. This means that Coal is more brittle under static loading, than under dynamic loading.
7. The Quartzite specimens maintain elasticity for

Level I and Level II tests for about 30 % of the failure load.

8. The Norite, Sandstone and Coal specimens maintain elasticity for Level II tests for 45 % from failure load, and for Level I tests for about 50 % of the failure load.
9. The differences in elastic phases for LPD and CMOD between Level I and Level II tests are within 11 - 15 % for Quartzite specimens, and +5 to -5 % for Norite specimens.
10. Sandstone specimen differences in elastic phases between Level I and Level II tests for LPD are within -100 to -150 % and for CMOD 10 to 25 %.
11. Coal specimen differences in elastic phases between Level I and Level II tests for LPD are within 10 and 70% and for CMOD 11 to -5 %.
12. The differences in plastic phases for LPD and CMOD between Level I and Level II tests are within 20 - 25 % for Quartzite, -10 to -15 % for Norite, -25 to -150 % for Sandstone and -50 % to -160 % for Coal specimens.

IX.2 **Fracturing**

The following conclusions can be made from the comparisons of the fracturing on investigated rocks.

1. Quartzite forms split crack in the tip of the V shape. Norite forms fracture process zone.
2. Quartzite maintains the straight direction of fracture propagation in contrast to Norite which fractures in a zigzag.

3. Quartzite forms secondary fracturing with smaller angles, compared to Norite, occurring within the quartz grains.

IX.3 **Tensile stress and Tensile strength**

The following conclusions can be made from the estimated values of tensile stress and tensile strength on investigated kind of rocks.

1. The tensile stress of the specimens σ_t, can be calculated by the following general formula, :

$$\sigma_t = \frac{14{,}41.P}{D^2}$$

   Where P is the load (N) and D is the diameter of the test specimen (m).
2. Tensile stress is dependant on applied loading rate. Tensile strength decreases with decreasing loading rate.
3. The peak resistance zone also depending on the loading rate. A zone increases its length with decreasing on loading rate.
4. The average tensile strength, which is calculated for Quartzite is 11.56 MPa, for Norite 13.45 MPa, for Sandstone 5.24 MPa and for Coal 0.58 MPa. The crack velocity on fracture toughness tests was higher then 0.001 m/sec.
5. The average yield tensile stress which is calculated for Quartzite is 5 MPa, for Norite 7 MPa, for Sandstone 2.3 MPa and for Coal 0.32 MPa. The crack

velocity on fracture toughness tests was higher then 0.001 m/sec.

IX 4 **Defining of J_{IC}**

The following conclusions can be made from the comparisons of the estimated values of J and the values of J as determined from equation VI.20.

1. Most accurately in this investigation was a variation of the Merkel-Corten technique given by Eq VI.22 for estimating of J_{IC} from three point bending specimens.
2. The stretch zone line $J = 2\sigma_{flow}\,\Delta a$ is not necessary for the rock specimens because this line is very steep and in general will absent from a stretch zone.
3. J_{IC} must be taken as the intersection between fitted curve to the J versus crack extension points and the axis of J-integral values.
4. Critical value of J-integral standing between the cycles where is calculated K_{IC}.

IX.5 **J-integral calculations**

From the evaluation of load-displacement curves and from experiments on three different kinds of rock, the following conclusions can be drawn for three-point bend specimens:

1. From the different equations for J-integral determination from load-displacement curve, the relation of Merkel and Corten yields the best results.
2. Crack extension begins below the J-value determined with the extrapolation method. This method can be applied only for specimens if data points beyond maximum load are included in a case when fracture with material separation begins under load nearby the load of failing (for example as Norite specimens).
3. Equation VI.27 can be use for calculation of K_{IC} by means of J_{IC} with admissible accuracy.

X RECOMENDATION FOR FUTURE WORK

Future studies on fracture toughness of rocks should consider the elements of both a J_{IC} and K_{IC} approach. J_{IC} testing appears to be less restrictive of specimen size and needs less verification due to a nonlinear stress-strain behaviour. K_{IC} measurement, on the other hand, requires fewer tests to be performed and data reduction follows a simpler procedure. However, an analysis by Ernst indicates that a complete J versus crack growth curve can be determined from a single load - displacement record with absolutely no measure of crack length.

One other aspect of rock fracture that needs further attention is the micro mechanics of crack propagation. Speculations of micro crack zones need direct substantiation in order to understand fully the rock behaviour. Crack front configurations need to be examined to understand the effects of plane stress and plane strain. Perhaps the most important reason for micro mechanics models is that guidance is needed when extrapolating data from one or several rock types to the various rocks encountered in a particular application.

The main application of the fracture toughness coefficients is in the field of numerical modelling. One of the problems is the presence of micro cracks in specimens, as mentioned above. At the present stage, Mode I fracture toughness tests don't give a successful evaluation of the percentage of cracks in tested specimens, unlike in ceramics, metals and other homogeneous materials. For future investigations three point bending specimens should be combined with three-axial compressive stress tests, which is possible with the MTS - testing machine. The three-axial compressive stress tests must be terminated at predefined stress levels and then speci ens should be tested to determine the fracture toughness coefficient. Then the rock might have different K_{Ic} values for different percentages of micro cracks and different pressures.

REFERENCES

1. **Atkinson, B.K.**, *Fracture Mechanics of Rock*, Academic Press, 1987.
2. **Atkinson, B.K., MacDonald, D., Meredith, P.G.**, In: *Proc. 3rd Int. Conf. on Acoustic Emission/Microseismic Activity in Geological Structures and Materials* (eds Hardy, H.R. and Leighton, F.W.). Trans. Tech. Pubs. Clausthal, 5-18, 1984.
3. **Barton, C.C.**, *EOS, Trans. Am. Geophys. Union* 62, 396, 1981.
4. **Brown, W.S., Swanson, S.R., Mason, W.E.**, "*Fracture Mechanics Applications to Rock*", Report UTECME 72-027, Univ. of Utah, Salt Lake City, Utah, 1972.
5. **Cook N.G.W.**, *Seismicity associated with mining*, 1st Int. Symp. on Inland Seismicity, Canada, 1976.
6. **Evans, A.G.**, *J. Mater. Sci.*, 7, 1137-1146, 1972.
7. **Goodman, D.J., Tabor, D.** *J. Glaciol.* 21., 651 - 660, 1980
8. **Griffit, A.A.**, *The theory of rupture*, Proc. 1st Int. Congr. Appl. Mech., pp 56 - 63, 1924
9. **Jaeger, J.C., Cook, N.G.W.**, *Fundamentals of Rock Mechanics*, 3Edn., Fleatcher & Son Ltd, Norwich, Great Britan, 1976.
10. **Ingraffea, A.R., Schmidt, R.A.**, *Proc. 19th. U.S. Symp. Rock Mech.*, Reno, Nevada, 247-253, 1978
11. **Ingreffea, A.R., Heuse, F.E., Ko, H.Y., Gerstle, K.**, *An analysis of discrete fracture propagation in rock loaded in compression*, Energy Research and Excavation Technology, Proc. 18th US Symp. on Rock Mech., 2A4-1 - 2A4-7, 1977.

12. **ISRM,** Commission of Testing Methods., *Suggested Methods for Determining the Fracture Toughness of Rock,* Int. J. Rock Mech. Min. Sci. & Geomech. Abstr., 1988

13. **Irwin, G.R.,** "*Plastic Zone Near a Crack and Fracture Toughness*", Proc. 7th, Sgamore Conf.,IV-63, 1960.

14. **Labuz, J.F., Shah, S.P., Dowding, C.H.,** *Int. J. Rock Mech. Min. Sci. Geomech.* Abstr. 22, 85-98, 1985.

15. **Lawn, B.R., Swain, M.V.,** *Int. J. Frac.* 9, 481-483, 1983.

16. **Lawn, B.R., Swain, M.V.,** *Int. J. Rock Mech. Min. Sci. Geomech. Abstr.* 13,, 311-319, 1976.

17. **Meredith, P.G.,** *A Fracture Mechanics Study of Experimentally Deformed Crustal Rocks,* PhD Thesis, Univ. of London., 1983.

18. **Munz, D.,** *Minimum Specimen Size for the Application of Linear-Elastic Fracture Mechanics,* ASTM, STP 668, 406 - 425, 1979.

19. **Nolen-Hoeksema, R.C., Gordon, R.B.,** *J. Geophys. Res.*, 90, 7827-7836, 1985

20. **Ouchterlony, F.,** "*Evaluation Formulas for Rock Fracture Toughness Testing with Standart Core Specimens*". Presented at SEM Spring Conf., New Orleans, LA, 1986.

21. **Ouchterlony, F., Sun, Z.,** "*New Methods of Measuring Fracture Toughness on Rock Cores*", SveDeFo, Report No 1983: 10, Swed. Detonic Res. Found., Stockholm, Sweden, 1983

22. **Ouchterlony, F.,** *Fracture testing of rocks, Cources and Lectures on Rock Fracture Mechanics,* No 275, H.P.Rossmanith, (Ed.), Univ. of Minnesota, Minneapolis, 159-167, 1984

23. **Ouchterlony, F.**, *A New Core Specimen for the Fracture Toughness Testing of Rocks*, Swedish Detonic Research Foundation, Rep, DS, Stockholm, Sweeden, 1980.

24. **Peng, S.S., Johnson, A.M.**, *Int. J. Rock Mech. Min. Sci.*, 9, 37-86, 1992

25. **Rice, J.R.**, *J. Appl. Mech.*, 35, 368-379, 1968.

26. **Rice, R.W., Freiman, S.W., Pohanka, R.C., Mecholsky, J.J., Wu, C.C.**, In "*Fracture Mechanics of Ceramics*" Vol. 4, (eds Bradt, R.C., Hasselman, D.P.H., Lange, F.F.). Plenum, New York, 849-876, 1978.

27. **Schmidt, R.A., Lutz, T.J.**, In "*Fracture Mechanics of Brittle Materials*", ASTM STP 678, Am. Soc. Testing Materials, Philadelphia, 166-182, 1979.

28. **Schmidt, R.A.**, *Proc. 21st. U.S. Symp. Rock Mech.*, Univ. Missouri, Rolla, 1980.

29. **Sih, G.C., Godoutos, E.E.**, Discussion on "*A modified strain energy density criterion applied to crack propagation*" by Theocaris, P.S., J. Appl. Mech., 49, 678-681, 1982

30. **Swartz,S.E., Hu, K.K., Fartash, M.**, *Stress intensity facror for plain concrete in bending prenotched versus precracked beams*, Expl. Mech., 412-417, 1982

31. **Tharp, T.M., Travers, M.A.**, *A simple precracking procedure for fracture toughness testing in rock* - application to roof rock above No.V coal (Indiana), 27th U.S.Symp on Rock Mech., 24 - 31, 198(.

32. **Whittaker, B.N., Singh, R.N., Sun, G.**, *Rock Fracture Mechanics -Principles, Design and Applications;* Elsevier, 1992.

33. **Begley, J.A. and Landes, J.D.** in *Fracture toughness*, ASTM, STP 514, American Society for Testing and

Materials, 1972, pp 1-20.

34. **Landes, J.D. a gly, J.A.** in *Fracture toughness,* ASTM, STP 514, American Society for Testing and Materials, 1972, pp 24-39.

35. **Landes D.J., Walker H., Clarke G.A.,** *Evaluation of Estimation Procedures Used in J-integral Testing,* Elastic-Plastic Fracture, ASTM, STP 668, Nov. 1977.

36. **Merkle J.R, Corte H.T.,** *Journal of Pressure Vessel Technology, Transactions,* Am.Soc.Mech.Eng. Vol 96.

37. **Eftis J., Jones D.L., Lebowitz H.,** *Engineering Fracture Mechanics,* Vol 7, pp. 491-503, 1975.

38. **Landes J.D., Begley J.A.,** *Test Results from J-integral Studies: An Attempt to Establish a* J_{IC} *Testing Procedure,* "Fracture Analysis", ASTM, STP, 27-29 Aug., pp. 170-186, 1973.

39. **Gere, Timoshenko,** *Mechanics of materials,* Third Edition, Chapman & Hill, 1991

40. **Rice J.R.,** *Journal of Applied Mechanics,* Vol. 35, pp. 379-386, 1968.

41. **Rice J.R.,** *in "Fracture",* **H. Liebowitz,** *Ed.,* Vol. 2, Academic press, New York, pp 191-311, 1968.

42. **Begley , J.A., Landes, J.D.,** *in "Fracture Toughness",* ASTM, STP, 514, pp. 1-23, 1972.

43. **Begley, J.A., Landes, J.D.,** *in "Fracture Toughness",* ASTM, STP, 514, pp. 24-39, 1972.

44. **Bucci, R.J., Paris, P.C., Landes, J.D., Rice, J.R.,** *in "Fracture Toughness",* ASTM, STP, pp. 40-69, 1972.

45. **Rice, J.D., Paris, P.C., Merkle, J.G.,** *in "Progress in Flaw growth and Fracture Toughness testing",* ASTM, STP, pp231-245, 1973.

46. **Landes, J.D., Begley, J.A.,** *in "Fracture Analysis",* ASTM, STP 560, pp.170-186, 1974.

47. **Begley, J.A.**, *"Recommended Practices for the Determination of the J_{Ic} Point from the J vs a R-curve"*, ASTM, E-24, Philadelphia, Ra., 7Oct, 1974.

48. **Clarke, G.A., Andrews, W.R., Begley, J.A., Donald, J.K., Embley, G.T., Landes, J.D., Mc Cabe, D.E.**, *J. of Testing and Evaluation*, Vol 7, No 1, pp. 49-56, Jan. 1974.

49. **Wilkening, W.W.**, *in Proceeding, 19th U.S. Symposium on Rock Mechanics*, Y.S. Kim Ed., Univ. of Nevada, pp.254-258.

50. **Schmidt, R.A., Lutz, T.J.**, *in "Fracture Mechanics Applied to Brittle Materials"*, ASTM, STP 678, Philadelphia, pp. 166-182, 1979.

51. **Paranjee, S.A.**, *"Interrelation of crack opening displacement with stress intensity factor and J-integral"*, Ph.D. Thesis, I.I.T. Bombay 1976.

52. **Benerjee, S.**, *"Influence of specimen size and configuration on the plastic zone size, toughness and crack growth"*, Engineering Fracture Mechanics, 15, p. 343, 1981.

53. **Kahoff,J.F., Beinert, J., Winkler, S.**, *"Influence of dynamic effects on crack arrest"*, IWM-Report V22/80, prepared for ERRI, 1981.

54. **Crosley, P.B., Ripling, E.J.**, *"Dynamic fracture toughness of A533 steel, Journal of basic Engineering"*, Transcriptions, ASME, Ser.D, Vol. 91, p. 525, 1969.

55. **Crosley, P.B., Ripling, E.J.**, *"Crack arrest toughness of Pressure vessel steel"*, Nuclear Engineering and Design, Vol.17, No 1, p. 32, 1971.

56. **Crosley, P.B., Ripling, E.J.**, *"Crack arrest in on increasing K-field"*, proceedings of the Second International Conference on Pressure Vessel

Technology, San Antonio, Texas, p. 995, 1973.

57. **Crosley, P.B., Ripling, E.J.**, *"Characteristics of a run arrest segment of crack extension"*, ASTM, STP 627, Philadelphia, Pa., p. 203, 1977.

58. **Crosley, P.B., Ripling, E.J.**, *"Towards development of a standard test for measuring K_{IC}"*, ASTM, STP 627, Philadelphia, Pa, p.372, 1977.

59. **Hahn, G.T., Kanninen, M.F., Rosenfield, A.R., Hoagland, R.G.**, *"A preliminary study of fast fracture and arrest in the DCB test specimen"*, in Dynamic Crack Propagation, Lehigh Univ., Part VII, Leyden p. 649, 1972.

60. **Hahn, G.T., Kanninen, M.F., Rosenfield, A.R., Hoagland, R.G.**, *"The characterisation of fracture arrest in structural steel"*, Proceeding of the Second International Conference on Pressure Vessel Technology, San Antonio, Texas, ASME, 1973.

61. **Hahn, G.T., Kanninen, M.F., Rosenfield, A.R., Hoagland, R.G.**, *"Rectangular DCB-specimen for fast fracture and crack arrest measurement"*, Report No BMI-1933, Battelle Columbus Laboratories, Columbus, Ohio, 1974.

62. **Hahn, G.T., Kanninen, M.F., Rosenfield, A.R., Hoagland, R.G.**, *"Acrack arrest measuring procedure for K_{IM}, K_{ID} and K_{IA} properties"*, ASTM, STP 627, Philadelphia, Pa, p.177, 1977.

63. **Kanninen, M.F., Popelar, C., Gehlen, P.C.**, *"Dynamic analysis of crack arrest in controled stright - sided DCB-test specimens for wedge loading and machine loading conditions"*, Fast fracture and crack arrest, ASTM, STP, 627, Philadelphia, Pa., p.19, 1977.

64. **MTS - 815 Testing Machine,** *"Manual book".*

65. *"Standard Test Method for Plane-Strain Fracture Toughness of Metallic Materials".* ASTM, E-399, Philadelphia, Pa, 1974,1978, 1982, 1984.

66. **Srawley, J.E.,** *International Journal of fracture,* Vol. 12, No. 3, pp. 470-474, 1976.

67. **Costin, L.,** *"Static and Dynamic Fracture Behaviour of Oil Shale"* in "Fracture Mechanics for Ceramics, Rocks and Concrete", ASTM, STP 745, pp.169-184, Chicago, 1980.

68. **Ouchterlony, F.,** *"Extension of the Compliance and Stress Intensity Formulas for the Single Edge Crack Round Bar in Bending",* in "Fracture Mechanics for Ceramics, Rocks and Concrete", ASTM, STP 745, pp.237-255, Chicago, 1980.

69. **Joyce, J.A., Gudas, J.P.,** *"Computer Interactive J_{IC} Testing of Navy Alloys",* in "Elastic-Plastic Fracture", ASTM, STP 668, pp. 451-467, Atlanta, 1977.

70. **Zhu Zhe-Ming,** *"A New Method for Measurement of Fracture Toughness K_{IC} by Three Point Bend Specimen",* in J. "Engineering Fracture Mechanics", Vol. 45, No. 2, pp. 141-147, 1993.

71. **Shih, C.F., deLorenzi, H.G.,** in *"Elastic-Plastic Fracture",* ASTM, STP 668, pp. 65-120, 1979.

APPENDIX 1

Schematic presentation of the Chevron Notched
Short Rod (SR) specimen (not to scale)

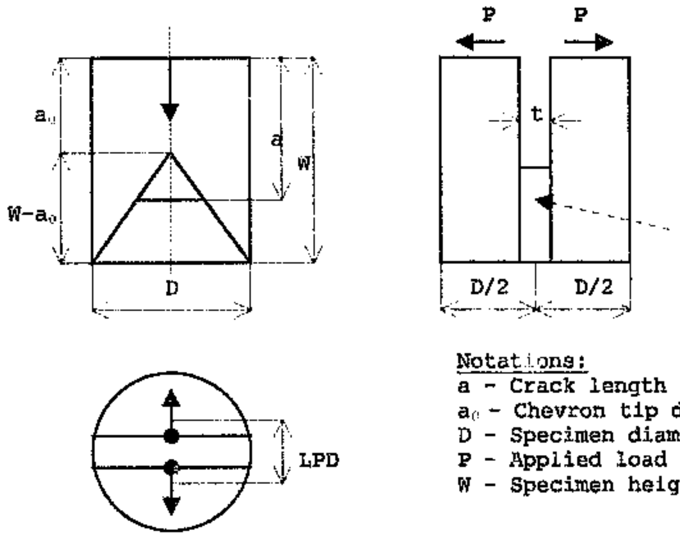

Notations:
a - Crack length
a_0 - Chevron tip distance
D - Specimen diameter
P - Applied load
W - Specimen height

Schematic presentation of the Single Edge Notched
Round Bar in Bending Short Rod (CB) specimen
(not to scale)

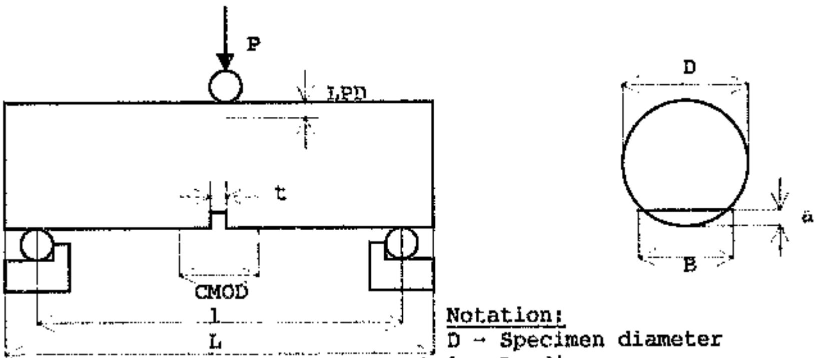

Notation:
D - Specimen diameter
l - Loading span
L - Specimen length
a - Crack length
P - Applied load
t - Notch width
CMOD - Crack mouth opening displacement
LPD - Load point displacement

Schematic presentation of the Brazil disk
in diametrical compression (not to scale)

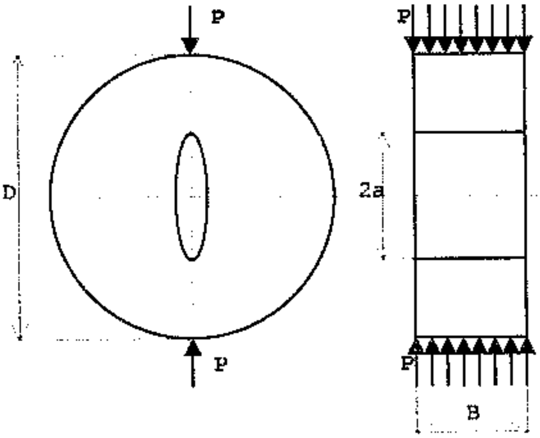

Notation:
P - Applied load
B - Specimen thickness
D - Specimen diameter
a - Half crack length

Schematic presentation of the Radial cracked
ring test (RCRT) (not to scale)

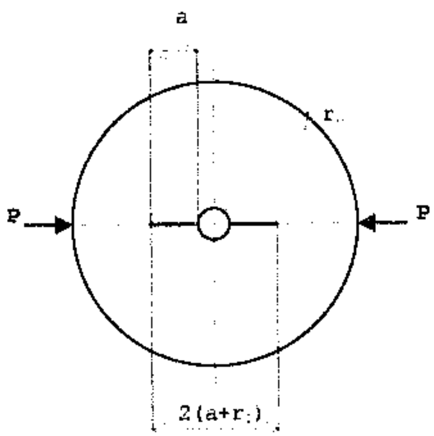

Notation:
P - Applied load
a - Half crack length
r_i - The inner radius
r_o - The outer radius

Schematic presentation of the Modified ring test (MRT) (not to scale)

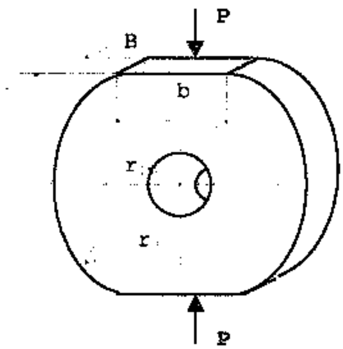

Notation:
b - Loading surface width
B - Specimen thickness
r - The outer radius
r_i - The inner radius
P - Applied load

Schematic presentation of the Single edge cracked half disk specimen in three point bending test (not to scale)

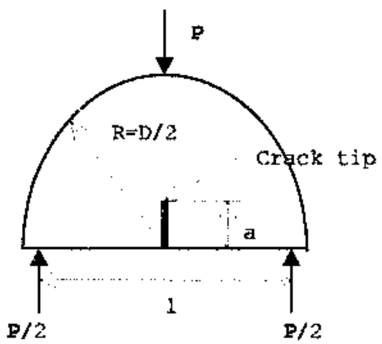

Notation:
P - Applied load
l - Loading span
a - Crack length

Schematic presentation of the Round compact disk in tension test (not to scale)

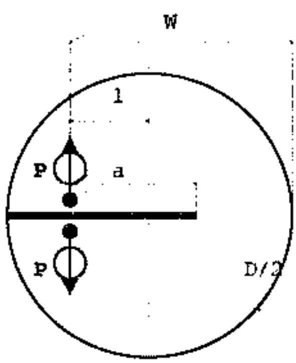

Notation:
P - Applied load
a - Crack length
D - Specimen diameter
l - Distance between axes of disk and holes
W - Specimen width

APPENDIX 2

Bottom

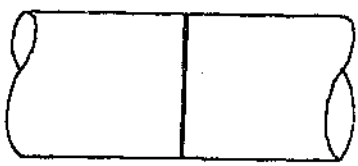

Chevron Face

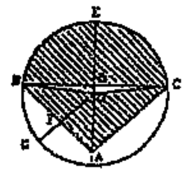

Side

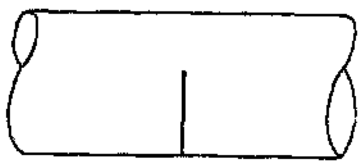

Parameters of the V shape

	D = 53 mm	D = 54 mm
AB = AC = 0.68D	36.04	36.72
AO = 0.35D	18.55	18.90
BC = 0.96D	50.88	51.84
DO = 0.14D	7.42	7.56
CD = 0.48D	25.44	25.92
DE = 0.36D	19.08	19.44
AD = 0.49D	25.97	26.46
BEC = 1.29D	68.37	69.66
OF = 0.25D	13.25	13.50
AE = 0.85D	45.05	45.90
< BOC = 163.9 deg. or 1.43 rad.		

APPENDIX 3

QUARTZITE

Results from fracture toughness calculations

B=0.053 m; K_{CB}=1.886 MPa/m

Table 1-a

	Eq.No	Q1L2	Q2L2	Q3L2	Q4L2
Loading rate (mm/sec)	VI.1	5.9E-04	1.1E-03	1.1E-03	9.7E-04
Initial tangent s_{it} (N/m)	VI.2	1.01E+05	8.65E+04	8.95E+04	8.95E+04
Slope value s_c (N/m)	VI.6	9.64E+04	7.11E+04	6.53E+04	7.36E+04
Displacement ratio p (-)	VI.9	0.17	0.16	0.18	0.14
Calculated F_c (N)	N/A	810	N/A	N/A	1930
Young's modulus E (GPa)	VI.13	54.33	46.91	48.52	48.52
En. Rel. Rate G^c_{CB} (J/m²)	VI.15	91.40	107.77	110.19	95.72
Frac. Tough. K^c_{CB} (MPa√m)	VI.12	2.21	2.22	2.26	2.13

Table 1-b

	Eq.No	Q5L2	Q6L2	Q6-5	Q6-4
Loading rate (mm/sec)	VI.1	8.5E-04	6.7E-04	9.3E-04	8.9E-04
Initial tangent s_{it} (N/m)	VI.2	9.42E+04	9.92E+04	9.12E+04	8.52E+04
Slope value s_c (N/m)	VI.6	7.74E+04	7.42E+04	8.27E+04	7.62E+04
Displacement ratio p (-)	VI.9	0.17	0.15	0.17	0.15
Calculated F_c (N)	N/A	1750	N/A	N/A	1870
Young's modulus E (GPa)	VI.13	50.81	52.44	49.35	46.30
En. Rel. Rate G^c_{CB} (J/m²)	VI.15	95.44	93.20	104.04	107.31
Frac. Tough. K^c_{CB} (MPa√m)	VI.12	2.18	2.19	2.24	2.20

Average fracture toughness coefficient:	2.20 MPa√m
Standard Deviation:	0.043
Variance:	0.002

N O R I T E

Results from fracture toughness calculations

B=0.053 m; K=1.974 MPa/m

Table 2-a

	Eq.No	N1L2	N3L2	N4L2	N5L2
Loading rate (mm/sec)	VI.1	5.55E-04	4.92E-04	6.29E-04	4.77E-04
Initial tangent s_i (N/m)	VI.2	1.81E+05	1.92E+05	1.73E+05	1.89E+05
Slope value s (N/m)	VI.6	1.49E+05	1.58E+05	1.42E+05	1.53E+05
Displacement ratio p (-)	VI.9	0.20	0.18	0.19	0.14
Calculated F_Q (N)	N/A	2190	2114	2344	2146
Young's modulus E (GPa)	VI.13	91.9	97.5	87.9	96.0
En. Rel. Rate G (J/m²)	VI.15	52.48	50.76	53.46	42.72
Frac. Tough. K (MPa√m)	VI.12	2.31	2.34	2.28	2.13

Table 2-b

	Eq.No	N6L2	N7L2	N7-5	N7-4
Loading rate (mm/sec)	VI.1	6.06E-04	5.64E-04	5.24E-04	6.72E-04
Initial tangent s_i (N/m)	VI.2	1.84E+05	1.79E+05	1.85E+05	1.87E+05
Slope value s (N/m)	VI.6	1.57E+05	1.47E+05	1.61E+05	1.58E+05
Displacement ratio p (-)	VI.9	0.15	0.15	0.25	0.17
Calculated F_Q (N)	N/A	N/A	2210	1875	N/A
Young's modulus E (GPa)	VI.13	93.3	90.9	94.0	95.0
En. Rel. Rate G (J/m²)	VI.15	51.25	46.82	56.31	52.10
Frac. Tough. K (MPa√m)	VI.12	2.30	2.17	2.42	2.34

Average fracture toughness coefficient: 2.29 MPa√m

Standard Deviation: 0.094

Variance: 0.009

S A N D S T O N E

Results from fracture toughness calculations

B=0.054 K_{IC}=0.822 MPa/m

Table 3

	Eq.No	SST4L2	SST5L2	SST6L2	SST7L2
Loading rate (mm/sec)	VI.1	4.3E-08	4.5E-08	4.7E-08	4.4E-08
Initial tangent s_{it} (N/m)	VI.2	7.93E+04	7.82E+04	8.42E+04	8.18E+04
Slope value s_c (N/m)	VI.6	6.7E+04	6.4E+04	6.9E+04	6.9E+04
Displacement ratio p (-)	VI.9	0.1	0.1	0.1	0.1
Calculated F_c (N)	N/A	282	268	352	318
Young's modulus E (GPa)	VI.13	40.26	39.71	42.75	41.53
En. Rel. Rate G^c_{IC} (J/m^2)	VI.15	3.38	2.14	2.26	2.94
Frac. Tough. K^c_{IC} (MPa/m)	VI.12	0.38	0.30	0.32	0.36

Average fracture toughness coefficient:	0.34 MPa/m
Standard Deviation:	0.037
Variance:	0.001

C O A L

Results from fracture toughness calculations

B=0.054 m; K_{IC}=0.152 MPa/m

Table 4

	Eq.No	C1L2	C2L2	C3L2	C4L2
Loading rate (mm/sec)	VI.1	7.91E-07	1.99E-06	1.16E-06	9.65E-07
Initial tangent s_{it} (N/m)	VI.2	2.44E+04	2.56E+04	2.53E+04	2.47E+04
Slope value s_c (N/m)	VI.6	9.35E+03	7.71E+03	6.43E+03	8.42E+03
Displacement ratio p (-)	VI.9	0.1	0.1	0.1	0.1
Calculated F_c (N)	N/A	128	150	145	137
Young's modulus E (GPa)	VI.13	2.44	3.01	2.85	2.59
En. Rel. Rate G^c_{IC} (J/m^2)	VI.15	1.27	1.52	1.40	1.49
Frac. Tough. K^c_{IC} (MPa/m)	VI.12	0.134	0.150	0.143	0.146

Average fracture toughness coefficient:	0.143 MPa/m
Standard Deviation:	0.007
Variance:	4.62E-05

APPENDIX 4

Calculation on the moment of inertia
Of intersection

1. Circular segment

$$\alpha = 1{,}43 \text{ radians } (\alpha < \pi/2)$$
$$r = D/2$$

- calculation of the area on circular segment

$$A_1 = r^2(\alpha - \sin\alpha.\cos\alpha) = (\frac{D}{2})^2.(1{,}43 - \sin 1{,}43.\cos 1{,}43) = 0{,}323.D^2$$

- calculation of the moment of inertia

$$J_y = \frac{r^4}{12}.(3\alpha - 3\sin\alpha\cos\alpha - 2\sin^3\alpha\cos\alpha)$$

$$J_y = \frac{D^4}{192}.(3.1{,}43 - 3.\sin 1{,}43.\cos 1{,}43 - 2.\sin^3 1{,}43.\cos 1{,}43) = 0{,}019.D^4$$

- calculation on the centre of the axis

$$y_{1C} = \frac{2r}{3}.(\frac{\sin^3\alpha}{\alpha - \sin\alpha.\cos\alpha}) = \frac{D}{3}(\frac{\sin^3 1,43}{1,43 - \sin 1,43.\cos 1,43}) = 0,251.D$$

$$y = y_{1c} - OD = 0,251.D - 0,14.D = 0,111.D$$

2. Triangle part

- calculation of the area

$$A_2 = \frac{b.h}{2} = \frac{0,96D.0,49D}{2} = 0,235\,D^2$$

- calculation of the moment of inertia

$$J_y = \frac{h.b^3}{48} = \frac{0,49D.(0,96D)^3}{48} = 0,009\,D^4$$

- calculation on the centre of the axis

$$y_{2c} = \frac{1}{3}.h = \frac{1}{3}.0,49D = 0,163D$$

3. Defining of the neutral axis

$$y^{*} = \frac{A_1.y - A_2.y_{2c}}{A_1 + A_2} = \frac{0,323\,D^2.0,111D - 0,235\,D^2.0,163D}{0,323\,D^2 + 0,235\,D^2} = -0,004D$$

new "y" coordinates of figures are;

C_1 = DE - y* = 0,36D - (-0,004D) = 0,364D

C_2 = AD + y* = 0,49D - 0,004D = 0,486D

4.Calculation of sectional modules

$$J = J_{1c} + J_{2c} = 0,019\,D^4 + 0,009\,D^4 = 0,028\,D^4$$

- Compressive stress

$$S_1 = \frac{J}{C_1} = \frac{0,028\,D^4}{0,364D} = 0,077\,D^3$$

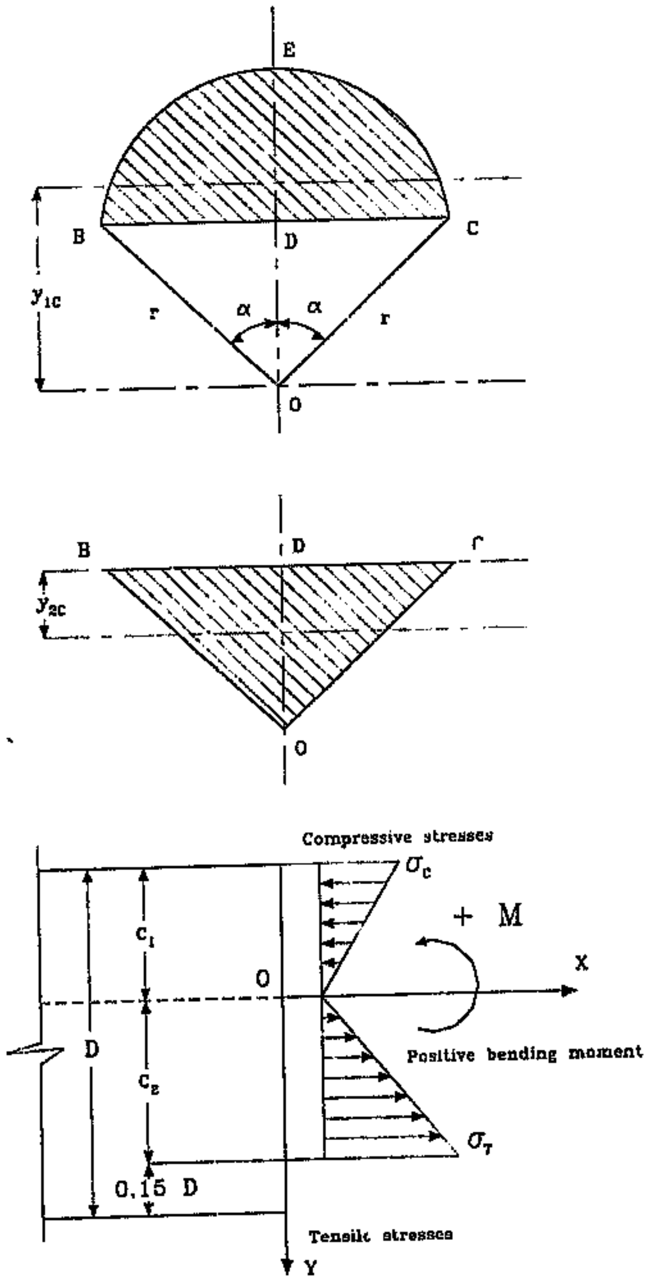

Figure A.1

Figures for calculation of moment of inertia

- Tensile stress

$$S_2 = \frac{J}{C_2} = \frac{0,028\,D^4}{0,486D} = 0,058\,D^3$$

5. Calculation of stresses

- bending moment

$$M = \frac{P.3,33D}{4} = 0,832.P.D$$

- Compressive stress

$$\sigma_C = \frac{M}{S_1} = \frac{0,832.P.D}{0,077.D^3} = \frac{10,81.P}{D^2}$$

- Tensile stress

$$\sigma_T = \frac{M}{S_1} = \frac{0,832.P.D}{0,058.D^3} = \frac{14,34.P}{D^2}$$

APPENDIX 5

Q U A R T Z I T E

Values for J-integral calculations (Table 1)

B = 0.053 m; K_{IC} = 2.20 (MPa$\sqrt{m}$); E = 49.63 (GPa); ν = 0.20

	Q 5-1	Q 5-2	Q 5-3	Q 5-4	Q 5-5	Q max
Cracked Ligament **a** (m)	8.62E-03	9.174E-03	1.087E-02	1.571E-02	1.714E-02	1.978E-02
Uncracked Ligament **b** (m)	3.62E-02	3.588E-02	3.418E-02	2.934E-02	2.791E-02	2.527E-02
a/b	0.24	0.26	0.32	0.53	0.61	0.78
Load (N)	300	700	1050	1650	1900	2050
LPD (m)	2.38E-06	8.25E-06	1.67E-05	2.44E-05	3.96E-05	4.25E-05
Work Done (N.m)	3.57E-04	4.48E-03	1.91E-02	4.48E-02	0.1151	0.1990
Final Load (N)	100	100	100	100	100	100
Final LPD (m)	7.31E-07	1.84E-06	3.61E-06	4.98E-06	9.32E-06	1.09E-05
B.b	1.92E-03	1.90E-03	1.81E-03	1.55E-03	1.48E-03	1.34E-03
a/W	0.16	0.17	0.21	0.30	0.32	0.37
σ (MPa)	1.53	3.57	5.36	8.42	9.70	10.46
K_I (MPa$\sqrt{m}$)	0.265	0.678	1.109	2.09	2.52	2.92
J_I (N/m) - Landes, Bergley	0.37	4.72	21.10	62.40	155.54	297.01
$J_{[illegible]}$ (N/m)-Landes, Bergley	0.26	3.33	17.09	56.11	143.10	285.13
J_I (N/m) - Merkel, Corten	0.42	5.27	23.25	72.55	164.22	310.55

N O R I T E

Results for J-integral calculations (Table 2)

B = 0.053 m; K_{IC} = 2.29 Mpa$\sqrt{m}$; E = 93.31 GPa; ν = 0.31.

	N-2	N-3	N-4	N-5-1	N-5	N3L2	N-7
Cracked Ligament (m) **(a)**	8.91E-03	9.79E-03	1.08E-02	1.34E-02	2.89E-02	4.44E-02	5.04E-02
Uncracked Ligam. (m) **(b)**	4.41E-02	4.33E-02	4.22E-02	3.96E-02	1.41E-02	8.55E-03	2.65E-03
a/b	0.2	0.23	0.26	0.34	1.20	5.19	19.02
Load (N)	750	1250	1800	1950	1650	1250	650
LPD (m)	3.90E-06	7.20E-06	1.15E-05	1.83E-05	3.55E-05	5.36E-05	9.92E-05
Work done (N.m)	1.27E-03	4.14E-03	1.03E-02	2.34E-02	5.65E-02	8.23E-02	1.21E-01
Final Load (N)	100	100	100	100	100	100	100
Final LPD (m)	2.75E-07	5.94E-07	9.29E-07	2.12E-05	6.90E-05	6.9E-05	6.9E-05
B.b	2.30E-03	2.30E-03	2.20E-03	1.19E-03	0.70E-03	0.45E-03	0.14E-03
a/W	0.17	0.18	0.20	0.25	0.54	0.84	0.95
σ (MPa)	3.82	6.38	9.19	9.66	8.42	6.38	3.32
K_I (MPa$\sqrt{m}$)	0.72	1.25	1.82	2.22	2.84	2.67	1.48
J_I (N/m) -Landes, Bergley	1.10	3.60	9.36	62.32	161.43	365.78	1728.57
$J_{[illegible]}$ (N/m) -Landes, Bergley	0.78	2.66	7.82	62.32	161.43	365.78	1728.57
J_I (N/m) - Merkel, Corten	1.44	4.08	10.49	58.16	174.39	379.56	1734.20

S A N D S T O N E

Values for J - integral calcu.ation

Table 3

B = 0.054 m; K_{IC} = 0.34 MPa$\sqrt{m}$; E = 41.06 GPa; v = 0.24.

	SST-2	SST-3	SST-4	SST-5
Cracked Ligam.(m) **(a)**	0.0217	0.0258	0.0343	0.0455
Uncrack. Ligam.(m) **(b)**	0.0313	0.0277	0.0187	0.0075
a/b	0.69	0.93	1.83	6.07
Load (N)	450	550	650	750
LPD (m)	1.58E-05	3.38E-05	4.20E-05	5.33E-05
Work done (N.m)	0.0055	0.0152	0.0231	0.0346
Final Load (N)	100	100	100	100
Final PLD (m)	4.99E-06	1.27E-05	1.30E-05	2.16E-05
B.b	1.66E-03	1.44E-03	9.91E-04	3.98E-04
a/W	0.41	0.49	0.65	0.86
σ (MPa)	2.30	2.81	3.32	3.83
K_I (MPa$\sqrt{m}$)	0.67	0.90	1.22	1.62
J_I (N/m) - Landes, Bergley	6.32	21.11	46.62	173.87
$J_{[illegible]}$ (N/m) - Landes, Bergley	6.32	21.11	46.62	173.87
J_I (N/m) - Merkel, Corten	7.17	22.25	48.24	176.69

Stress intensity factor is calculated on a basis of equation:

$$K_I = 1.12 x \sigma x SQRT(a x \pi)$$

APPENDIX 6

Legend

Zone of interest

Main fracture

Featuring of Quartzite specimen

Figure A-Q-1

Crack initiation of Quartzite

Figure A-Q-2-a

Figure A-Q-2-b

Figure A-Q-2

Crack initiation of Quartzite specimen in the tip of the V shape

A-Q-2-a Magnification x 50
A-Q-2-b Magnification x 25

Figure Q1
Crack initiation in the left
Side of the V shape of Quartzite specimen

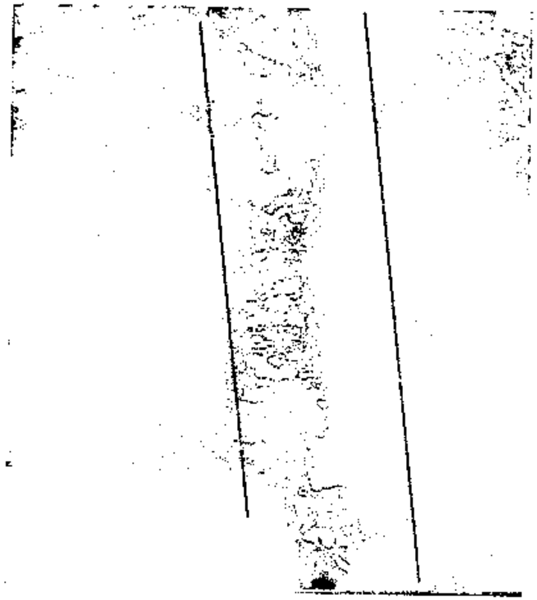

Figure Q2
Crack initiation in the right
Side of the V shape of Quartzite specimen

Figure Q3

30°, parallel- grain in a top left part of the picture. 45° - grain in central right part of the picture

Figure Q4

45°, 90°- grain in a central part of the picture. 45° - grain in a middle top part of the picture

Figure Q5

45° - grain in the left part of the picture
30° - grain in the top right side of the picture

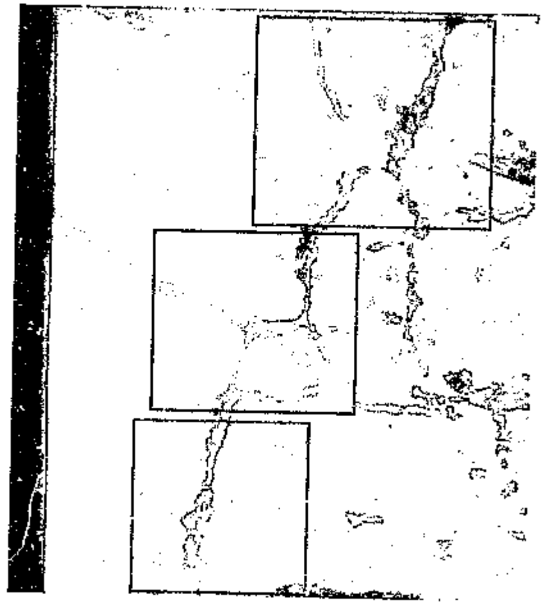

Figure Q6

45° - crack in the top part of the picture
90°,45° - crack in the central part of the picture
45° - crack in a bottom part of the picture

Figure Q7

30°,45° - crack in a entral
part of the picture

Figure Q8

30°,45° - grain in a left side
of the picture
90,45 - grain in a righ side
of the picture

Figure Q9

45 - grain in a middle right part of the picture

Figure Q10

45 - grain in a right side of the picture

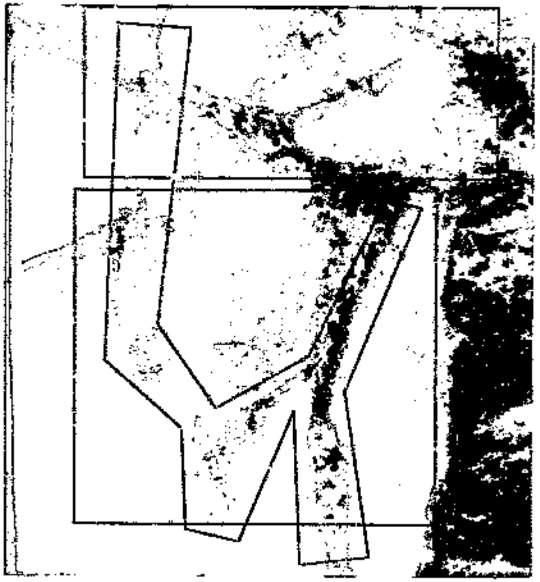

Figure Q11

45° - grain in a top part of the picture
35°,40° - grain in central part of the picture

Figure Q12

70 - grain in a top part of the picture
45 - grain in central part of the picture

Figure Q13

45 ,90 - grain in a right part
of the picture

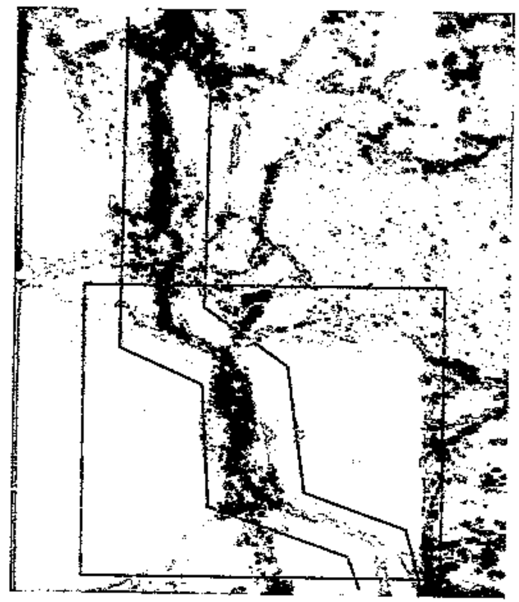

Figure Q14

45 ,90 - grain in a bottom half
of the picture

FRACTURING OF NORITE SPECIMENS

Figure N1

Fracturing in the tip of the V shape of Norite specimens under polarised light

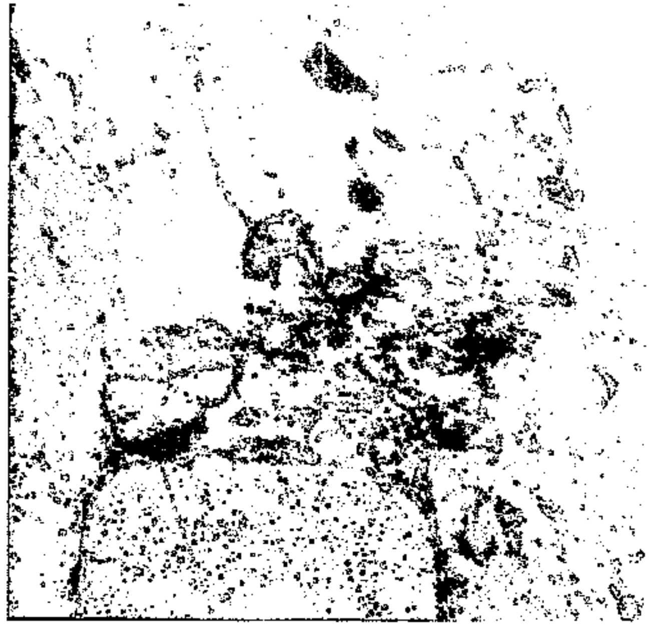

Figure N2

Fracturing in the tip of the V shape of Norite specimens under bottom light

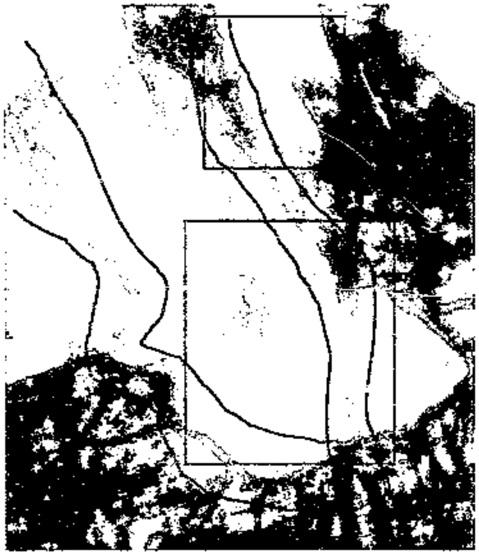

Figure N3

20° - grain in a middle top part of the picture
20°,40° - grain in a middle part of the picture

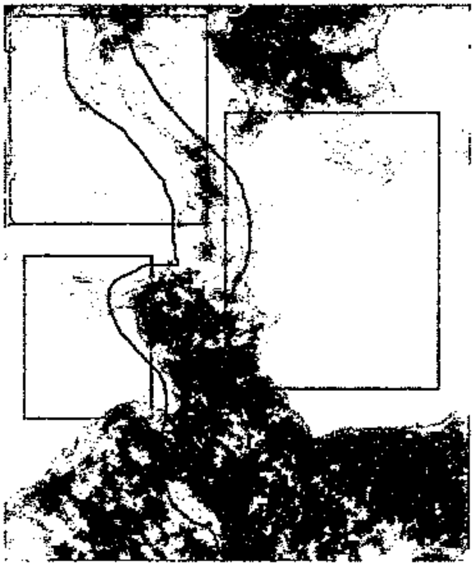

Figure N4

60° - grain in a top left part of the picture
90° - grain in a middle right side of the picture
80 - grain in a bottom left half of the picture

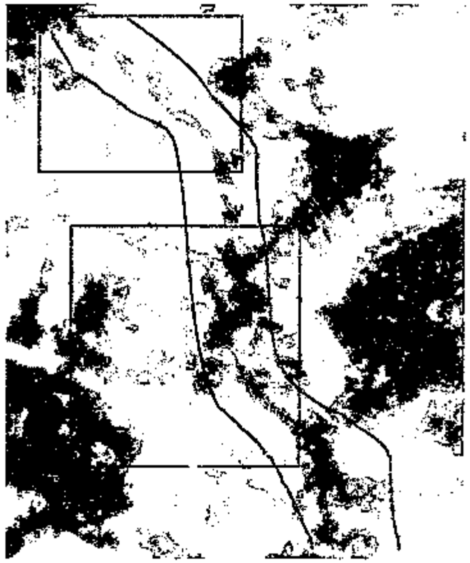

Figure N5

60° - grain in a center of the picture
80°,90° - grain in a top left corner of the picture

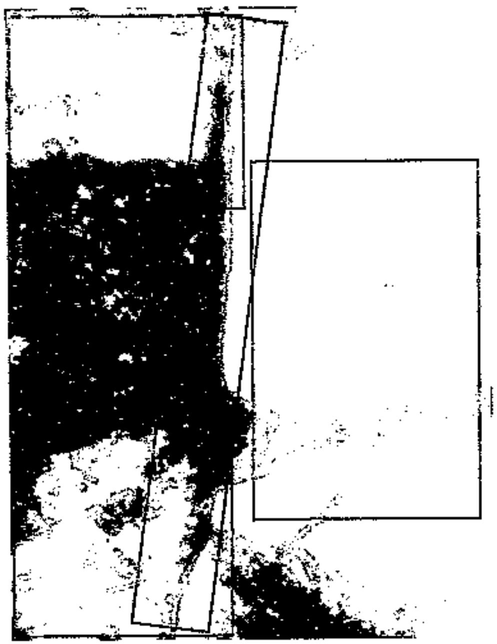

Figure N6

60′ - grain in top and bottom left part of the picture
90 ,parallel - grain in a right side of the picture

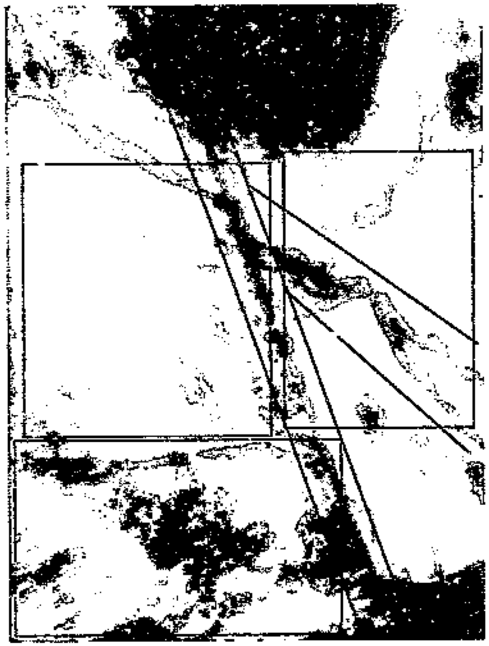

Figure N7

80′,90′ - grain in a middle left part of the picture
90′,parallel - grain in a central part of the picture
80′ - grain in a bottom left part of the picture

Figure N8

90′ - grain in top half of the picture
80′,parallel - grain in a center and bottom part of the picture

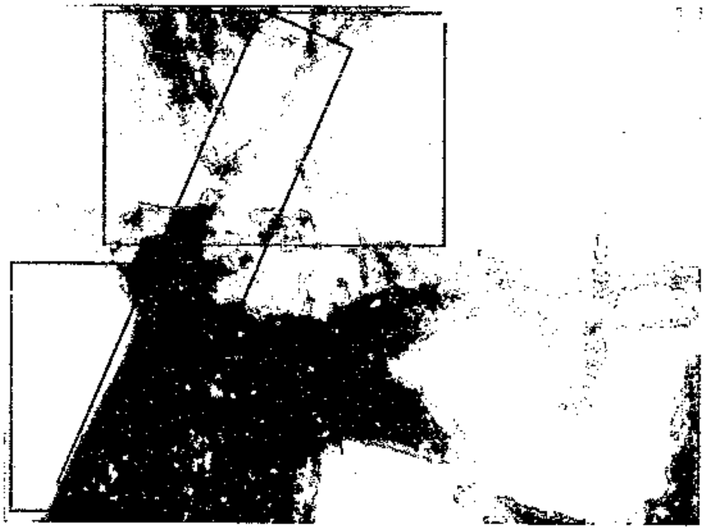

Figure N9

80 - grain in a top half of the picture
parallel - grain in a bottom left side
of the picture

Figure N10

90',parallel- grain in a bottom left part
of the picture

Figure N11

80 - grain in a top half of the picture
60 - grain in a bottom half of the picture

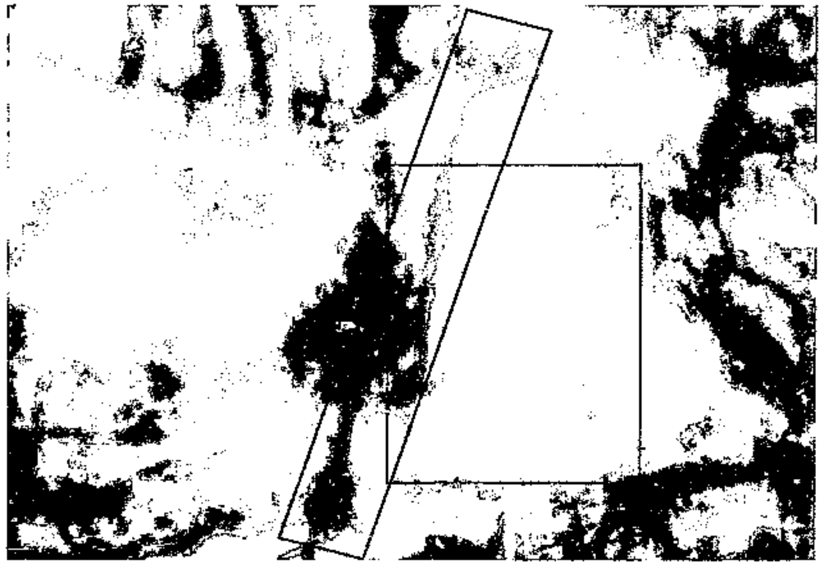

Figure N12

80' - grain in a middle right of the picture

FRACTURING OF SANDSTONE SPECIMENS

Figure S1

Figure S2

Chaotic fracture distribution in fracture process zone in the tip of the V shape

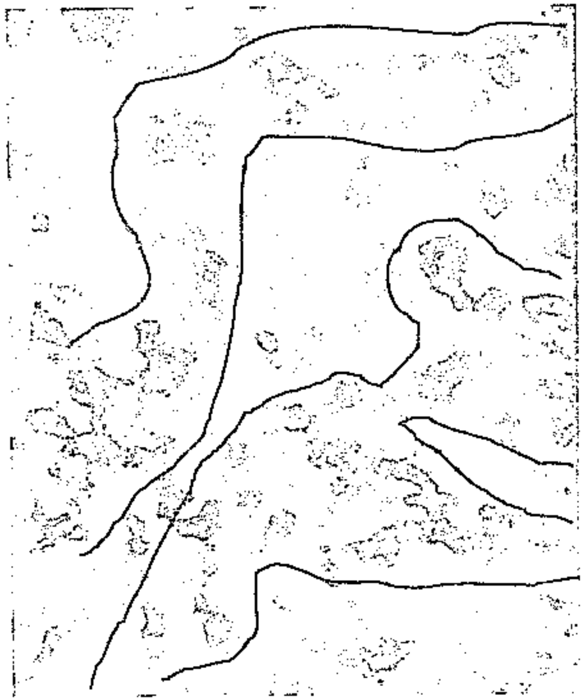

Figure S3

Can be seen shied of cracks from the left to the right side of tne picture

Figure S4

Can be seen shied of cracks from the left to the right side of the picture with joins between them

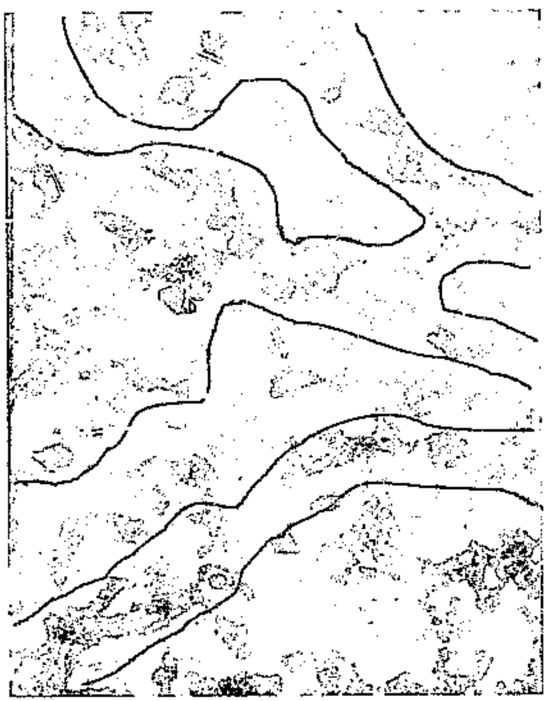

Figure S5

Can be seen shied of cracks from the left
to the right side of the picture

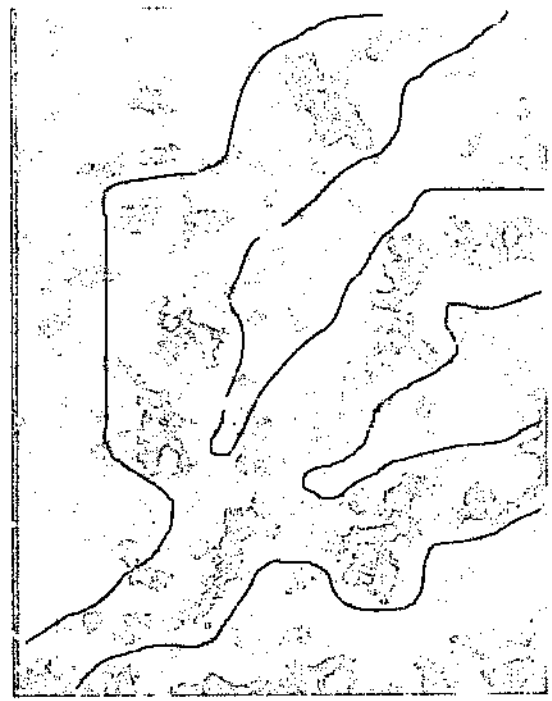

Figure S6

Can be seen shied of cracks from the left
to the right side of the picture with
joins between them